Supporting Information
for

C–H Bond Activation at Antimony(III): Synthesis and Reactivity of Sb(III)-Oxyaryl Species

Gabriel Duneş,[a,b] Marie Cordier,[a] Samia Kahlal[a] Alpar Pöllnitz,[b] Jean-Yves Saillard,[a]* Cristian Silvestru[b]* and Yann Sarazin[a]*

[a] *Université de Rennes, CNRS, Institut des Sciences Chimiques de Rennes, UMR 6226*
Campus de Beaulieu, 35042 Rennes, Cedex, France
E-mail: yann.sarazin@univ-rennes.fr; jean-yves.saillard@univ-rennes.fr

[b] *Dr. G. Duneş, Dr. A. Pöllnitz, Prof. Dr. C. Silvestru*
Department of Chemistry, Supramolecular Organic and Organometallic Chemistry Centre (SOOMCC)
Faculty of Chemistry and Chemical Engineering, Babeş-Bolyai University
11 Arany Janos, 400028 Cluj-Napoca, Romania
E-mail: cristian.silvestru@ubbcluj.ro

Table of Contents

List of Figures

List of Tables

Experimental Procedures

General Information

All manipulations were performed under an inert atmosphere by using standard Schlenk techniques or in a dry, solvent-free glovebox (Jacomex; O_2 < 1 ppm, H_2O < 3 ppm). THF was distilled under argon from Na/benzophenone prior to use. Petroleum ether (40-60 °C), toluene, dichloromethane, and Et_2O were collected from MBraun SPS-800 purification alumina columns and thoroughly degassed with argon before being stored on 4 Å molecular sieves. Deuterated solvents (Eurisotop, Saclay, France) were stored in sealed ampoules over activated 4 Å molecular sieves or a potassium mirror, and degassed by a minimum of three freeze–thaw cycles. Antimony(III) chloride (Alfa Aesar) was sublimed prior to use. CS_2 was degassed by three freeze-pump-thaw cycles and stored over molecular sieves 4 Å under argon. All other chemicals were provided by commercial suppliers and used as received. ESI mass spectra were recorded on a Thermo Scientific Orbitrap XL spectrometer equipped with standard ESI/APCI source. Data analysis and calculations of the theoretical isotopic patterns were carried out with the Xcalibur software package.[1] Melting points were measured with an Electrothermal 9200 apparatus and are not corrected. Elemental analyses were carried out on a Flash EA 1112 analyser.

2,6-$^{i}Pr_2C_6H_3OH$ (Sigma-Aldrich, 97%), 2,6-$^{t}Bu_2C_6H_3OH$ (Sigma-Aldrich, 98%), 2,4-$^{t}Bu_2C_6H_3OH$ (Alfa Aesar, 99%) and 2,4,6-$^{t}Bu_3C_6H_2OH$ (Thermo Fisher Scientific, 97%) were sublimed or distilled prior to use. The corresponding potassium salts [{2,6-$^{i}Pr_2$-C_6H_3O}K], [{2,6-$^{t}Bu_2$-C_6H_3O}K], [{2,4-$^{t}Bu_2$-C_6H_3O}K] and [{2,4,6-$^{t}Bu_3$-C_6H_2O}K] were synthesised by adding at room temperature a solution of the appropriate phenol in THF over a suspension of KH in THF, followed by filtration, removal of the solvent and washing the resulting off-white solid with hexane. 2,6-($^{i}Pr_2NCH_2)_2C_6H_3Br$,[2] [{2,6-$(Me_2NCH_2)_2C_6H_3$}$SbCl_2$] (aka [{*NCN*^{Me4}}$SbCl_2$]),[3] [2-$(Me_2NCH_2)C_6H_4$]$SbCl_2$ (aka [{*CN*^{Me4}}$SbCl_2$]),[4] [2,6-$(Me_2NCH_2)_2C_6H_3$]$Sb(OC_6H_3$-$^{i}Pr_2$-2,6)$_2$] (aka [{*NCN*^{Me4}}$Sb(OC_6H_3$-$^{i}Pr_2$-2,6)$_2$], **1**),[5] and $[H(OEt_2)_2]^+[H_2N\{B(C_6F_5)_3\}_2]^-$,[6] were prepared following literature procedures.

NMR spectra were recorded with Bruker AM-400 or AM-500 spectrometers. Assignment of the signals was assisted by 1D (^1H, ^{13}C) and 2D (COSY, HMBC, HMQC and NOESY/ROESY) NMR experiments. Abbreviations used in multiplicities are: s, singlet; d, doublet; dd, doublet of doublets; t, triplet; m, multiplet. The NMR spectra were processed using MestReNova software package.[7] The ^1H chemical shifts are reported in δ units (ppm) relative to the residual peak of the deuterated solvent ($CDHCl_2$, 5.32 ppm; C_6D_5H, 7.16 ppm; [$(CD_2)_3CHDO$], 1.73 ppm; CD_2HCN, 1.94 ppm; C_5D_4HN, 7.22 ppm). The ^{13}C chemical shifts are reported in δ units (ppm) relative to the peak of the deuterated solvent (CD_2Cl_2, 53.84 ppm; C_6D_6, 128.06 ppm; THF-d_8, 25.31; CD_3CN, 1.32 ppm; pyridine-d_5, 123.87 ppm).[8]

Synthesis and Characterisation

Synthesis of [{*NCN*^{Me4}}Sb(C_6H_2-^{t}Bu_2-3,5-O-4)] (3)

THF (10 mL) was added, at room temperature, over a mixture of solid [{2,6-^{t}Bu_2-C_6H_3O}K] (191 mg, 0.78 mmol) and [{*NCN*^{Me4}}$SbCl_2$] (150 mg, 0.39 mmol). The solids dissolved and the resulting orange solution was stirred for 2 h. The reaction mixture was filtered to remove the KCl by-product then the resulting solution was concentrated to *ca.* 3 mL. Addition of hot hexane (10 mL) generated a chartreuse insoluble material and the resulting suspension was stirred for 1 h, then filtered and the solid was washed with additional hot hexane (5 mL). After filtration, the resulting precipitate was dried under reduced pressure to afford **3** as a chartreuse air-sensitive solid (171 mg, 85%), m.p. 144 °C (dec).

Note: The remaining traces of unreacted [{NCN^{Me4}*}$SbCl_2$] and of the co-product 2,6-^{t}Bu_2-C_6H_3OH (observed in the ^{1}H NMR of **3**) can be removed by washing the resulting chartreuse solid with toluene (2 x 5 mL) and Et_2O (2 x 5 mL), followed by drying the resulting insoluble solid under vacuum.*

Single crystals of **3** suitable for X-ray diffraction were grown from a concentrated THF solution stored at −35 °C.

Elemental analysis calcd for $C_{26}H_{39}SbN_2O$ (517.37 g/mol): C, 60.36; H, 7.60; N, 5.41. Found: C, 60.13; H, 7.20; N, 5.79.

IR (Nujol mull): 3057w, 2936w, 1559s, 1479s, 1434s, 1375w, 1334m, 1301w, 1254m, 1200w, 1097s, 1011w, 998m, 924w, 884m, 835s, 769s, 714w, 617w, 569w. See Fig. S7

^{1}H NMR (CD_3CN, 400.13 MHz, 300 K): δ 7.47 (t, $^3J_{HH}$ = 7.5 Hz, 1H, H-4), 7.30 (d, $^3J_{HH}$ = 7.5 Hz, 2H, H-3), 6.96 (bs $v_{1/2}$ = 190 Hz, 2H, H-9), AB spin system with A at δ 3.73 and B at δ 3.80 ($^2J_{HH}$ = 14.9 Hz, 4H, H-5), 2.58 (s, 6H, H-6), 2.06 (s, 6H, H-7), 1.24 (bs $v_{1/2}$ = 90 Hz, 18H, H-13) ppm. See Fig. S1.

^{13}C{^{1}H} NMR (CD_3CN, 100.62 MHz, 300 K): δ (C_q, C-8) not detected, 145.79 (C_q, C-2), 144.08 (C_q, C-1), 138.80 (C_q, C-11), 131.28 (C-4), 126.36 (C-3), 126.04 (C-9), 121.00 (C_q, C-10), 64.94 (C-5), 47.10 (C-6), 46.61 (C-7), 35.63 (C-12), 30.00 (C-13) ppm. See Fig. S2.

^{1}H NMR (CD_2Cl_2, 400.13 MHz, 300 K): δ 7.46 (t, $^3J_{HH}$ = 7.6 Hz, 1H, H-4), 7.27 (d, $^3J_{HH}$ = 7.6 Hz, 2H, H-3), 6.65 (bs $v_{1/2}$ = 195 Hz, 2H, H-9), AB spin system with A at δ 3.69 and B at δ 3.77 ($^2J_{HH}$ = 14.6 Hz, 4H, H-5), 2.58 (s, 6H, H-6), 2.11 (s, 6H, H-7), 1.27 (bs $v_{1/2}$ = 160 Hz, 18H, H-13) ppm. See Fig. S3.

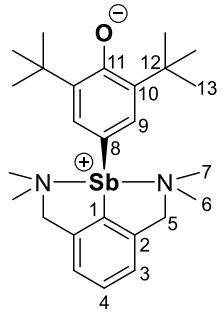

CD_3CN and CD_2Cl_2

^{13}C{^{1}H} NMR (CD_2Cl_2, 100.62 MHz, 300 K): δ (C_q, C-10) not detected, 176.33 (C_q, C-8), 144.76 (C_q, C-2), 143.59 (C_q, C-1), 138.97 (C_q, C-9), 130.74 (C-4), 125.94 (C-3), 112.72 (C_q, C-11), 64.82 (C-5), 47.04 (C-6), 46.60 (C-7), 34.57 (C-12), 29.72 (C-13) ppm. See Fig. S4.

^{1}H NMR (THF-d_8, 500.13 MHz, 300 K): δ 7.42 (t, $^3J_{HH}$ = 7.5 Hz, 1H, H-4), 7.27 (d, $^3J_{HH}$ = 7.5 Hz, 2H, H-3), 7.16 (s, 1H, H-9), 6.45 (s, 1H, H-13), 3.79 (s, 4H, H-5), 2.57 (s, 6H, H-6), 2.09 (s, 6H, H-7), 1.39 (s, 9H, H-15), 1.13 (s, 9H, H-17) ppm. See Fig. S5.

^{13}C{^{1}H} NMR (THF-d_8, 125.77 MHz, 300 K): δ 177.50 (C_q, C-8), 145.99 (C_q, C-2), 144.84 (C_q, C-1), 139.29 (C_q, C-12), 139.02 (C_q, C-10), 133.30 (C-9), 131.08 (C-4), 129.98 (C-13), 126.39 (C-3), 112.22 (C_q, C-11), 65.17 (C-5), 46.75 (C-6), 46.53 (C-7), 35.96 (C-14, C-16), 30.46 (C-15), 30.32 (C-17) ppm. See Fig. S6.

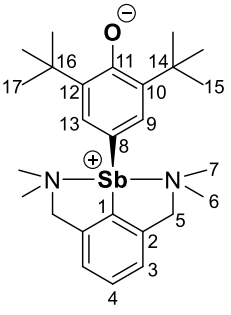

THF-d_8

Synthesis of [{*NCN*^{iPr4}}$SbCl_2$]

^{n}BuLi (1.4 mL, 2.3 mmol, 1.6 M in *n*-hexane solution) was added dropwise at −78 °C to a solution of 2,6-(^{i}Pr_2NCH_2)$_2$$C_6H_3Br$ (0.8 g, 2.09 mmol) in THF (15 mL). The resulting orange slurry was stirred for 1 h at −78 ºC, then added dropwise to a solution of $SbCl_3$ (0.48 g, 2.09 mmol) in THF (15 mL), at −78 °C. The reaction mixture was stirred for 3 h, at −78 °C, then was slowly allowed to reach room temperature and stirred overnight. Volatiles were removed under reduced pressure and the crude off-white solid was then extracted into toluene (2 x 15 mL). The resulting slurry was filtered and removal of the solvent under reduced pressure yielded the title compound as a pale-yellow solid which was further washed with 20 mL hexane (0.68 g, 66%), m.p. 183 °C (dec).

Elemental analysis calcd for $C_{20}H_{35}SbCl_2N_2$ (496.17 g/mol): C, 48.41; H, 7.11; N, 5.65. Found: C, 48.15; H, 6.99; N, 5.71.

^{1}H NMR (C_6D_6, 400.13 MHz, 300 K): δ 7.20 (t, $^3J_{HH}$ = 7.5 Hz, 1H, H-4), 6.91 (d, $^3J_{HH}$ = 7.5 Hz, 2H, H-3), 4.30 (s, 4H, H-5), 3.97 (sept, $^3J_{HH}$ = 6.7 Hz, 4H, H-6 and H-8), 1.32 (d, $^3J_{HH}$ = 6.7 Hz, 12H, H-7), 0.89 (d, $^3J_{HH}$ = 6.7 Hz, 12H, H-9) ppm. See Fig. S13.

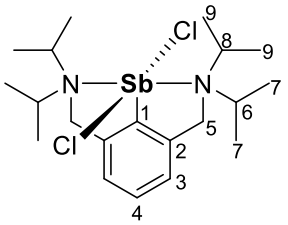

^{13}C{^{1}H} NMR (C_6D_6, 100.62 MHz, 300 K): δ 156.21 (C_q, C-1), 147.24 (C_q, C-2), 130.18 (C-4), 124.90 (C-3), 56.77 (C-5), 54.82 (C-6, C-8), 24.84 (C-7), 20.45 (C-9) ppm. See Fig. S14.

MS (ESI+, MeOH), *m/z* (relative intensity, %): 424.18 (8) $[M - 2Cl]^+$, 459.16 (100) $[M - Cl]^+$.

HRMS (ESI+, MeOH): $[M - Cl]^+$ calcd. for $C_{20}H_{35}N_2ClSb$ 459.15215. Found: 459.15355.

Synthesis of [{*NCN^{iPr4}*}Sb(C$_6$H$_2$-^{t}Bu$_2$-3,5-O-4)] (4)

A colourless solution of [{2,6-^{t}Bu$_2$-C_6H_3O}K] (148 mg, 0.60 mmol) in THF (5 mL) was added to a stirred slurry of [{*NCN^{iPr4}*}$SbCl_2$] (150 mg, 0.30 mmol) in THF (5 mL) at room temperature. The solids dissolved and the resulting dark-red solution was stirred for 2 h. KCl was eliminated by filtration and the resulting solution was concentrated to *ca.* 3 mL. Addition of hot hexane (10 mL) generated a dark-red insoluble material and the resulting suspension was stirred for 1 h then filtered. The orange solid was washed again with additional hot hexane (2 x 5 mL). After filtration, the resulting precipitate was dried under reduced pressure to afford **4** as an orange air-sensitive solid (172 mg, 91%), m.p. 130 °C (dec).

Suitable crystals for X-ray diffraction were obtained by slow diffusion of hexane into a saturated THF solution of **4** at −35 ºC.

Elemental analysis calcd for $C_{34}H_{55}SbN_2O$ (629.59 g/mol): C, 64.86; H, 8.81; N, 4.45. Found: C, 64.55; H, 8.47; N, 4.79.

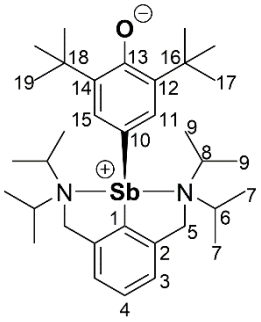

^{1}H NMR (CD_3CN, 400.13 MHz, 300 K): δ 7.46 (t, $^3J_{HH}$ = 7.5 Hz, 1H, H-4), 7.33 (s, 1H, H-11), 7.27 (d, $^3J_{HH}$ = 7.5 Hz, 2H, H-3), 6.43 (s, 1H, H-15), AB spin system with A at δ 3.70 and B at δ 4.11 ($^2J_{HH}$ = 16.0 Hz, 4H, H-5), 3.25 (m, 4H, H-6 overlapped with H-8), 1.37 (s, 9H, H-17), 1.36 (d, $^3J_{HH}$ = 6.7 Hz, 12H, H-7), 1.13 (d, $^3J_{HH}$ = 6.7 Hz, 12H, H-9), 1.07 (s, 9H, H-19) ppm. See Fig. S15.

^{13}C{^{1}H} NMR (CD_3CN, 100.62 MHz, 300 K): δ 177.15 (C_q, C-10), 149.49 (C_q, C-2), 143.38 (C_q, C-1), 139.62 (C_q, C-14), 139.46 (C_q, C-12), 137.73 (C_q, C-13), 135.18 (C-11), 132.41 (C-15), 131.25 (C-4), 125.09 (C-3), 54.04 (C-5), 35.72 (C-18), 35.59 (C-16), 35.24 (C-6, C-8), 30.48 (C-17), 30.10 (C-7), 29.81 (C-19), 22.31 (C-9) ppm. See Fig. S16.

Synthesis of [{*CN^{Me2}*}Sb(OC$_6$H$_3$-^{t}Bu$_2$-2,6)$_2$] (5)

A solution of [{2,6-^{t}Bu$_2$-C_6H_3O}K] (148 mg, 0.60 mmol) in THF (5 mL) was added to a suspension of [{*CN^{Me2}*}$SbCl_2$] (98 mg, 0.30 mmol) in THF (5 mL) at room temperature. The solids dissolved and the resulting yellow solution was stirred for 2 h. KCl was eliminated by filtration, and the resulting solution was concentrated to *ca.* 3 mL. Addition of hexane (10 mL) generated a brown insoluble material and the resulting suspension was stirred for 1 h. After filtration, the solvent was evacuated in vacuo and the resulting solid was dried to afford **5** as a green-yellow air-sensitive solid (156 mg, 78%), m.p. 135 °C (dec).

Elemental analysis calcd for $C_{37}H_{54}NO_2Sb$ (666.60 g/mol): C, 66.67; H, 8.17; N, 2.10. Found: C, 66.31; H, 7.95; N, 2.06.

^{1}H NMR (THF-*d$_8$*, 500.13 MHz, 300 K): δ 8.60 (dd, $^3J_{HH}$ = 6.5 Hz, 1H, H-6), 7.34 (tt, $^3J_{HH}$ = 7.5 Hz, $^4J_{HH}$ = 5.6 Hz, 2H, H-4 and H-5), 7.19 (d, $^3J_{HH}$ = 7.4 Hz, 1H, H-3), 7.08 (d, $^3J_{HH}$ = 7.7 Hz, 4H, H-11), 6.62 (t, $^3J_{HH}$ = 7.7 Hz, 2H, H-12), 3.56 (s, 2H, H-7), 1.79 (s, 6H, H-8), 1.31 (s, 36H, H-14) ppm. See Fig. S17.

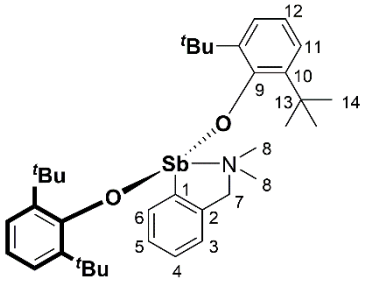

^{13}C{^{1}H} NMR (THF-*d$_8$*. 125.13 MHz, 300 K): δ 159.38 (C_q, C-1), 156.60 (C_q, C-2), 146.36 (C_q, C-9), 141.74 (C_q, C-10), 137.03 (C-6), 131.15 (C-5), 128.37 (C-4), 128.26 (C-3), 126.95 (C-11), 119.19 (C-12), 66.20 (C-7), 45.18 (C-8), 33.95 (C-14), 30.86 (C-13) ppm. See Fig. S18.

HRMS (ESI+, CD_2Cl_2): $[M - C_{14}H_{21}O]^+$ calcd. for $C_{23}H_{33}NOSb$ 460.15948. Found: 460.15983.

HRMS (ESI-, CD_2Cl_2): $[C_{14}H_{21}O]^-$ calcd. for $C_{14}H_{21}O$ 205.15869. Found: 205.15916.

Synthesis of [{*CN*^{Me2}}Sb(C_6H_2-^{t}Bu$_2$-3,5-O-4)]$_4$ (**6$_4$**)

THF (10 mL) was added at room temperature over a mixture of solid *N,N*-dimethyl-aminopyridine (DMAP) (28 mg, 0.23 mmol) and **5** (150 mg, 0.23 mmol). The solids dissolved and the resulting green solution was stirred for 3 h at 68 °C. During this time, a colourless, crystalline and insoluble material crashed out of the solution, and the resulting suspension was stirred for an additional hour. The supernatant was filtered off, and from the resulting green mother liquor, *N,N*-dimethyl-aminopyridine (DMAP) and HOC_6H_3-^{t}Bu$_2$-2,6 in an 1:1 molar ratio (based on ^{1}H NMR) were identified as the sole products (See Fig. S19). The separated crystalline material was insoluble in all common solvents (THF-d$_8$, CD_2Cl_2, C_6D_6, toluene-d$_8$, DMSO-d$_6$, D_2O) and was identified by SCXRD and HRMS as the cyclic tetramer [{*CN*^{Me2}}Sb(C_6H_2-^{t}Bu$_2$-3,5-O-4)]$_4$ (**6$_4$**). The white solid isolated by filtration was further washed with cold THF (5 mL) and hexanes (5 mL) and dried under reduced pressure to yield **6$_4$** as a white crystalline solid (90 mg, 85%), m.p. 160 °C.

Elemental analysis calcd for $C_{92}H_{128}N_4O_4Sb_4$ (1841.10 g/mol): C, 60.02; H, 7.01; N, 3.04. Found: C, 59.93; H, 6.91; N, 3.14.

HRMS (ESI+, CD_2Cl_2): $[M - H]^+$ calcd. for $C_{92}H_{128}N_4O_4Sb_4$ 1840.60908. Found: 1840.61078.

NMR data could not be recorded owing to the complete insolubility of the title compound in all common organic solvents.

Synthesis of [{*NCN*^{Me4}}Sb(OC_6H_2-^{t}Bu$_3$-2,4,6)$_2$] (**7**)

A colourless solution of [{2,4,6-^{t}Bu$_3$-C_6H_2O}K] (150 mg, 0.50 mmol) in THF (5 mL) was added to a stirred suspension of [{*NCN*^{Me4}}$SbCl_2$] (96 mg, 0.25 mmol) in THF (5 mL) at room temperature. The solids dissolved and the resulting orange solution was stirred for 2 h. The reaction solution was filtered to remove KCl, and the resulting solution was then concentrated to *ca.* 1 mL. Addition of toluene (5 mL) generated a brown insoluble material and the resulting suspension was stirred for 1 h then filtered. After filtration, the solvent was pumped off under vacuum and the resulting solid was dried to constant weight to afford **7** as an orange air-sensitive solid (140 mg, 67%), m.p. 166 °C (dec).

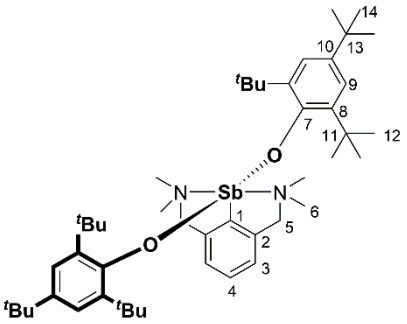

Elemental analysis calcd for $C_{48}H_{77}N_2O_2Sb$ (835.92 g/mol): C, 68.97; H, 9.29; N, 3.35. Found: C, 68.91; H, 9.10; N, 3.33.

^{1}H NMR (C_6D_6, 500.13 MHz, 300 K): δ 7.31 (s, 4H, H-9), 7.06 (t, $^3J_{HH}$ = 7.5 Hz, 1H, H-4), 6.79 (d, $^3J_{HH}$ = 7.5 Hz, 2H, H-3), 3.63 (s, 4H, H-5), 2.03 (s, 12H, H-6), 1.44 (m, 54H, H-12 and H-14) ppm. See Fig. S20.

^{13}C{^{1}H} NMR (C_6D_6, 125.13 MHz, 300 K): δ 161.47 (C_q, C-7), 157.65 (C_q, C-1), 146.46 (C_q, C-2), 138.07 (C_q, C-10), 134.97 (C_q, C-8), 130.72 (C-4), 125.26 (C-3), 122.03 (C-9), 66.41 (C-5), 46.94 (C-6), 35.92 (C-13), 34.26 (C-11), 32.34 (C-12), 30.55 (C-14) ppm. See Fig. S21.

HRMS (ESI+, CD_2Cl_2): $[M - C_{18}H_{29}O]^+$ calcd. for $C_{30}H_{48}N_2OSb$ 573.27993. Found: 573.27905.

HRMS (ESI-, CD_2Cl_2): $[C_{18}H_{29}O]^-$ calcd. for $C_{14}H_{21}O$ 261.22129. Found: 261.22237.

Synthesis of [{*NCN*^{Me4}}Sb(OC_6H_2-^{t}Bu$_2$-2,4)$_2$] (**8**)

In a glovebox, a J-Young NMR tube was charged with [{*NCN*^{Me4}}$SbCl_2$] (30 mg, 0.078 mmol) and [{2,4-^{t}Bu$_2$-C_6H_3O}K] (38 mg, 0.16 mmol). The tube was removed from the glovebox and connected to a Schlenk line where THF-d$_8$ (0.5 mL) was added, then was inserted into the NMR probe to record the ^{1}H and ^{13}C{^{1}H} NMR spectra. Yield 95% (55 mg, 0.076 mmol), isolated as a pale-yellow solid.

^{1}H NMR (400.13 MHz, THF-d_8): δ 7.31 (t, $^3J_{HH}$ = 7.5 Hz, 1H, H-4), 7.18 (d, $^3J_{HH}$ = 7.5 Hz, 2H, H-3), 7.03 (bs $v_{1/2}$ = 37 Hz, 2H, H-9), 6.82 (bs $v_{1/2}$ = 85 Hz, 2H, H-11), 6.69 (m, 2H, H-12), 3.93 (bs $v_{1/2}$ = 280 Hz, 4H, H-5), 1.18 (s, 18H, H-14), 1.04 (s, 18H, H-16) ppm. See Fig. S22.

^{13}C{^{1}H} NMR (100.62 MHz, THF-d_8): δ 159.85 (C_q, C-1), 157.70 (C_q, C-7), 149.43 (C_q, C-2), 139.46 (C_q, C-10), 138.13 (C_q, C-8), 130.46 (C-4), 127.46 (C-3), 124.15 (C-9), 123.23 (C-12), 120.05 (C-11), 65.47 (C-5), 45.16 (C-6), 35.71 (C-13), 34.71 (C-15), 32.35 (C-14), 31.20 (C-16) ppm. See Fig. S23.

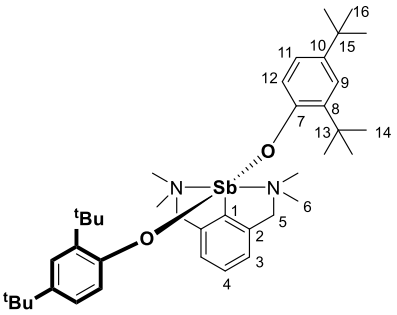

Synthesis of [{*NCN^{Me4}*}Sb(C$_6$H$_2$-^{t}Bu$_2$-3,5-OH-4)][Cl] (12)

A colourless solution of [Me$_3$NH][Cl] (37 mg, 0.39 mmol) in CH_2Cl_2 (3 mL) was added to a stirred green-yellow solution of **3** (200 mg, 0.39 mmol) in THF (5 mL) at room temperature. During the addition, the solution turned colourless. It was stirred for 20 min, after which the solvent was evaporated under vacuum and the white solids were washed with cold THF (10 mL). The resulting solid was dried under reduced pressure, yielding the titled compound **12** as a colourless, air-sensitive solid (162 mg, 75%).

X-ray quality colourless crystals were grown by slow diffusion of hexanes into a saturated CH_2Cl_2 solution at −35 °C.

Elemental analysis calcd for $C_{26}H_{40}ClN_2OSb$ (553.83 g/mol): C, 56.39; H, 7.28; N, 6.40. Found: C, 56.11; H, 7.04; N, 6.40.

^{1}H NMR (CD_2Cl_2, 500.13 MHz, 300 K): δ 7.55 (t, $^3J_{HH}$ = 7.6 Hz, 1H, H-4), 7.37 (d, $^3J_{HH}$ = 7.6 Hz, 2H, H-3), 7.14 (bs $v_{1/2}$ = 266 Hz, 2H, H-9), 5.82 (s, 1H, O*H*), AB spin system with A at δ 4.12 and B at δ 3.72 ($^2J_{HH}$ = 14.8 Hz, 4H, H-5), 2.80 (bs $v_{1/2}$ = 295 Hz, 6H, H-6), 2.11 (bs $v_{1/2}$ = 295 Hz, 6H, H-7), 1.33 (bs $v_{1/2}$ = 165 Hz, 18H, H-13) ppm. See Fig. S24.

^{13}C{^{1}H} NMR (CD_2Cl_2, 125.13 MHz, 300 K): δ 157.33 (C_q, C-8), 144.86 (C_q, C-2), 142.92 (C_q, C-1), 138.34 (C_q,C-10), 131.74 (C-4), 131.36 (C_q, C-11), 125.25 (C-9), 126.30 (C-3), 65.23 (C-5), 47.65 (C-12), 34.88 (C-6, C-7), 30.32 (C-13) ppm. See Fig. S25.

HRMS (ESI+, CD_2Cl_2): [M − Cl]$^+$ calcd. for $C_{26}H_{40}N_2OSb$ 517.21733. Found: 517.21623.

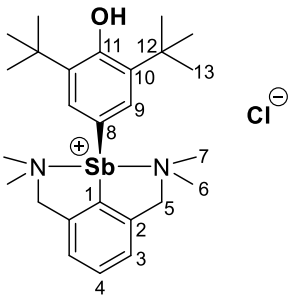

Synthesis of [{*NCN^{Me4}*}Sb(C$_6$H$_2$-^{t}Bu$_2$-3,5-OH-4)]$^+$[H$_2$N{B(C$_6$F$_5$)$_3$}$_2$]$^-$ (12')

A colourless solution of [H(OEt$_2$)$_2$]$^+$[H$_2$N{B(C$_6$F$_5$)$_3$}$_2$]$^-$ (226 mg, 0.19 mmol) in CH_2Cl_2 (5 mL) was added dropwise to green-yellow solution of **3** (100 mg, 0.19 mmol) in CH_2Cl_2 (10 mL), upon which the colour immediately discharged. After stirring for 3 h, the solvent was evaporated under reduced pressure, yielding **12'** as an off-white air sensitive solid. Suitable single crystals for X-ray diffraction were obtained by slow diffusion of hexanes into a saturated CH_2Cl_2 solution at –35 °C (204 mg, 69%).

Elemental analysis calcd for $C_{62}H_{42}B_2F_{30}N_3OSb$ (1558.37 g/mol): C, 47.79; H, 2.72; N, 2.70. Found: C, 47.79; H, 2.70; N, 2.71.

IR: 3626m, 3385w, 2964br, 1645m, 1522s, 1457s, 1275m, 1100br, 1082s, 984m, 957w, 778s, 612w. See Fig. S30.

^{1}H NMR (CD_2Cl_2, 500.13 MHz, 300 K): δ 7.60 (t, $^3J_{HH}$ = 7.6 Hz, 1H, H-4), 7.39 (d, $^3J_{HH}$ = 7.6 Hz, 2H, H-3), 7.15 (bs $v_{1/2}$ = 230 Hz, 2H, H-9), 5.70 (bs $v_{1/2}$ = 160 Hz, 2H, N*H*$_2$), 5.66 (s, 1H, O*H*), AB spin system with A at δ 3.88 and B at δ 3.75 ($^2J_{HH}$ = 15.0 Hz, 4H, H-5), 2.71 (s, 6H, H-6), 2.08 (s, 6H, H-7), 1.33 (bs $v_{1/2}$ = 130 Hz, 18H, H-13) ppm. See Fig. S26.

^{13}C{^{1}H} NMR (CD_2Cl_2, 125.13 MHz, 300 K): δ (C-11, not detected), 157.82 (C_q, C-8), 149.52, 147.14, 140,67, 138.32, 138.16, 135.86 (all *C*$_6$F$_5$), 144.50 (C_q, C-1), 140.94 (C_q,C-2), 138.47 (C_q, C-10), 132.52 (C-4), 129.37 (C-9), 126.75 (C-3), 65.23 (C-5), 48.02 (C-6), 47.25 (C-7), 34.86 (C-12), 30.16 (C-13) ppm. See Fig. S27.

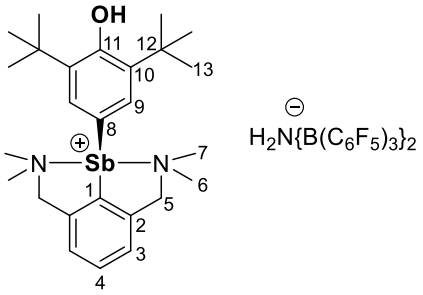

^{19}F{^{1}H} NMR (CD_2Cl_2, 188.29 MHz, 300 K): δ −132.92 (d, $^3J_{FF}$ = 18.9 Hz, 12F, *o*-F), −160.22 (t, $^3J_{FF}$ = 18.9 Hz, 6F, *p*-F), −165.70 (t, $^3J_{FF}$ = 18.9 Hz, 12F, *m*-F) ppm. See Fig. S28.

^{11}B NMR (CD_2Cl_2, 96.29 MHz, 300 K): δ −8.31 ppm. See Fig. S29.

Synthesis of [{*NCN*^{Me4}}Sb(S$_2$C-C$_6$H$_2$-^{t}Bu$_2$-3,5-O-4)] (13)

A colourless solution of CS_2 (0.1 mL, 1.74 mmol) in THF (5 mL) was added dropwise at room temperature to a chartreuse solution of **3** (300 mg, 0.58 mmol) in THF (10 mL). The mixture instantly turned orange, with concomitant formation of an orange precipitate. After 4 h, the orange suspension was concentrated to ca. 5 mL and the solids were isolated *via* cannula filtration. The resulting orange solids were dissolved in hot pyridine (3 mL) and allowed to slowly cool down to ambient temperature, affording formation of X-ray quality single crystals. The mother liquor was decanted and the orange crystalline solid was dried under reduced pressure to afford **13** (306 mg, 89%).

Elemental analysis calcd for $C_{27}H_{39}N_2OS_2Sb$ (593.50 g/mol): C, 54.64; H, 6.62; N, 4.72. Found: C, 54.27; H, 6.69; N, 4.44. See Fig. S31.

IR: 2952s, 2832w, 1601m, 1560s, 1418s, 1350m, 1305s, 1245s, 1202m, 1100m, 1011s, 911w, 908w, 835s, 762w, 745w, 667s, 527s.

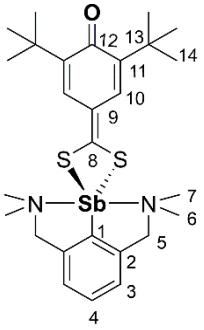

^{1}H NMR (Pyridine-d_5, 500.13 MHz, 300 K): δ 8.01 (s, 2H, H-9), 7.40 (t, $^3J_{HH}$ = 7.6 Hz, 1H, H-4), 7.25 (d, $^3J_{HH}$ = 7.6 Hz, 2H, H-3), AB spin system with A at δ 4.48 and B at δ 3.43 ($^2J_{HH}$ = 14.6 Hz, 4H, H-5), 2.55 (s, 6H, H-6), 1.97 (s, 6H, H-7), 1.58 (s, 18H, H-14) ppm. See Fig. S32.

^{13}C{^{1}H} NMR (Pyridine-d_5, 125.13 MHz, 300 K): δ 185.99 (C_q, C-9), 176.10 (C-8), 147.34 (C_q, C-1), 141.71 (C_q, C-11), 130.78 (C-4), 128.63 (C_q, C-2), 128.47 (C-3), 127.22 (C_q, C-12), 126.45 (C-10), 64.99 (C-5), 47.16 (C-6), 43.19 (C-7), 35.87 (C-13), 30.40 (C-14) ppm. See Fig. S33.

Synthesis of [{*NCN*^{Me4}}SbI$_2$]

A solution of KI (432 mg, 2.6 mmol) in distilled water (10 mL) was added to a solution of [{*NCN*^{Me4}}SbCl$_2$] (200 mg, 0.52 mmol) in CH_2Cl_2 (15 mL), and the resulting mixture was stirred for 3 h. The resulting bright yellow CH_2Cl_2 solution was separated and the title compound was further extracted by washing the aqueous phase with CH_2Cl_2 (2 x 10 mL). The organic layers were combined and dried over anhydrous $MgSO_4$. The solution was filtered and the solvent was pumped off under vacuum. The resulting solid was washed with hexanes (2 x 5 mL) and dried under reduced pressure to yield the title compound as a yellow powder (200 mg, 68%), m.p. 165 °C.

Elemental analysis calcd for $C_{12}H_{19}I_2N_2Sb$ (566.87 g/mol): C, 25.43; H, 3.38; N, 4.94. Found: C, 25.43; H, 3.37; N, 4.95.

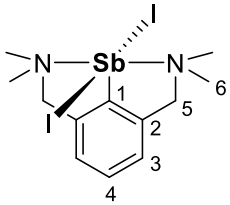

^{1}H NMR ($CDCl_3$, 500.13 MHz, 300 K): δ 7.41 (t, $^3J_{HH}$ = 7.5 Hz, 1H, H-4), 7.24 (d, $^3J_{HH}$ = 7.5 Hz, 2H, H-3), 4.26 (s, 4H, H-5), 3.00 (s, 12H, H-6) ppm. See Fig. S34.

^{13}C{^{1}H} NMR ($CDCl_3$, 125.13 MHz, 300 K): δ 148.26 (C_q, C-1), 145.21 (C_q, C-2), 131.13 (C-4), 125.94 (C-3), 66.64 (C-5), 50.84 (C-6) ppm. See Fig. S35.

HRMS (ESI+, MeOH): $[M - I]^+$ calcd. for $C_{12}H_{19}IN_2Sb$ 438.96256. Found: 438.96363.

Synthesis of 2,6-^{t}Bu$_2$-C$_6$H$_3$OD

A 50 mL Schlenk flask was charged with [{2,6-^{t}Bu$_2$-C$_6$H$_3$O}K] (200 mg, 0.82 mmol) and 10 mL of THF. The mixture was stirred for 5 minutes until the solids dissolved and 45 μL (2.46 mmol, 3 eq.) of D_2O was added and the resulted mixture was left to stir for 1h. The mixture was concentrated to 3 mL and petroleum ether (15 mL) was added, inducing the formation of a precipitate. The precipitate was isolated by filtration, dried under vacuum and sublimed at 40 °C at 10^{-3} mm Hg. The deuterated title compound was isolated as a colourless crystalline solid (165 mg, 97%, 98%-D based on NMR data, See Fig. S36).

Reaction of [{*NCN*^{Me4}}Sb(C$_6$H$_2$-^{t}Bu$_2$-3,5-O-4)] (3) with S$_8$

A 50-mL Schlenk tube was charged with [{*NCN*^{Me4}}Sb(C$_6$H$_2$-^{t}Bu$_2$-3,5-O-4)] (**3**) (100 mg, 0.19 mmol) and THF (10 mL). The resulting solution was added dropwise over a suspension of S_8 (7 mg, 0.026 mmol) in THF (5 mL). The mixture was stirred for 1 h until a dark orange suspension was formed. The suspension was concentrated to ca. 3 mL and petroleum ether (10 mL) was added. A pale yellow insoluble solid precipitated. The solid was separated by filtration and identified by NMR as [{*NCN*^{Me4}}Sb(μ^2-S)]$_2$ (50 mg, 75%). In the filtrate, the presence of 3,3',5,5'-tetra-tert-butyldiphenoquinone (**A**) was identified by

NMR; it crystallised (38 mg, 95%) together with a small crop of orange crystals (8 mg) of [({*NCN*^{Me4}}Sb(μ-S_5))$_2$] based on XRD.[9] See Fig. S58.

Reaction of [{*NCN*^{Me4}}Sb(C_6H_2-^{t}Bu$_2$-3,5-O-4)] (3) with excess of TEMPO

NMR scale procedure: A J-Young NMR tube was charged with [{*NCN*^{Me4}}Sb(C_6H_2-^{t}Bu$_2$-3,5-O-4)] (**3**) (30 mg, 0.06 mmol), TEMPO (31 mg, 0.20 mmol) and THF-d_8 (0.5 mL) under inert atmosphere. The ^{1}H NMR was recorded each day for seven consecutive days. The data reveal a slow process, where compound **3** is consumed with concomitant formation of new species identified as tetramethylpiperidine (TMP-H) and the known [{*NCN*^{Me4}}Sb(μ^2-O)]$_2$;[10] crystals of the latter were isolated, and XRD analysis confirmed its identity. See Fig. S59.

Preparative reaction: A 50 mL Schlenk flask was loaded with [{*NCN*^{Me4}}Sb(C_6H_2-^{t}Bu$_2$-3,5-O-4)] (**3**) (50 mg, 0.097 mmol) and TEMPO (53 mg, 0.34 mmol) and THF (10 mL). The mixture was stirred for 4 d and a dark green solution formed. The solution was then concentrated to 3 mL and kept in the freezer at −35 °C. Several types of crystals grew from this mixture. They were identified by SC-XRD as unreacted **3**, [{*NCN*^{Me4}}Sb(μ^2-O)]$_2$,[10] and 3,3',5,5'-tetra-*tert*-butyldiphenoquinone (**A**).

Reaction of [{*NCN*^{Me4}}Sb(C_6H_2-^{t}Bu$_2$-3,5-O-4)] (3) with N-iodosuccinimide

A 50-mL Schlenk tube was charged with [{*NCN*^{Me4}}Sb(C_6H_2-^{t}Bu$_2$-3,5-O-4)] (**3**) (100 mg, 0.19 mmol) and *N*-iodosuccinimide (43 mg, 0.19 mmol), and THF (10 mL) was added. The mixture was stirred for 1 h until a dark orange suspension formed. The orange insoluble solid was isolated by filtration, dried *in vacuo* and identified by ^{1}H NMR spectroscopy in CD_2Cl_2 as a mixture of [{*NCN*^{Me4}}Sb(I)(succinimide)] (ca. 80%) and [{*NCN*^{Me4}}SbI_2] (ca. 20%). We were unable to obtain crystals of the presumably [{NCN^{Me4}}Sb(I)(succinimide)]; all attempts failed, and SC-XRD analysis only confirmed the presence of crystals as [{NCN^{Me4}}SbI_2] in this mixture. From the supernatant, once taken to dryness, 3,3',5,5'-tetra-tert-butyldiphenoquinone (**A**) was identified by ^{1}H NMR and XRD as the only product soluble in THF. See Fig. S60.

General procedure for reactivity and mechanistic studies of Sb-oxyaryl species in THF-*d8*. A J-Young NMR tube was loaded with the appropriate solid reagents in a glovebox under inert atmosphere. The NMR tube was then removed from the glovebox, connected to a double-manifold Schlenk line, and loaded with the appropriate amount desired solvent using standard Schlenk techniques. Reaction times were measured from this point.

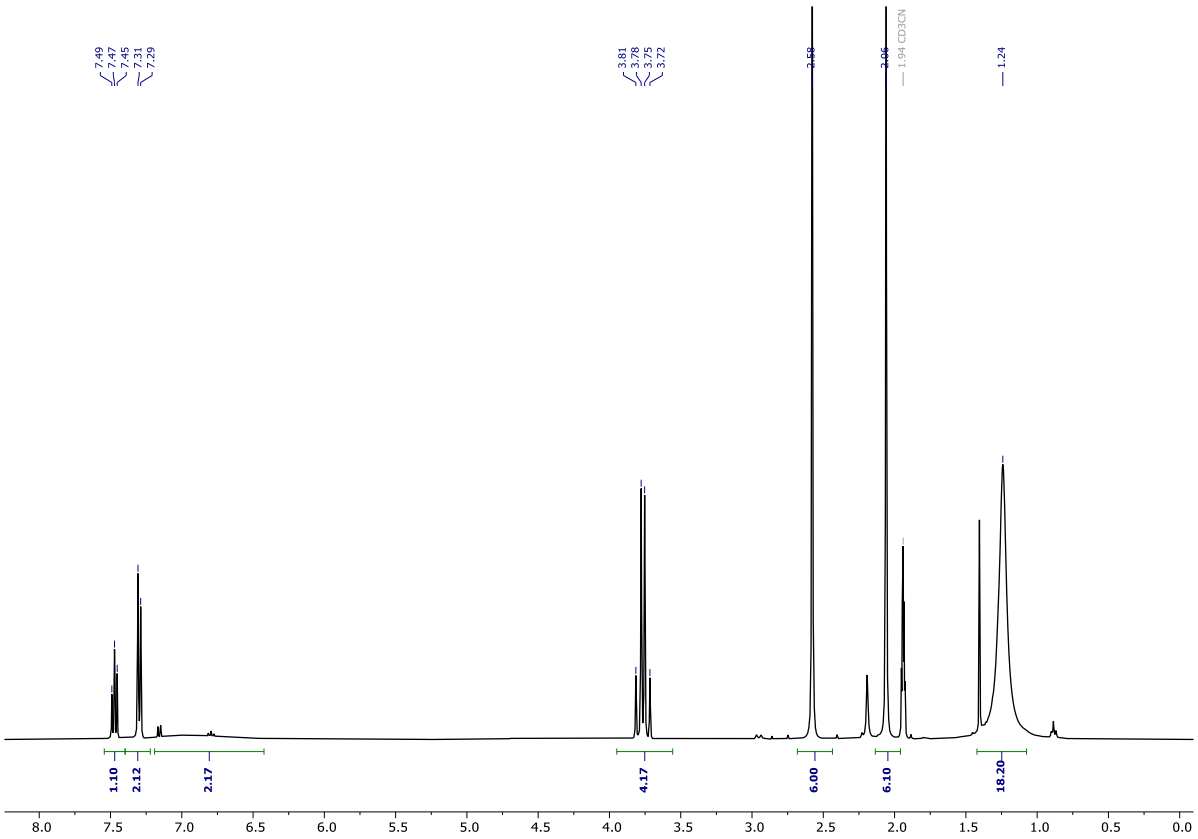

Figure S1. ^{1}H NMR spectrum (CD_3CN, 400.13 MHz, 300 K) of [{*NCN*^{Me4}}Sb(C_6H_2-$^{t}Bu_2$-3,5-O-4)] (**3**).

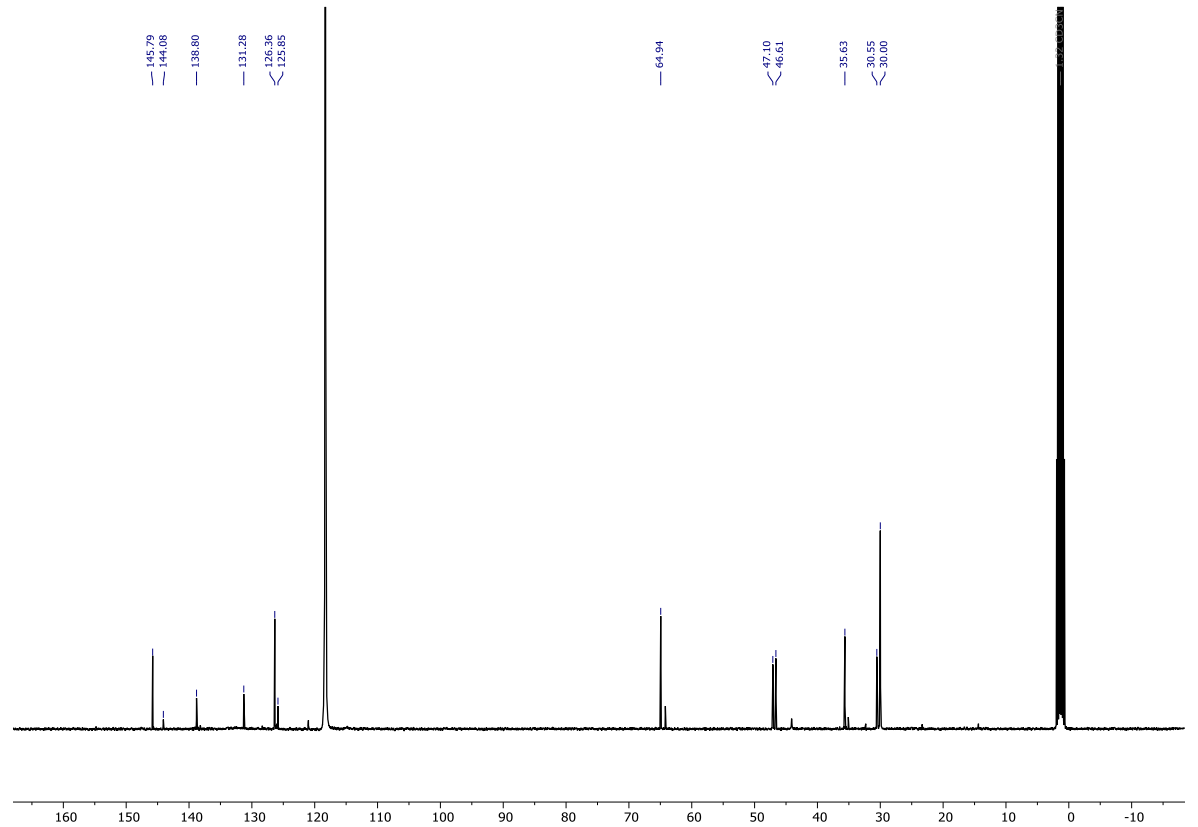

Figure S2. $^{13}C\{^{1}H\}$ NMR spectrum (CD_3CN, 100.62 MHz, 300 K) of [{*NCN*^{Me4}}Sb(C_6H_2-$^{t}Bu_2$-3,5-O-4)] (**3**).

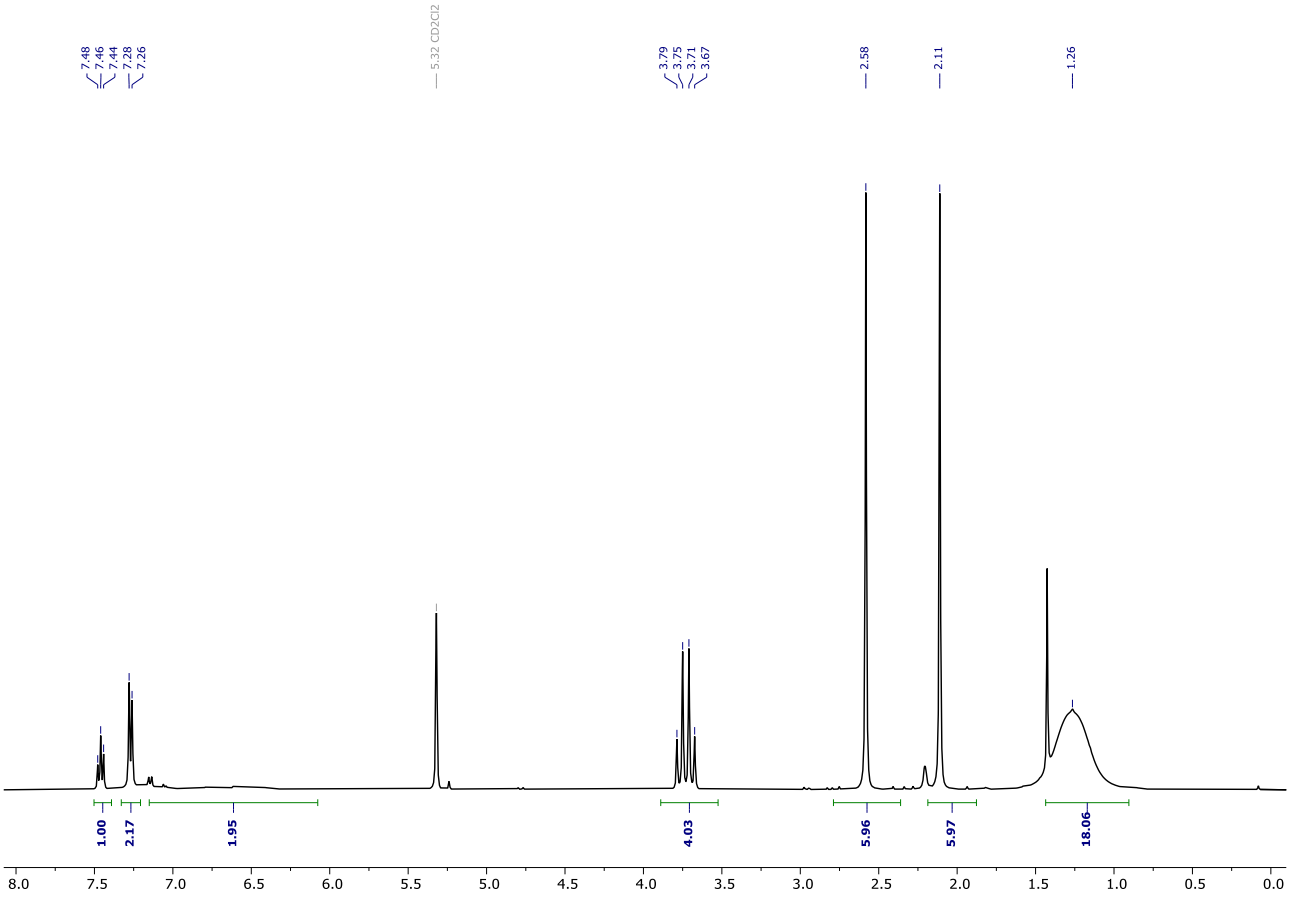

Figure S3. ^{1}H NMR spectrum (CD_2Cl_2, 400.13 MHz, 300 K) of [{*NCN*^{Me4}}Sb(C_6H_2-$^{t}Bu_2$-3,5-O-4)] (**3**).

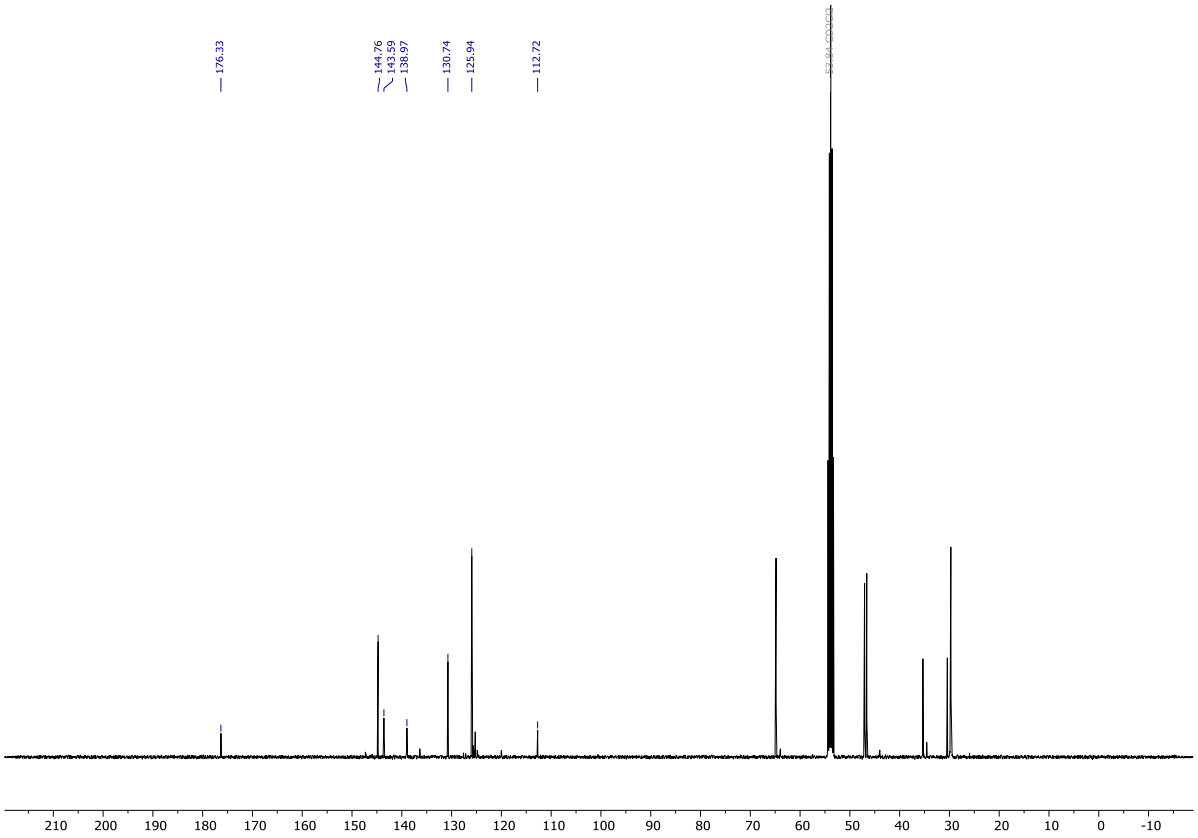

Figure S4. ^{13}C{^{1}H} NMR spectrum (CD_2Cl_2, 100.62 MHz, 300 K) of [{*NCN*^{Me4}}Sb(C_6H_2-$^{t}Bu_2$-3,5-O-4)] (**3**).

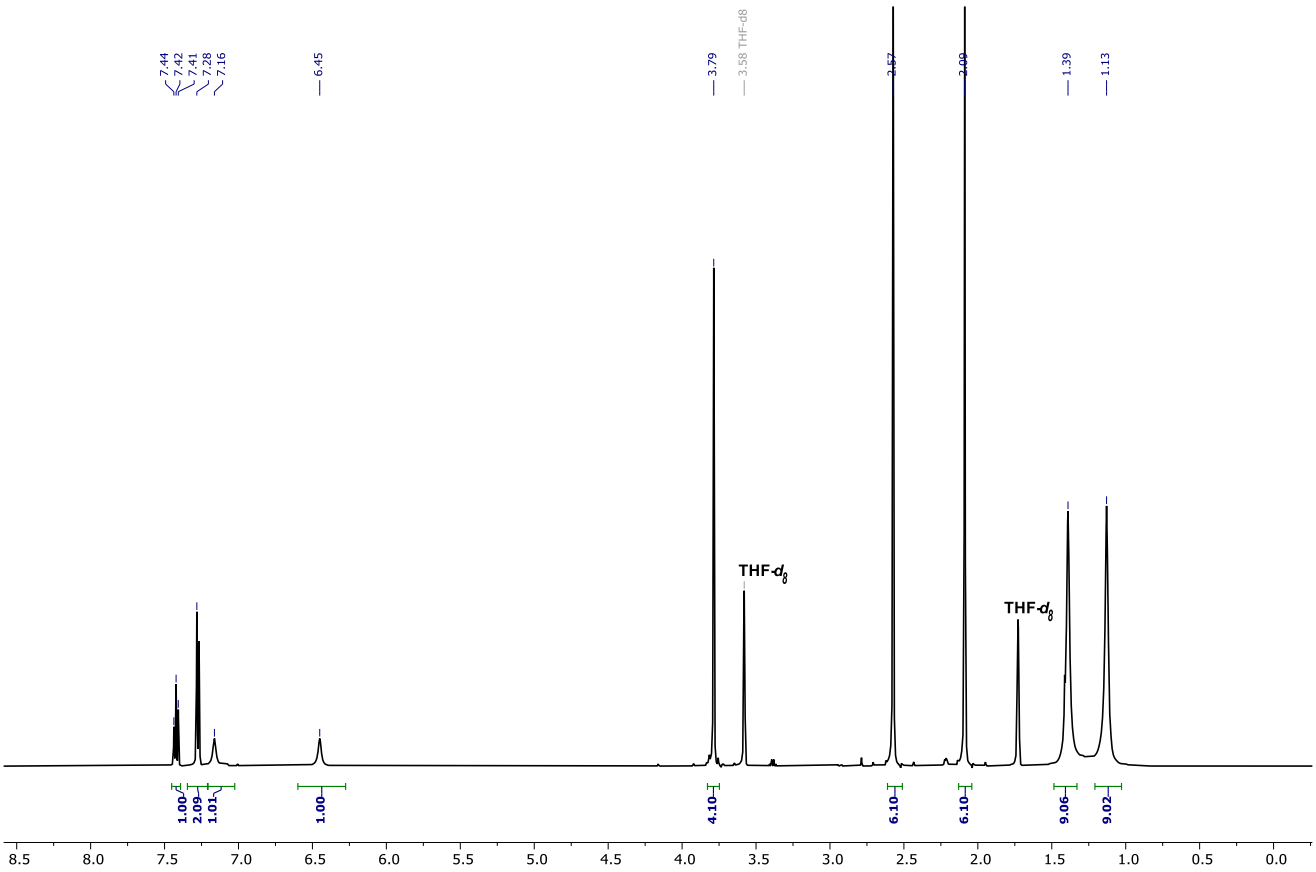

Figure S5. ^{1}H NMR spectrum (THF-d_8, 500.13 MHz, 300 K) of [{*NCN*^{Me4}}Sb(C$_6$H$_2$-^{t}Bu$_2$-3,5-O-4)] (**3**).

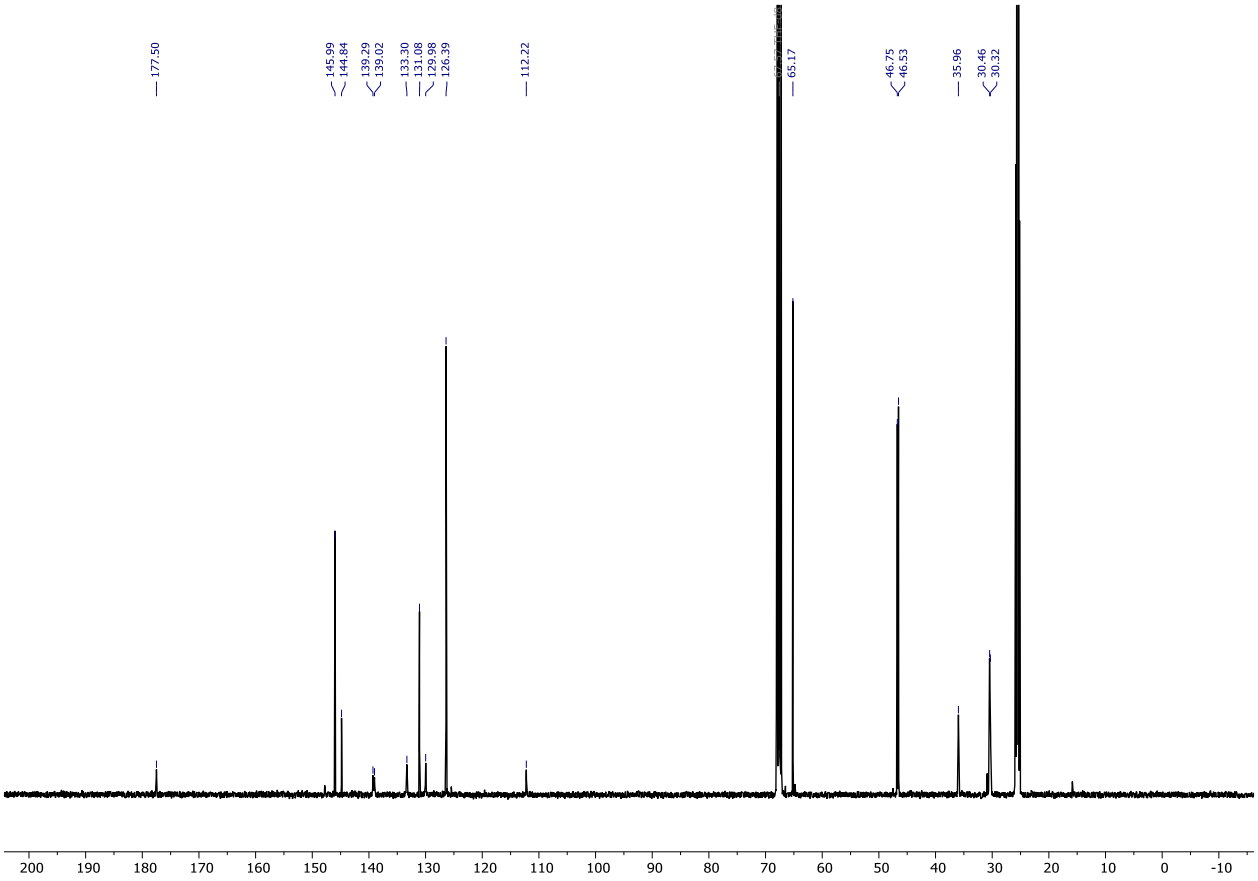

Figure S6. ^{13}C{^{1}H} NMR spectrum (THF-d_8, 125.77 MHz, 300 K) of [{*NCN*^{Me4}}Sb(C$_6$H$_2$-^{t}Bu$_2$-3,5-O-4)] (**3**).

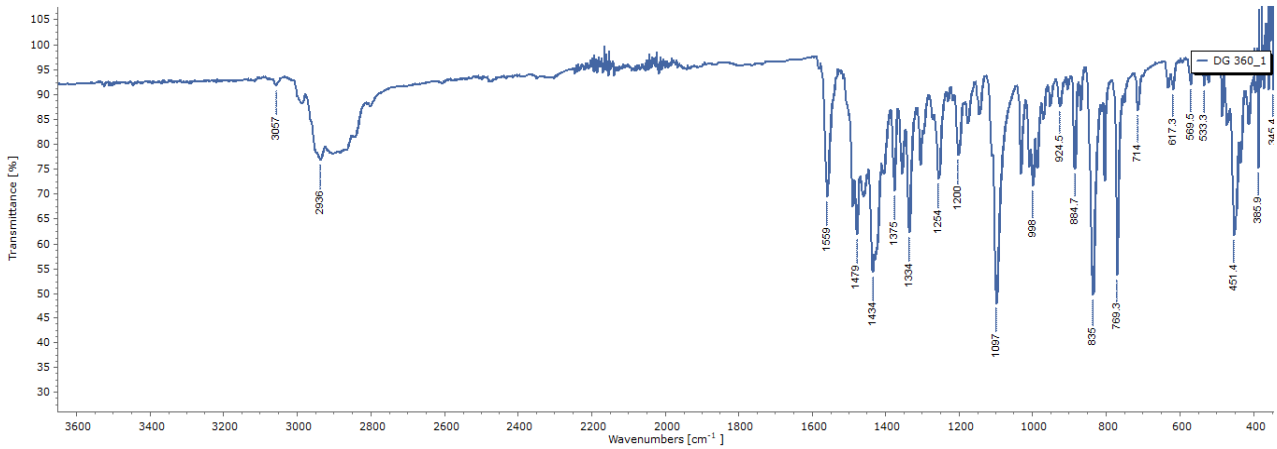

Figure S7. Infrared spectrum of [{*NCN*^{Me4}}Sb(C$_6$H$_2$-^{t}Bu$_2$-3,5-O-4)] (**3**).

Discussion of the ^{1}H NMR data for [{*NCN*^{Me4}}Sb(C$_6$H$_2$-^{t}Bu$_2$-3,5-O-4)] (3)

The ^{1}H NMR spectrum in THF-d_8 at room temperature (Fig. S5) displays two broad singlets at δ_H 1.13 and 1.39 ppm for inequivalent ^{t}Bu groups, and two others at 2.09 and 2.57 ppm (6H each) for N-C*H*$_3$ methyls. All ArC*H*$_2$-N hydrogens atoms are isochronous (resonance at 3.79 ppm), but the hydrogens in position 9 and 13 of the oxyaryl give rise to two separate singlets at 6.45 and 7.16 ppm. The dynamic nature of the system was probed by VT NMR (see below, Fig. S8-S10). Coalescence of the two ^{t}Bu resonances occurred at 338 K ($\Delta G^{\ddagger}$ = 16.0 kcal.mol^{-1}); it is accompanied by the merging of the two resonances for H$_9$ and H$_{13}$ atoms in the oxyaryl, and agree with free rotation around the Sb-C$_{oxyaryl}$ bond at high temperature.[11] Upon cooling the solution, all peaks become sharply resolved, but the resonance observed at room temperature for the Ar-C*H*$_2$-N atoms splits at 263 K into two distinct doublets (2H each) diagnostic of an AB spin system ($\Delta G^{\ddagger}$ = 14.0 kcal mol^{-1}), indicating that edge-inversion processes typical of heavy pnictogens are frozen at this temperature.[12] All thermally induced changes are reversible on return to 298 K; the two singlets for the NC*H*$_3$ hydrogens do not merge into a single one, showing that dissociation-recoordination of the side-arm does not take place.

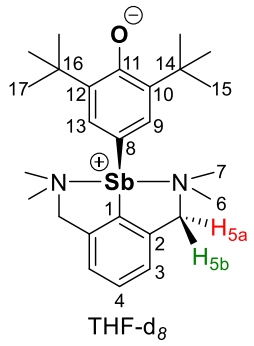

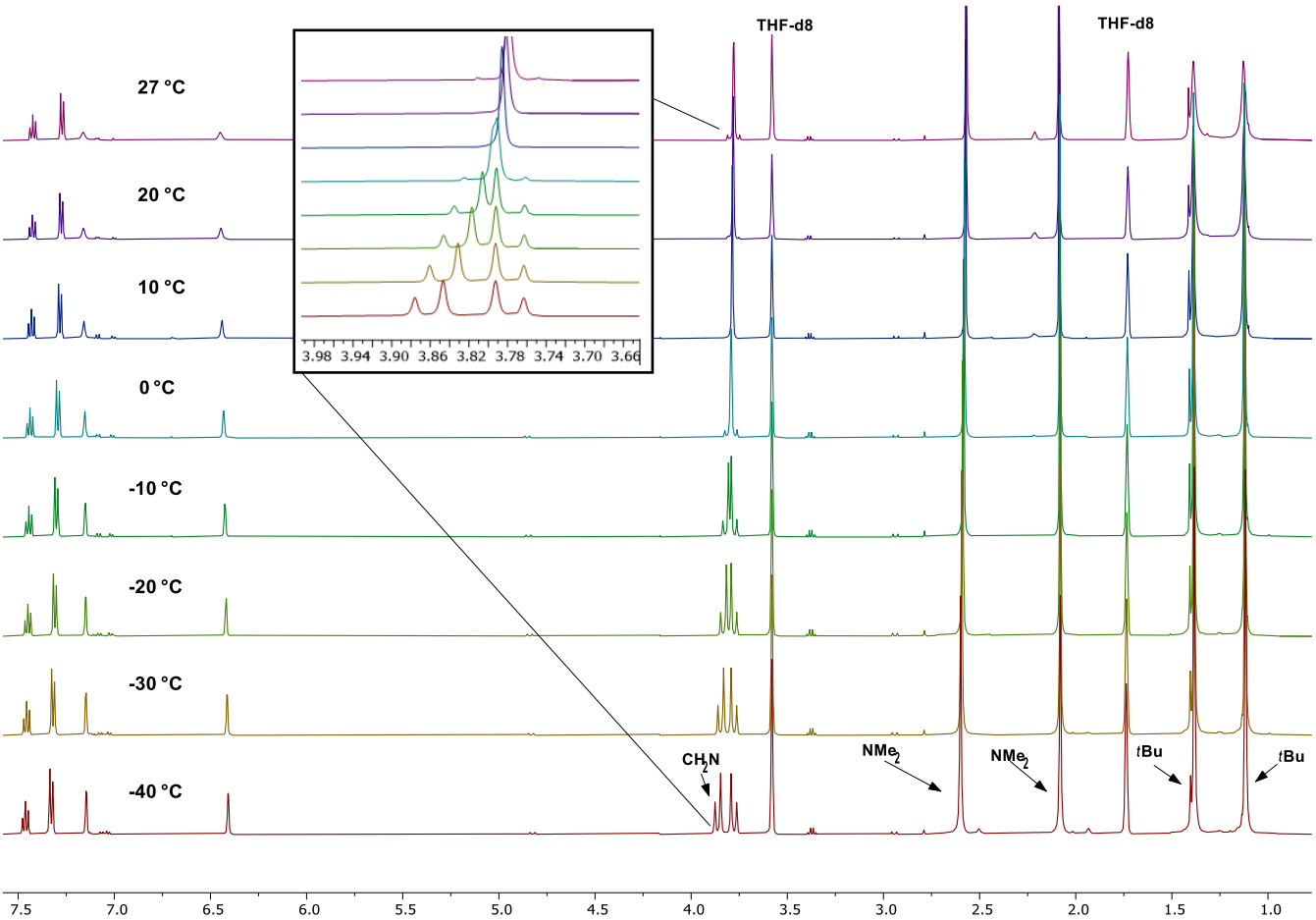

Figure S8. Variable temperature NMR studies: Stack of 1H low temperature NMR spectra (THF-d_8, 500.13 MHz, +27 to −40 °C) of [{*NCN*^{Me4}}Sb(C$_6$H$_2$-^{t}Bu$_2$-3,5-O-4)] (**3**).

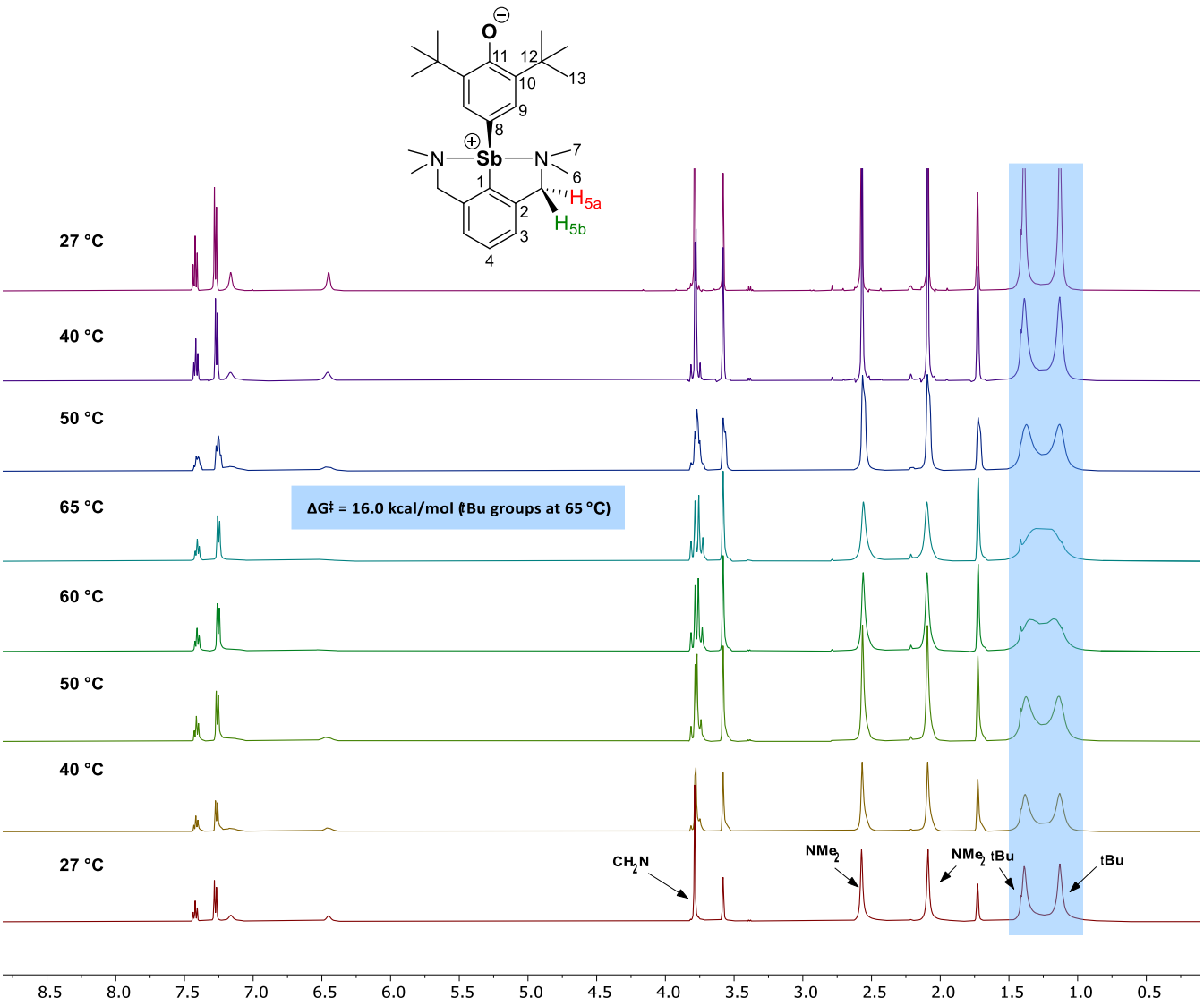

Figure S9. Variable temperature NMR studies: Stack of ^{1}H high temperature NMR spectra (THF-d_8, 500.13 MHz, +27 to +65 °C) of [{*NCN*^{Me4}}Sb(C$_6$H$_2$-^{t}Bu$_2$-3,5-O-4)] (**3**).

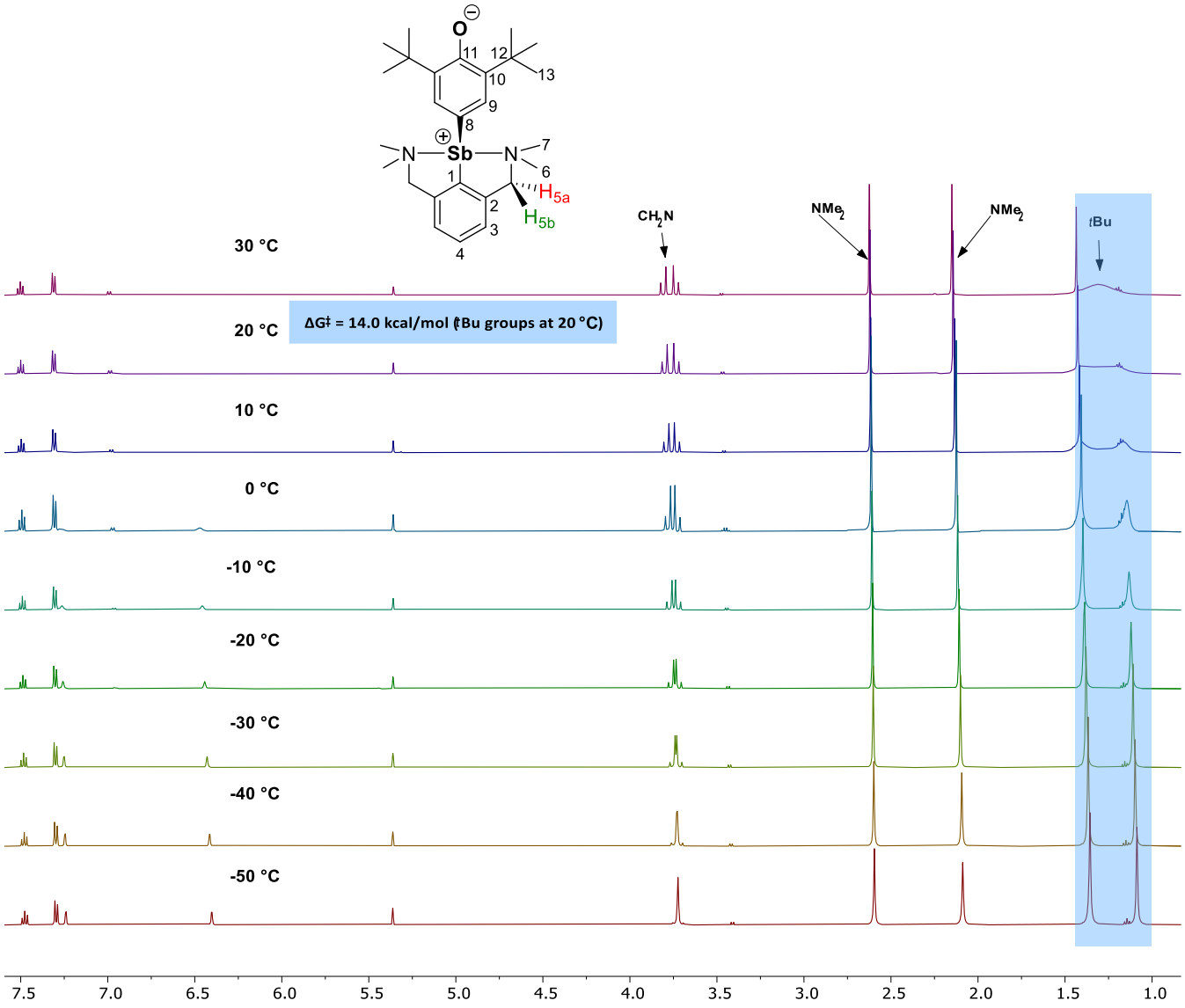

Figure S10. Variable temperature NMR studies: Stack of ^{1}H low temperature NMR spectra (CD_2Cl_2, 500.13 MHz, +30 to −50 °C) of [{*NCN*^{Me4}}Sb(C_6H_2-$^{t}Bu_2$-3,5-O-4)] (**3**).

A solution of [{*NCN*^{Me4}}Sb(C_6H_2-^{t}Bu$_2$-3,5-O-4)] (**3**) in THF-d_8 (0.4 mL) was prepared in a J-Young NMR tube under inert atmosphere. The ^{1}H NMR spectrum in THF-d_8 was recorded a first time at 300 K. In the glove-box, the same solution was transferred into a Quartz EPR Capillary, and the EPR spectrum was then recorded, showing the absence of Sb-centred signal. In a glove-box, the THF-d_8 solution was transferred back into a J-Young NMR tube, and the ^{1}H NMR spectrum was recorded a second time at 300 K, showing that the sample had remained intacted within the detection limit.

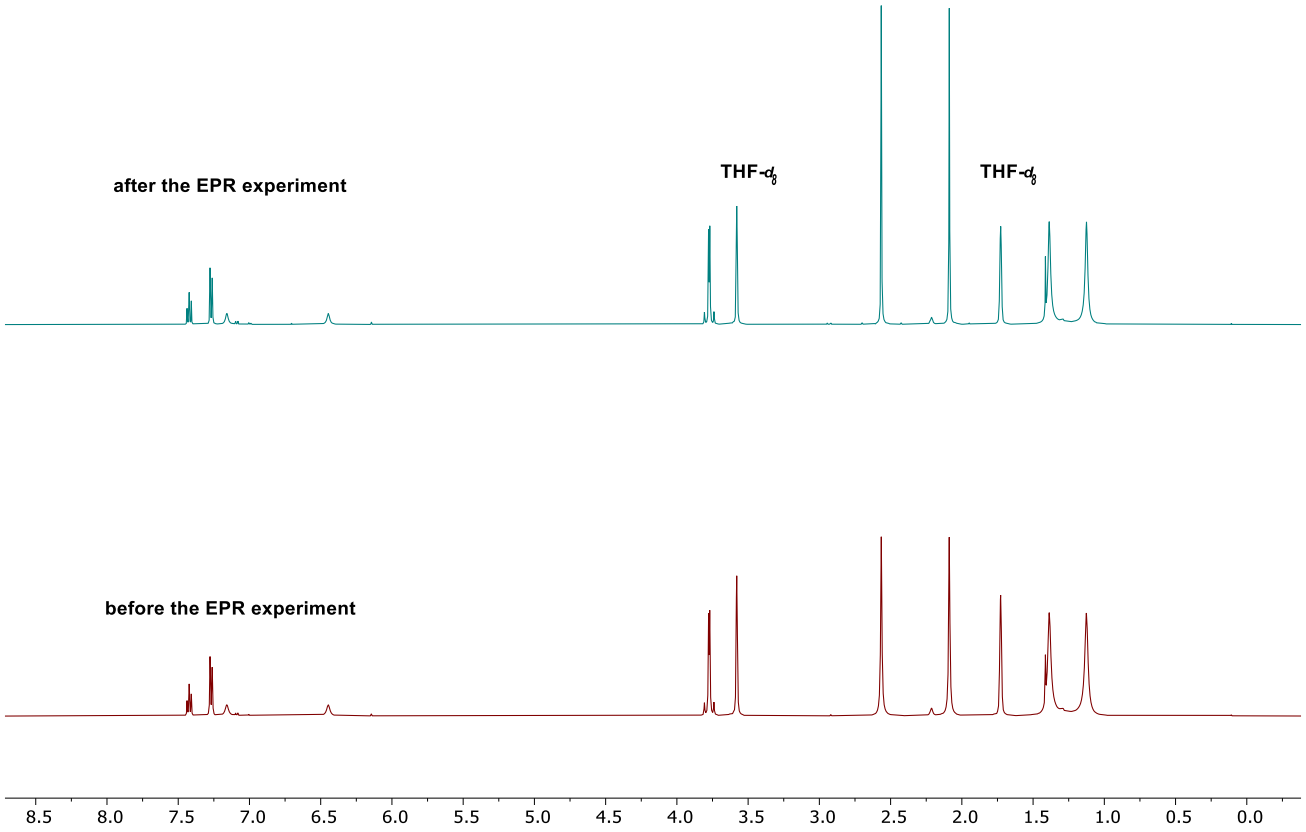

Figure S11. Sequential NMR-EPR-NMR spectroscopic analysis of [{*NCN*^{Me4}}Sb(C_6H_2-^{t}Bu$_2$-3,5-O-4)] (**3**): Stacked ^{1}H NMR spectra (THF-d_8, 400.13 MHz, 300 K) before (bottom) and after (top) the EPR experiment. The complex remained intact throughout the whole sequence within the limits of the detection method. See Fig. S12 for the corresponding EPR spectrum.

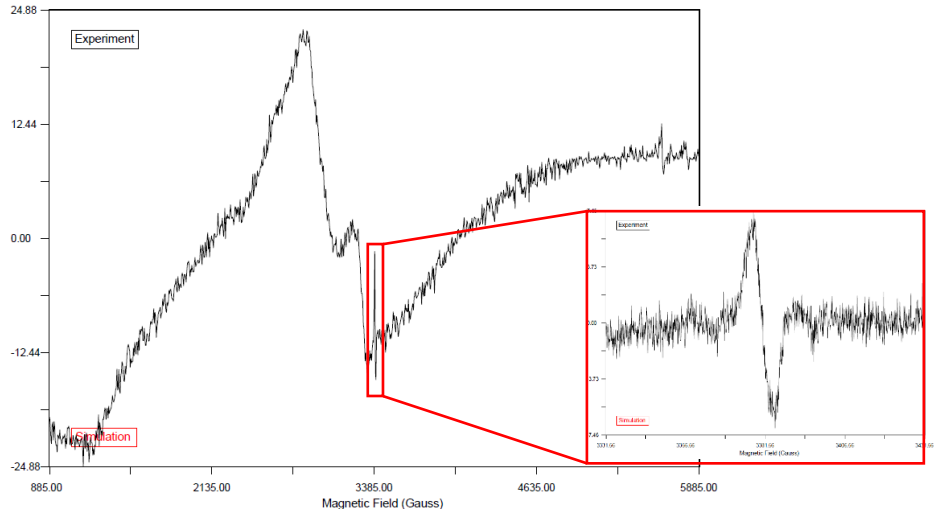

Figure S12. Sequential NMR-EPR-NMR spectroscopic analysis of [{*NCN*^{Me4}}Sb(C_6H_2-^{t}Bu$_2$-3,5-O-4)] (**3**)EPR spectrum of [{*NCN*^{Me4}}Sb(C_6H_2-^{t}Bu$_2$-3,5-O-4)] **3** in THF-d_8 solution at 300 K, showing the presence of a sole, weak resonance assigned to an organic molecule coming from minor decomposition of the complex. See Fig. S11 for the corresponding NMR spectra.

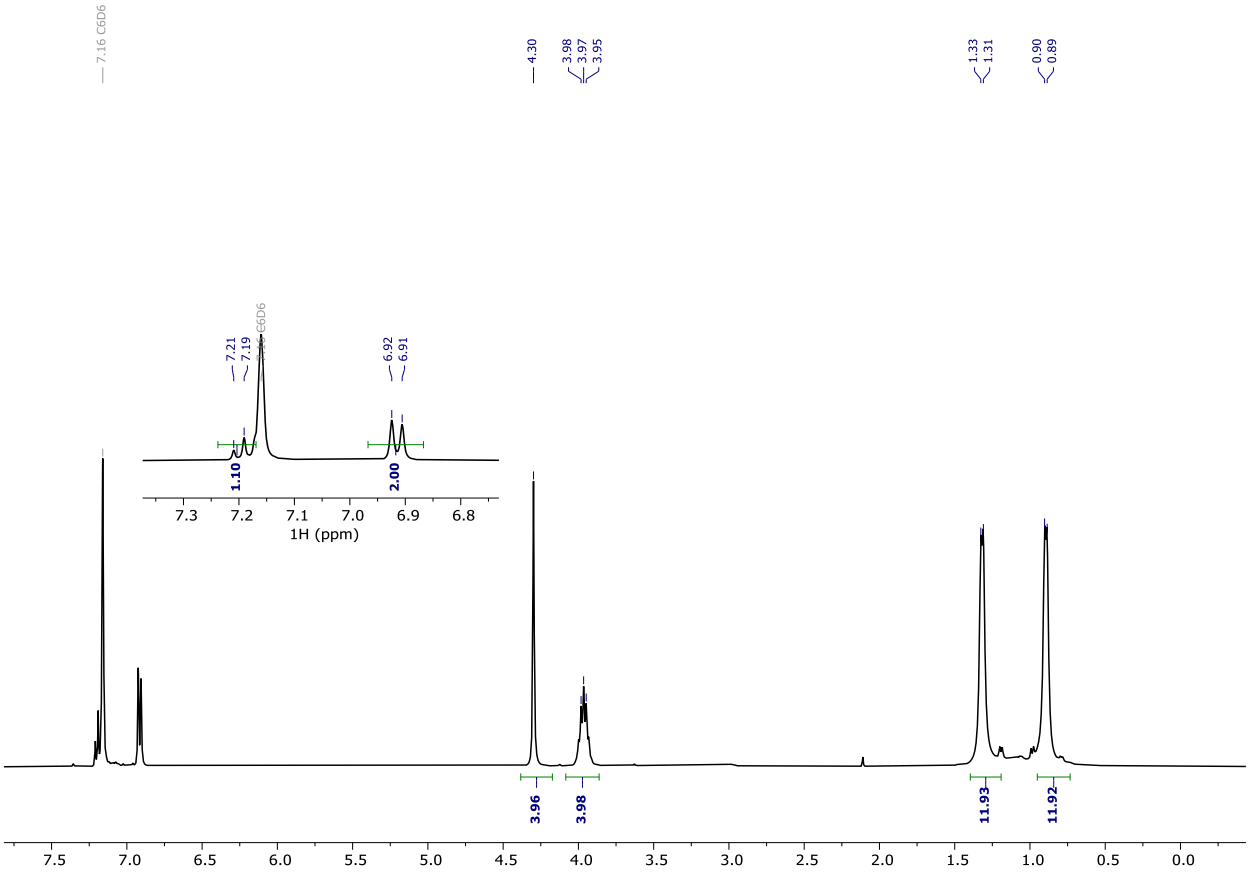

Figure S13. ^{1}H NMR spectrum (C_6D_6, 400.13 MHz, 300 K) of [{*NCN*^{iPr4}}$SbCl_2$].

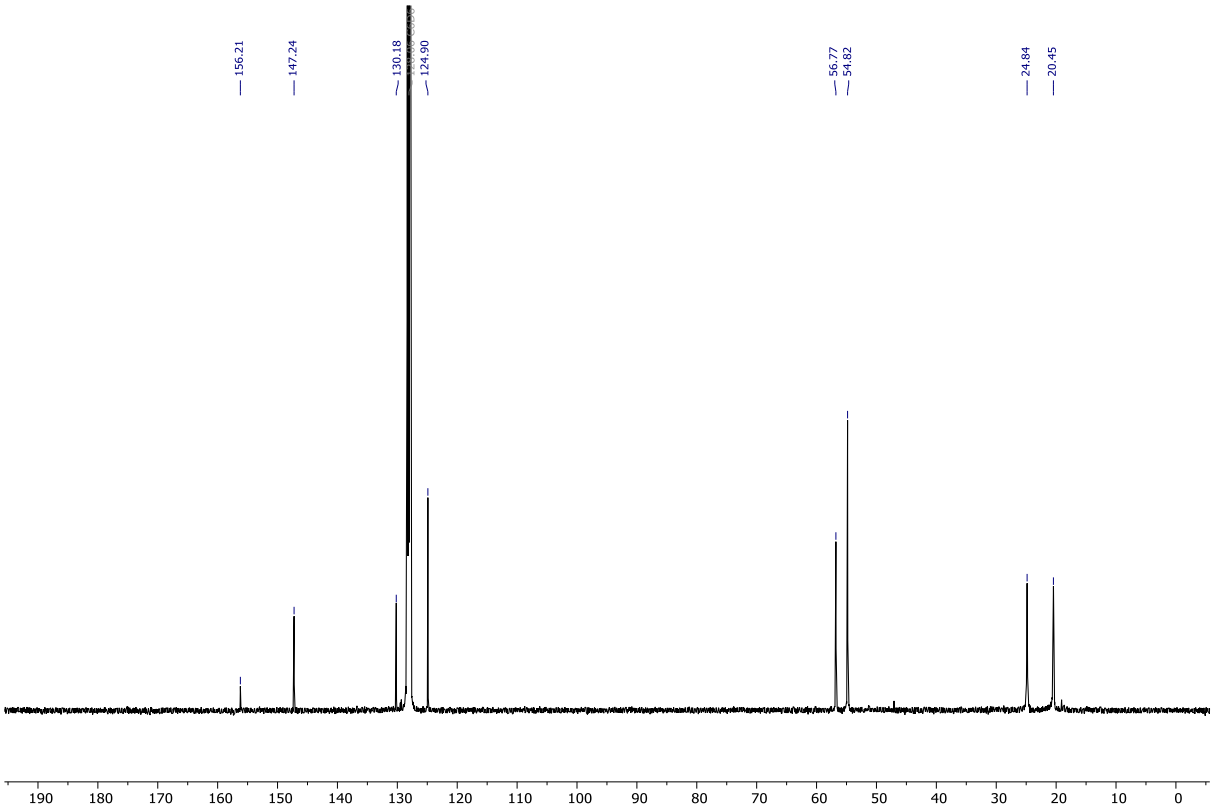

Figure S14. $^{13}C\{^{1}H\}$ NMR spectrum (C_6D_6, 100.62 MHz, 300 K) of [{*NCN*^{iPr4}}$SbCl_2$].

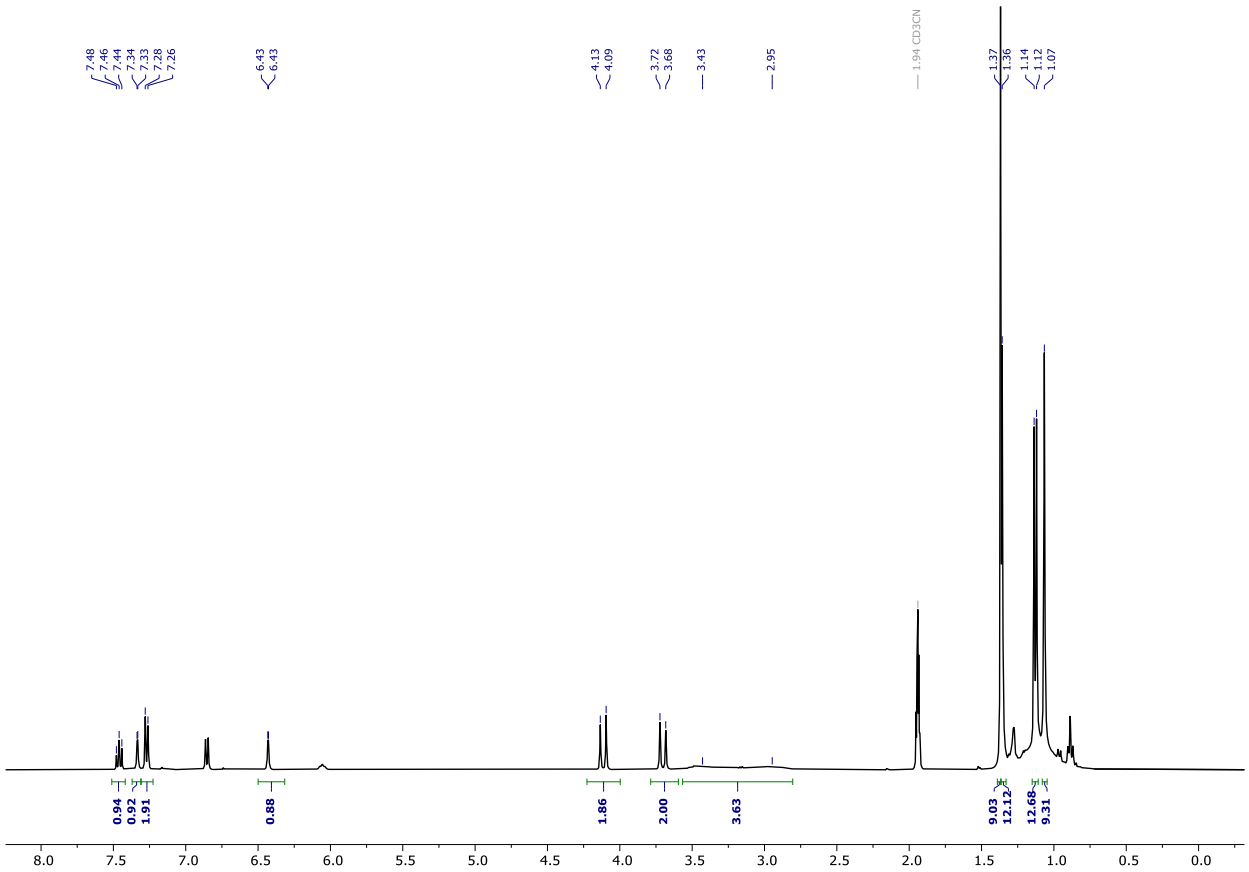

Figure S15. ^{1}H NMR spectrum (CD_3CN, 400.13 MHz, 300 K) of [{*NCN*^{iPr4}}Sb(C_6H_2-$^{t}Bu_2$-3,5-O-4)] (**4**).

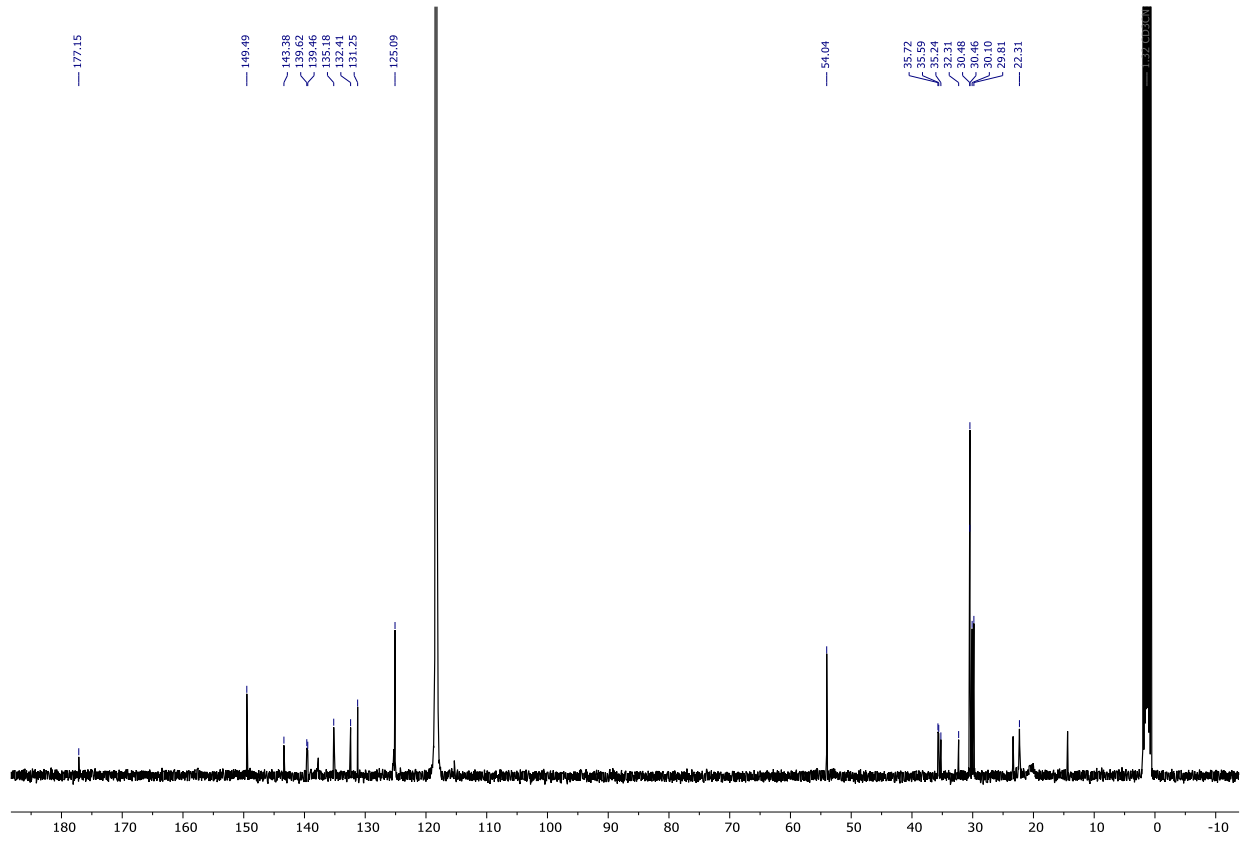

Figure S16. $^{13}C\{^{1}H\}$ NMR spectrum (CD_3CN, 100.62 MHz, 300 K) of [{*NCN*^{iPr4}}Sb(C_6H_2-$^{t}Bu_2$-3,5-O-4)] (**4**).

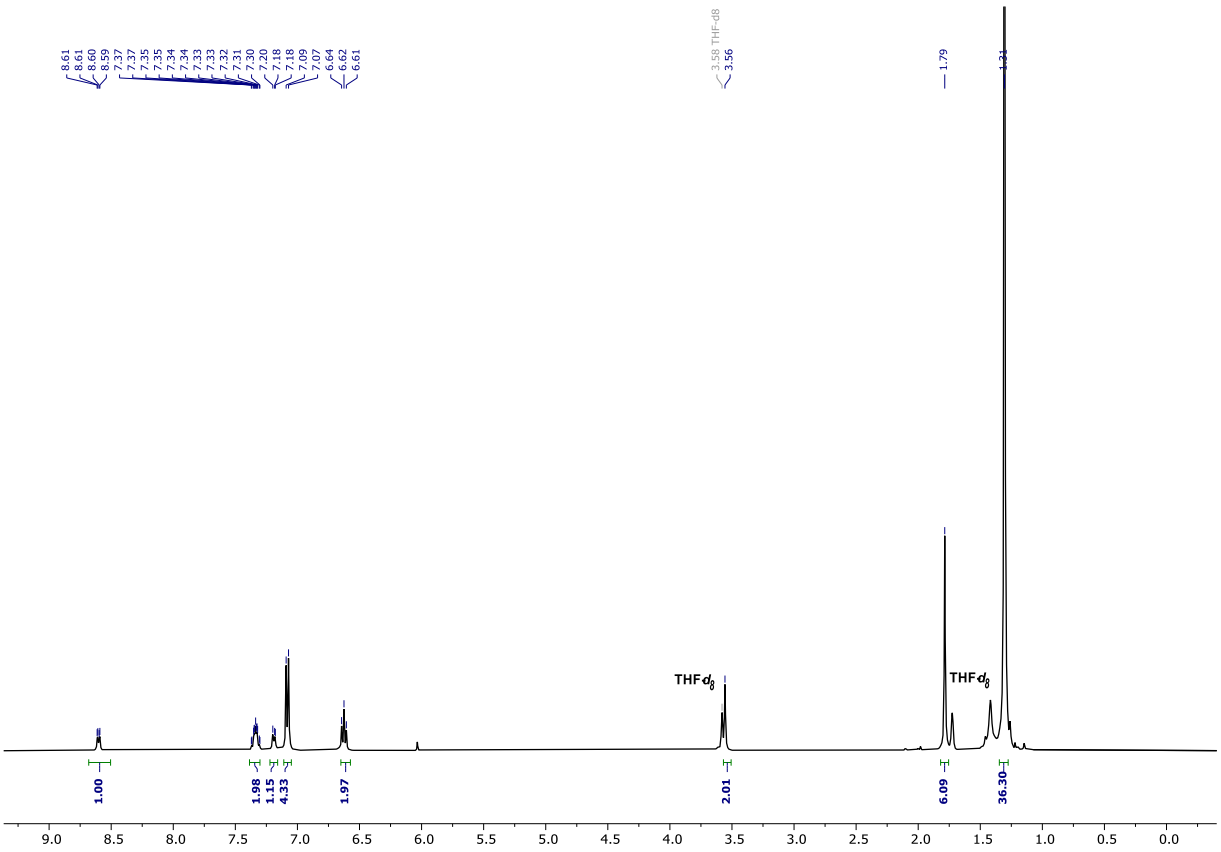

Figure S17. ^{1}H NMR spectrum (THF-d_8, 400.13 MHz, 300 K) of [{CN^{Me2}}Sb(OC$_6$H$_3$-^{t}Bu$_2$-2,6)$_2$] (**5**).

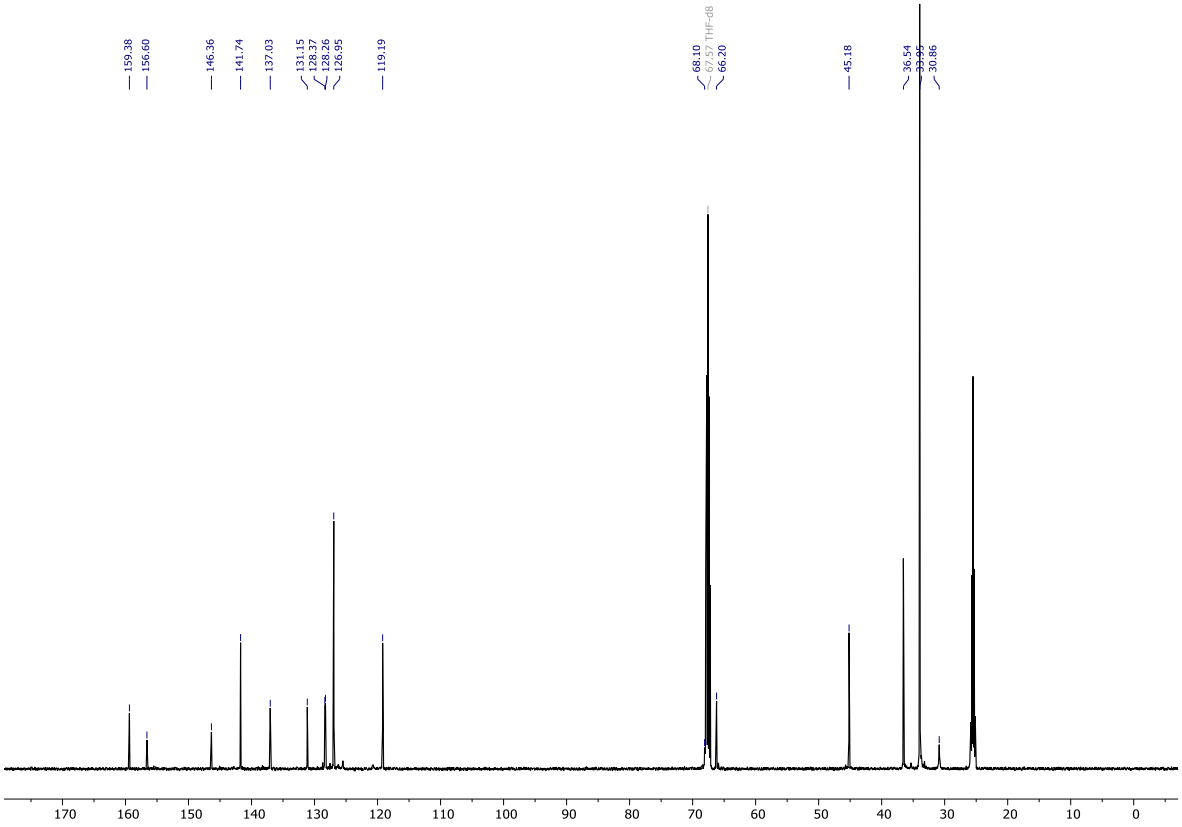

Figure S18. ^{13}C{^{1}H} NMR spectrum (THF-d_8, 100.62 MHz, 300 K) of [{CN^{Me2}}Sb(OC$_6$H$_3$-^{t}Bu$_2$-2,6)$_2$] (**5**).

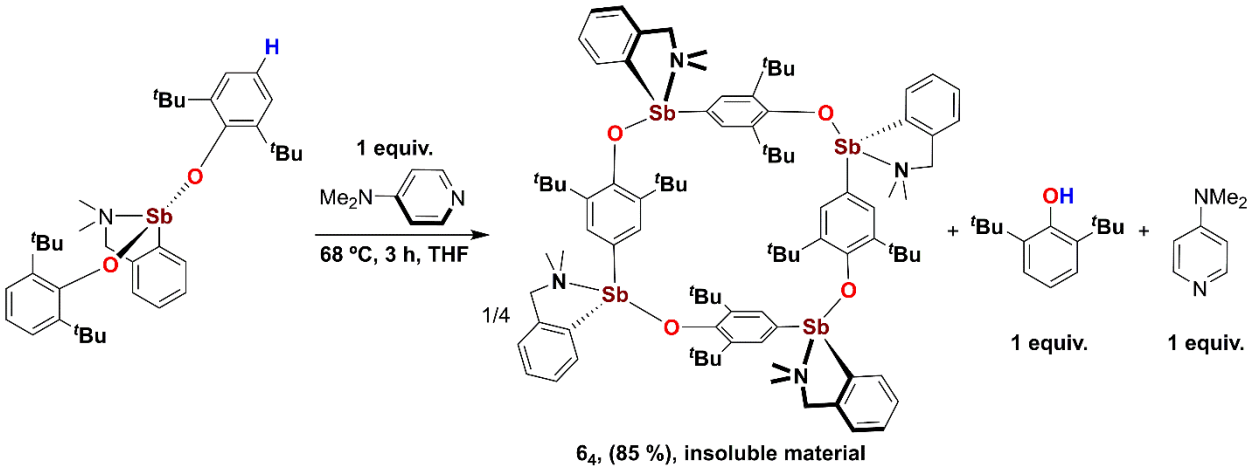

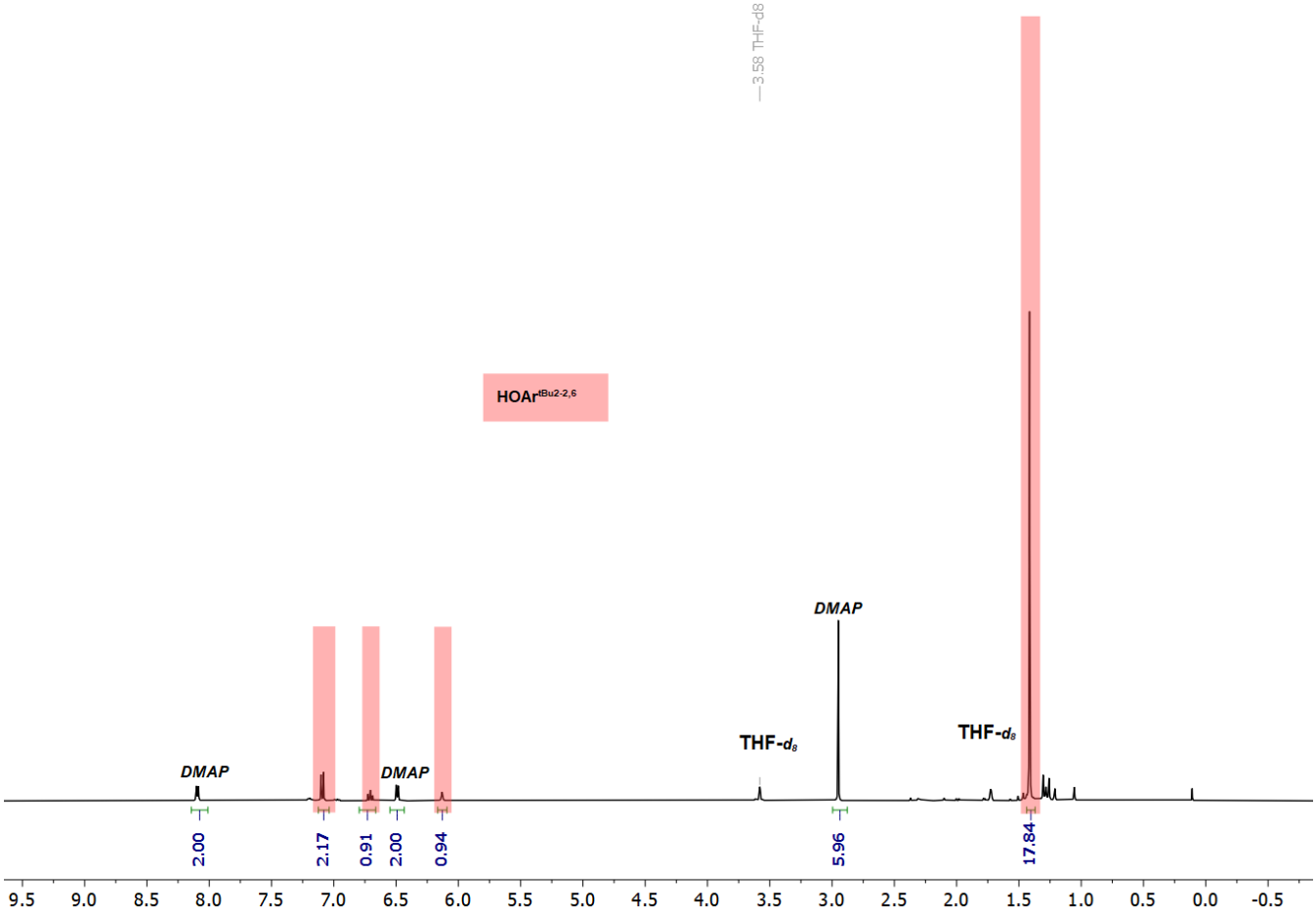

Figure S19. ^{1}H NMR spectrum (THF-d_8, 400.13 MHz, 300 K) of the *in situ* equimolar reaction of [{*CN*^{Me2}}Sb(OC$_6$H$_3$-^{t}Bu$_2$-2,6)$_2$] (**5**) with *N,N*-dimethylaminopyridine (DMAP).

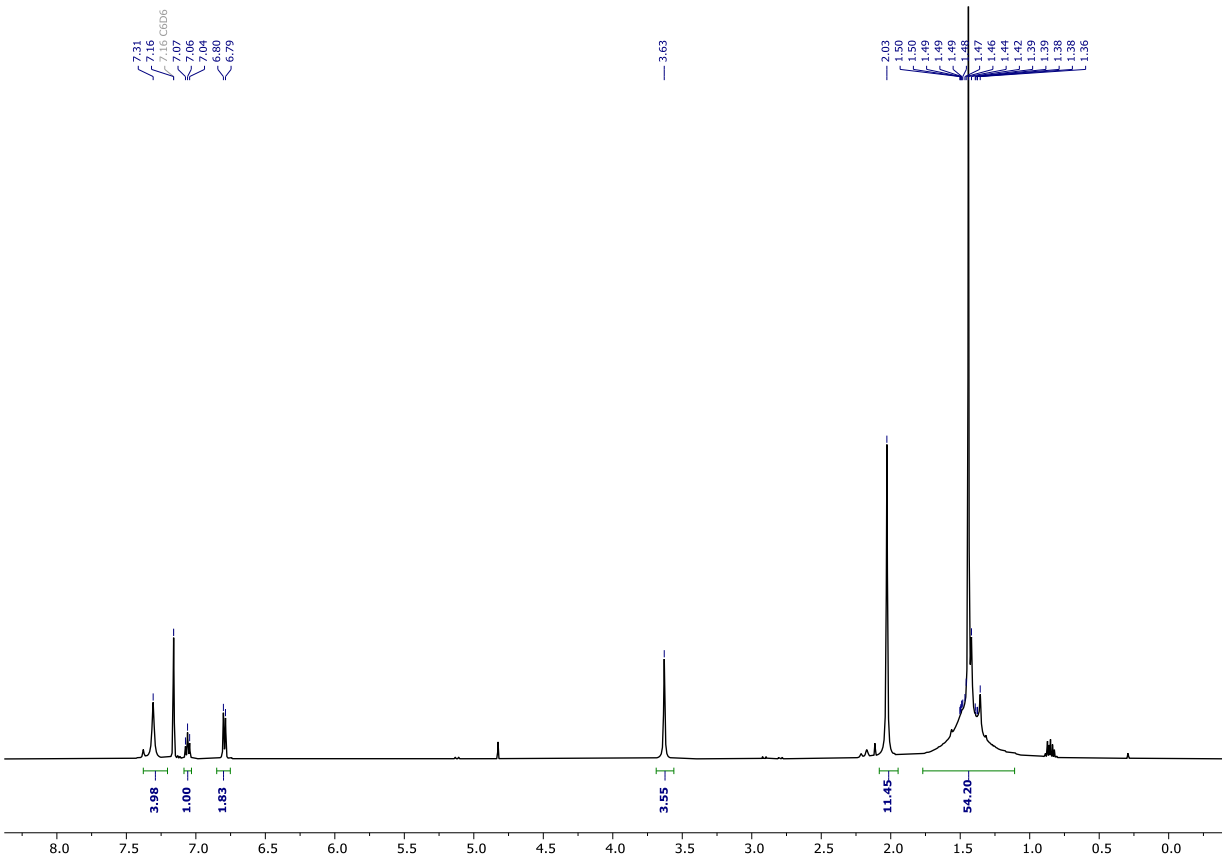

Figure S20. ^{1}H NMR spectrum (C_6D_6, 500.13 MHz, 300 K) of [{*NCN*^{Me4}}Sb(OC_6H_2-$^{t}Bu_3$-2,4,6)$_2$] (**7**).

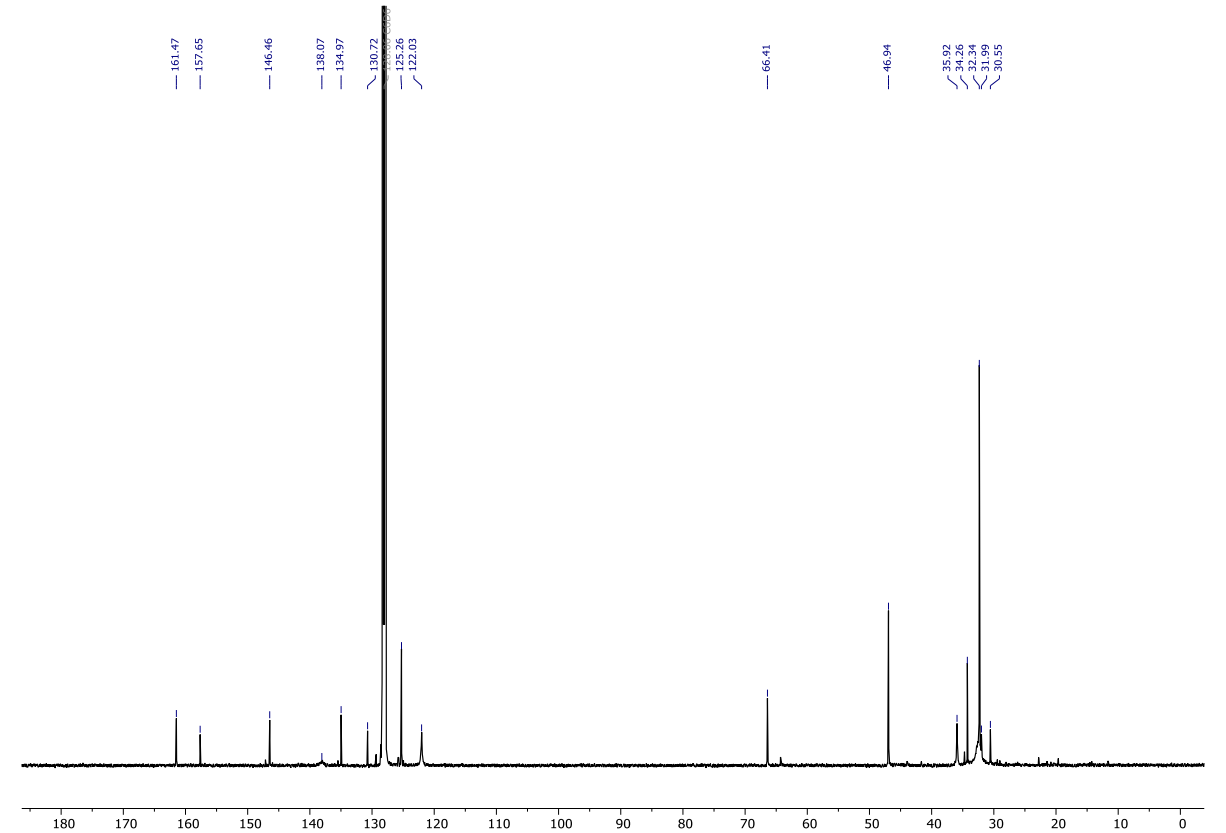

Figure S21. $^{13}C\{^{1}H\}$ NMR spectrum (C_6D_6, 125.13 MHz, 300 K) of [{*NCN*^{Me4}}Sb(OC_6H_2-$^{t}Bu_3$-2,4,6)$_2$] (**7**).

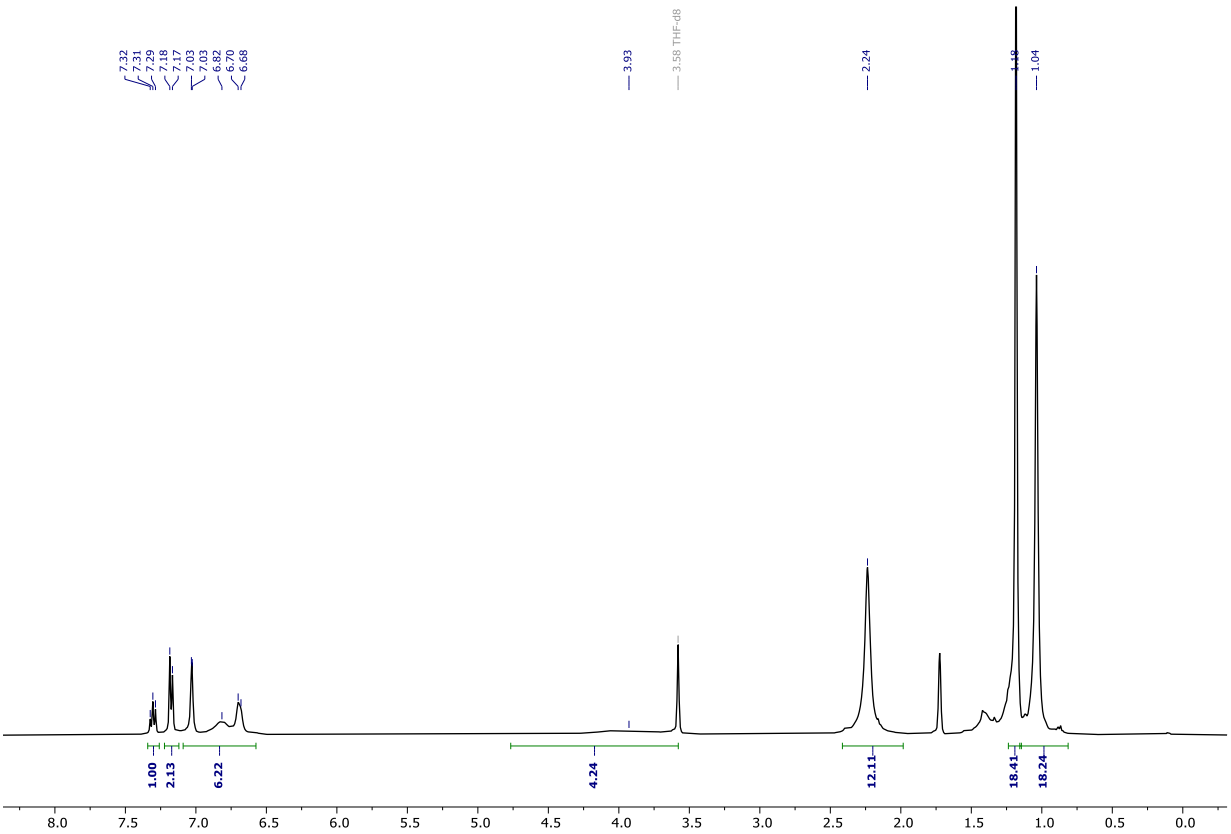

Figure S22. ^{1}H NMR spectrum (THF-d_8, 500.13 MHz, 300 K) of *in-situ* generated [{*NCN*^{Me4}}Sb(OC$_6$H$_2$-^{t}Bu$_2$-2,4)$_2$] (**8**).

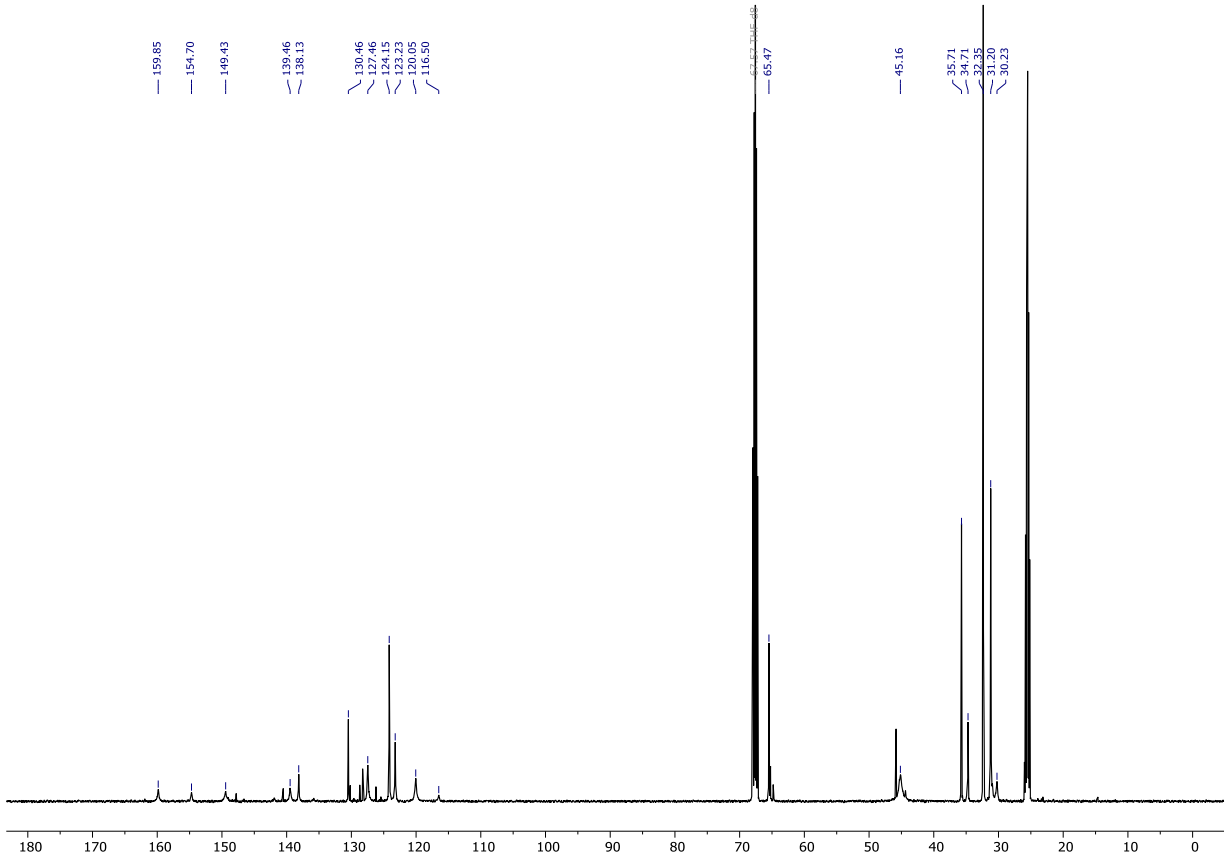

Figure S23. ^{13}C{^{1}H} NMR spectrum (THF-d_8, 125.13 MHz, 300 K) of *in-situ* generated [{*NCN*^{Me4}}Sb(OC$_6$H$_2$-^{t}Bu$_2$-2,4)$_2$] (**8**).

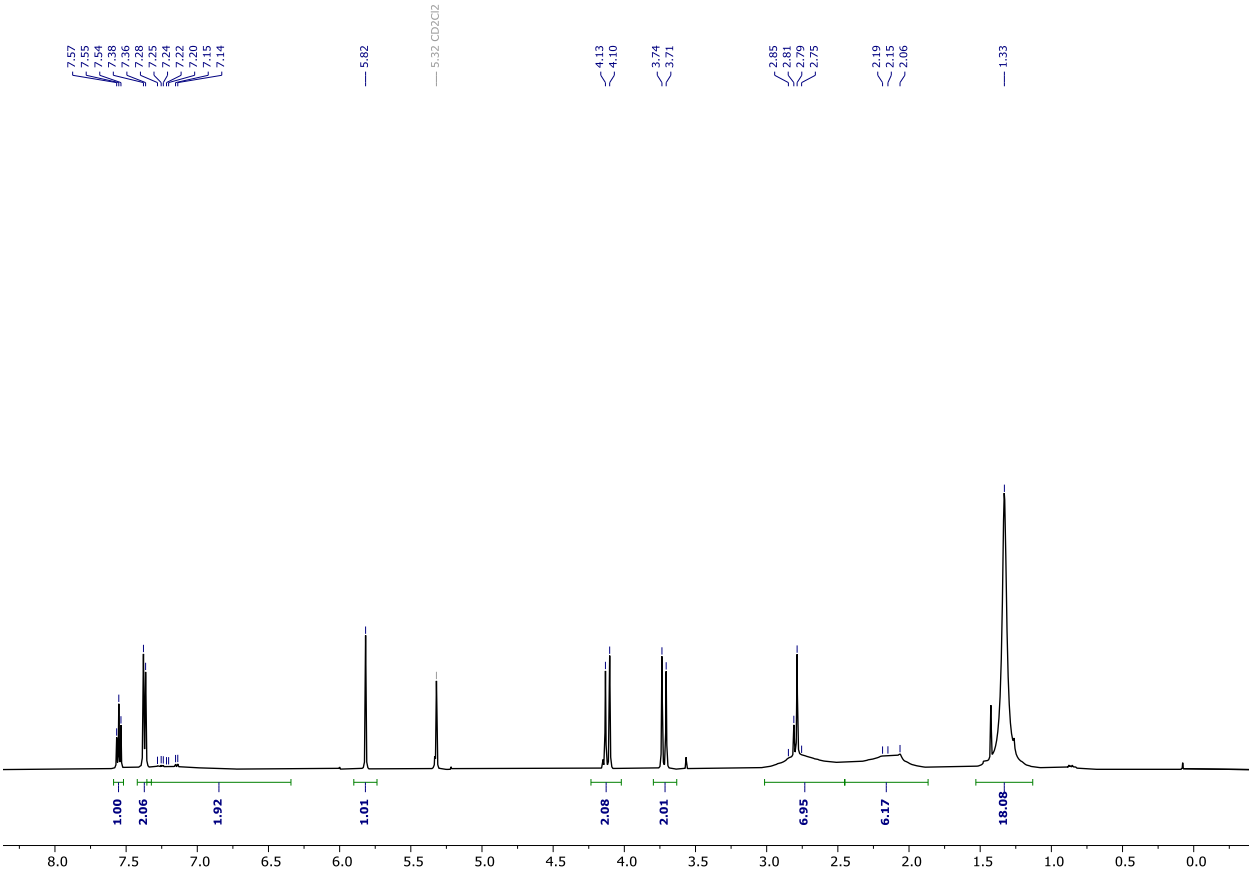

Figure S24. ^{1}H NMR spectrum (CD_2Cl_2, 500.13 MHz, 300 K) of [{*NCN*^{Me4}}Sb(C_6H_2-$^{t}Bu_2$-3,5-OH-4)][Cl] (**12**).

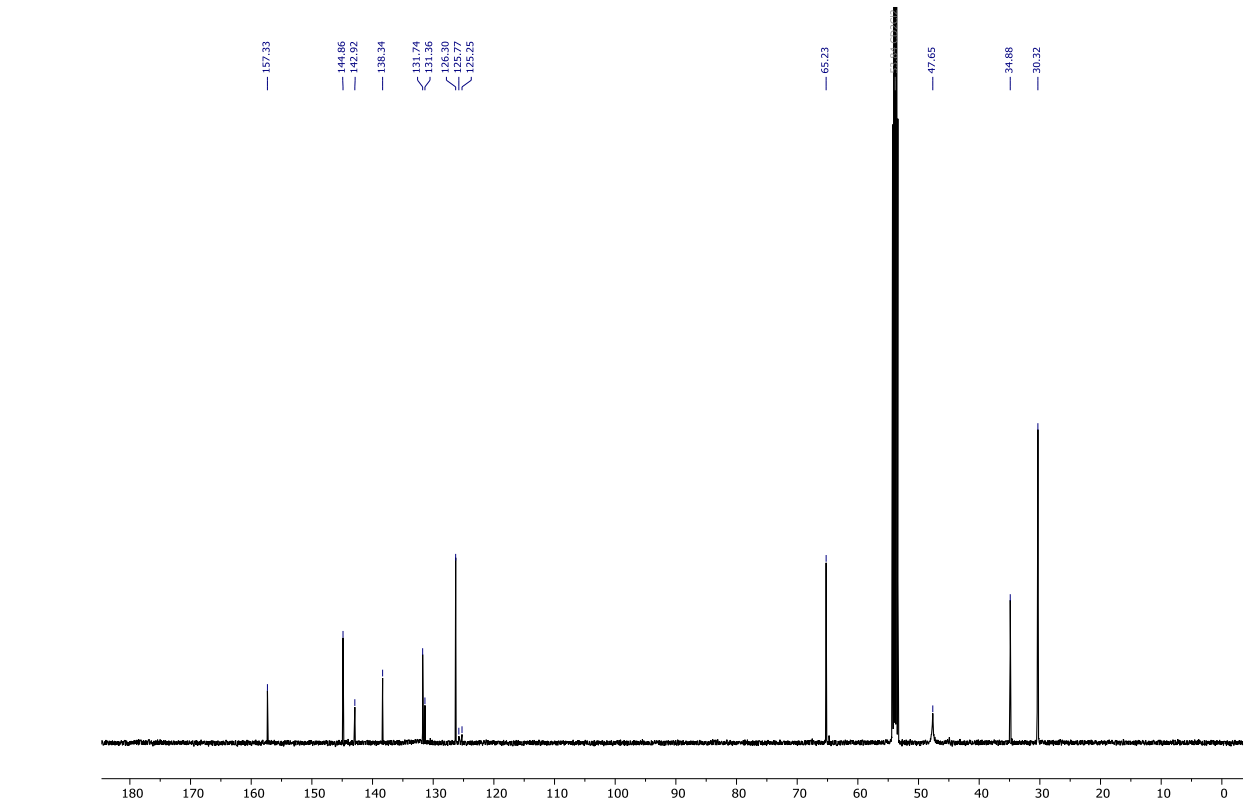

Figure S25. $^{13}C\{^{1}H\}$ NMR spectrum (CD_2Cl_2, 125.13 MHz, 300 K) of [{*NCN*^{Me4}}Sb(C_6H_2-$^{t}Bu_2$-3,5-OH-4)][Cl] (**12**).

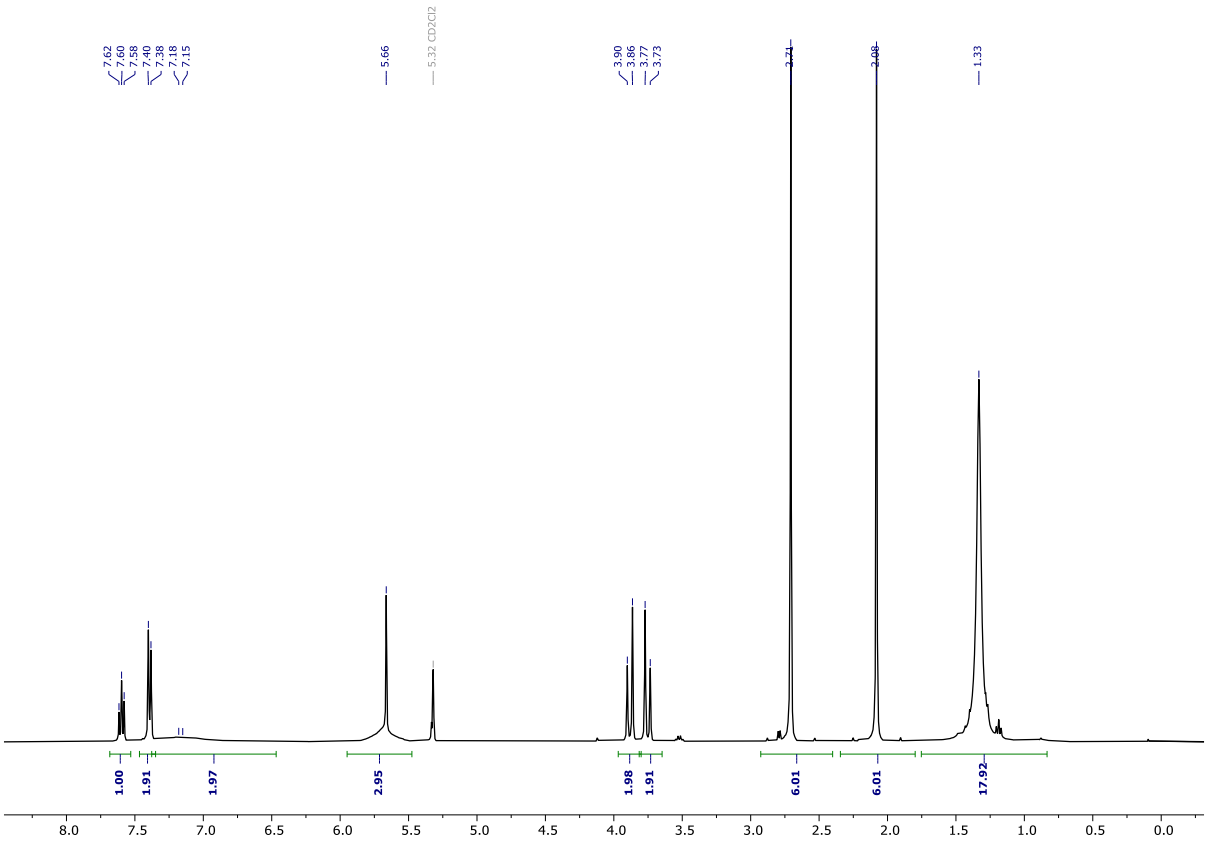

Figure S26. ^{1}H NMR spectrum (CD_2Cl_2, 500.13 MHz, 300 K) of [{*NCN*^{Me4}}Sb(C_6H_2-tBu_2-3,5-OH-4)]$^{+}$[H_2N{$B(C_6F_5)_3$}$_2$]$^{-}$ (**12'**).

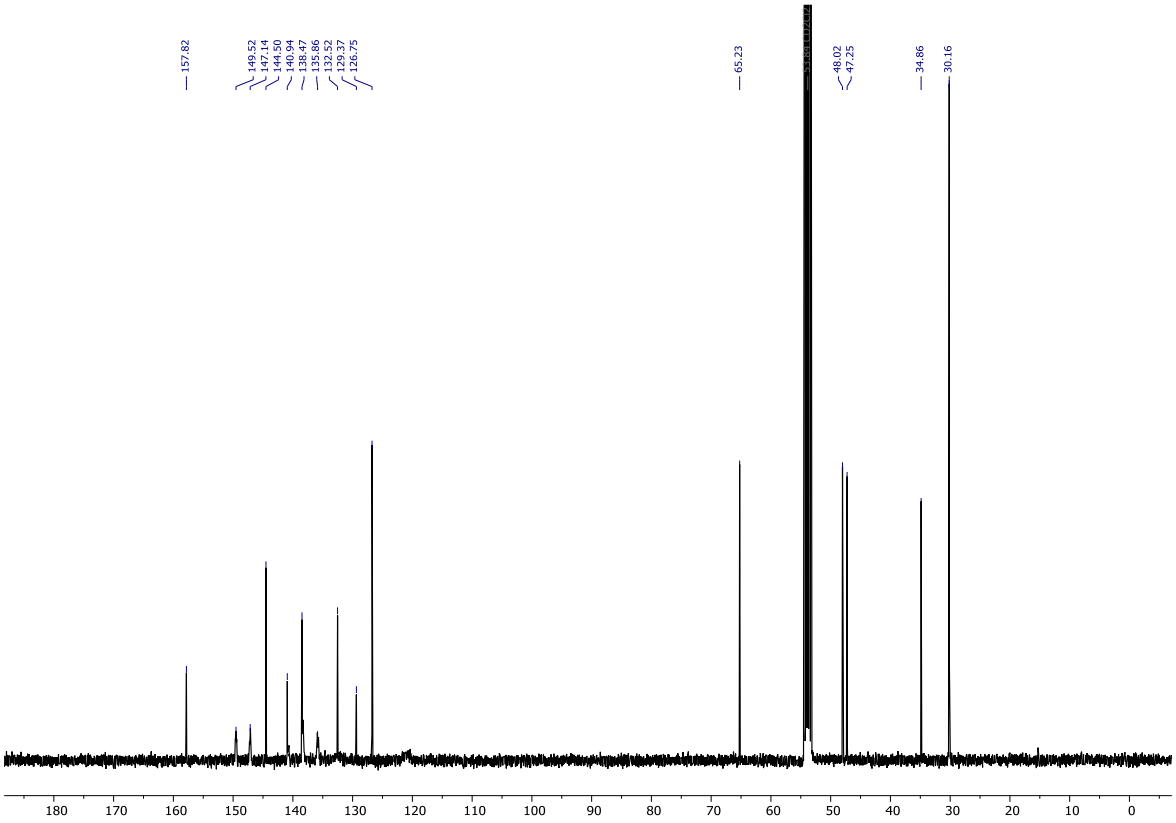

Figure S27. $^{13}C\{^{1}H\}$ NMR spectrum (CD_2Cl_2, 125.13 MHz, 300 K) of [{*NCN*^{Me4}}Sb(C_6H_2-tBu_2-3,5-OH-4)]$^{+}$[H_2N{$B(C_6F_5)_3$}$_2$]$^{-}$ (**12'**).

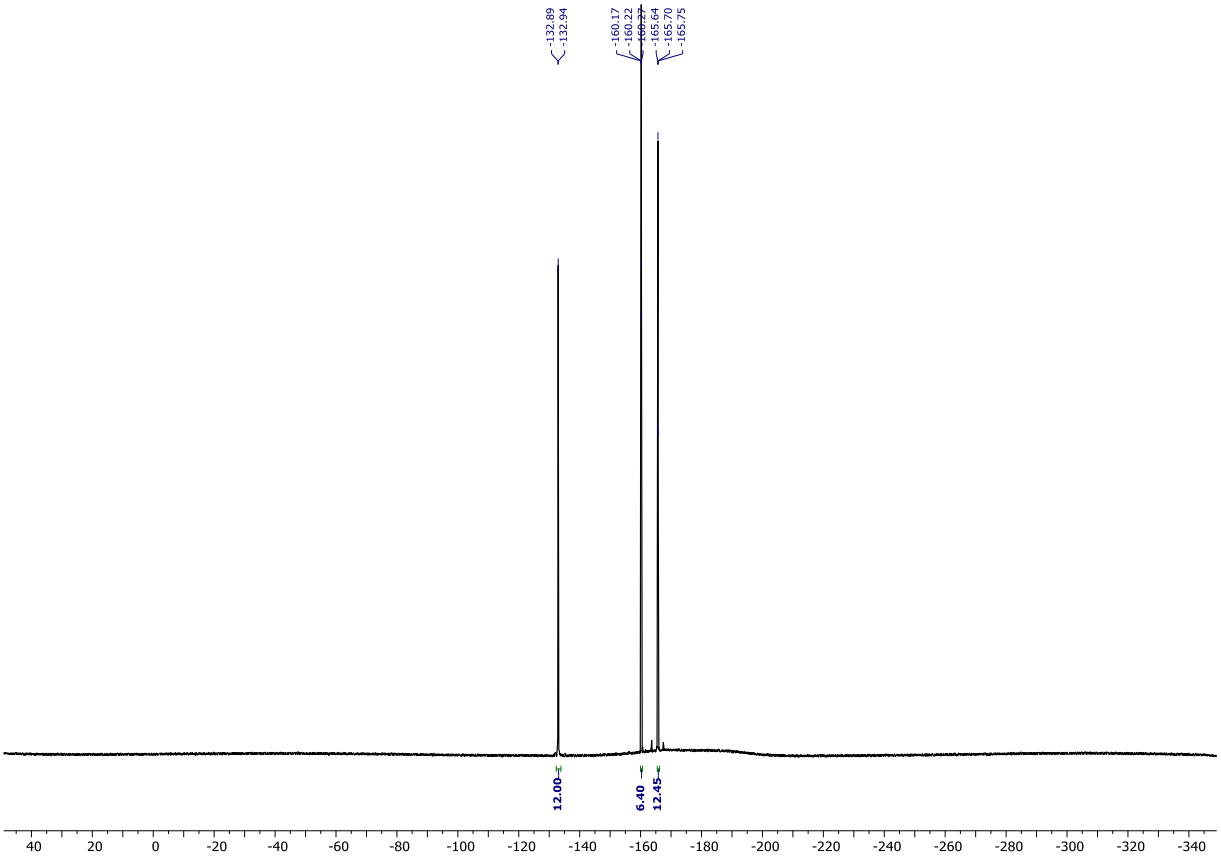

Figure S28. $^{19}F\{^{1}H\}$ NMR spectrum (CD_2Cl_2, 188.29 MHz, 300 K) of [{*NCN*^{Me4}}Sb(C_6H_2-tBu_2-3,5-OH-4)]$^+$[$H_2N\{B(C_6F_5)_3\}_2]^-$ (**12'**).

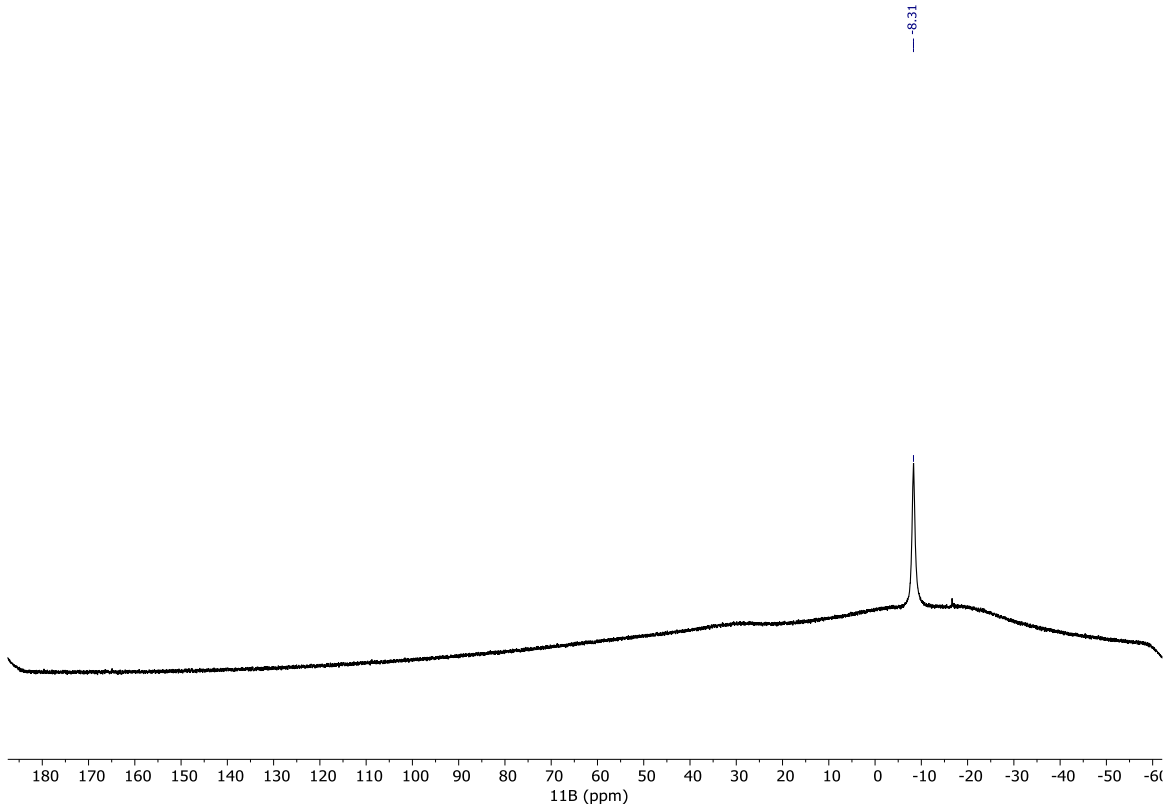

Figure S29. ^{11}B NMR spectrum (CD_2Cl_2, 96.29 MHz, 300 K) of [{*NCN*^{Me4}}Sb(C_6H_2-tBu_2-3,5-OH-4)]$^+$[$H_2N\{B(C_6F_5)_3\}_2]^-$ (**12'**).

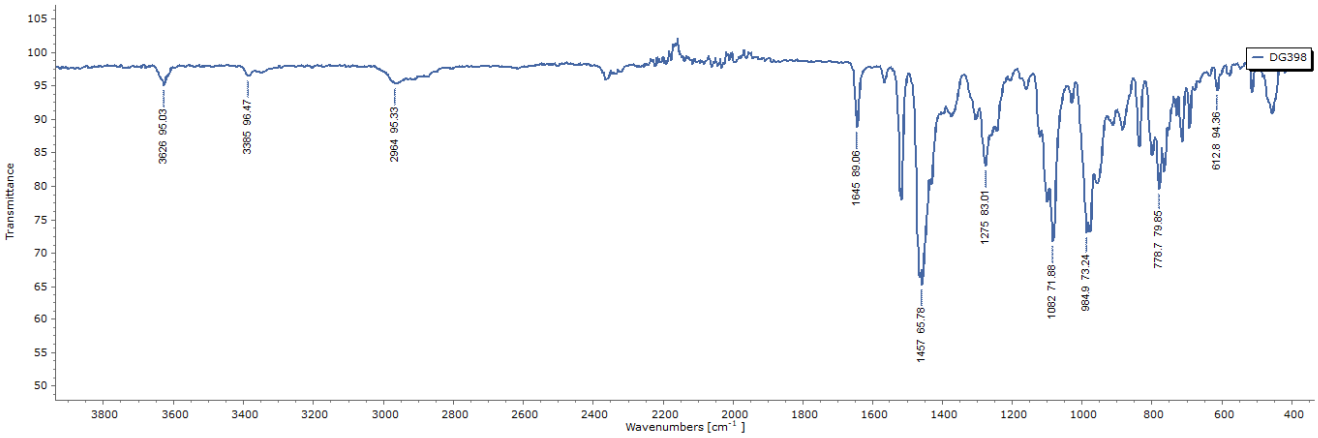

Figure S30. Infrared spectrum (Nujol mull) of [{*NCN*^{Me4}}Sb(C_6H_2-tBu_2-3,5-OH-4)]$^+$[H_2N{$B(C_6F_5)_3$}$_2$]$^-$ (**12'**).

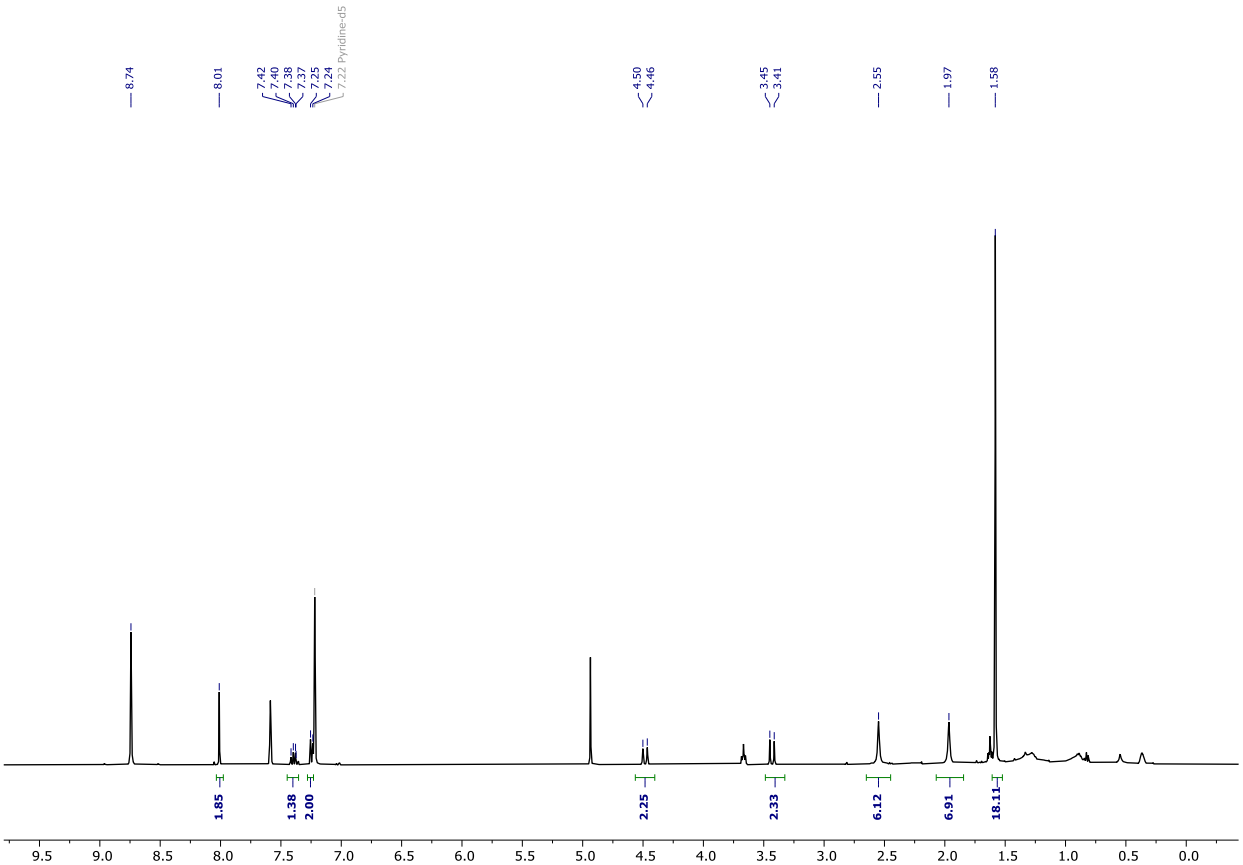

Figure S31. ^{1}H NMR spectrum (pyridine-d_5, 500.13 MHz, 300 K) of [{*NCN*^{Me4}}Sb(S_2C-C_6H_2-^{t}Bu_2-3,5-O-4)] (**13**).

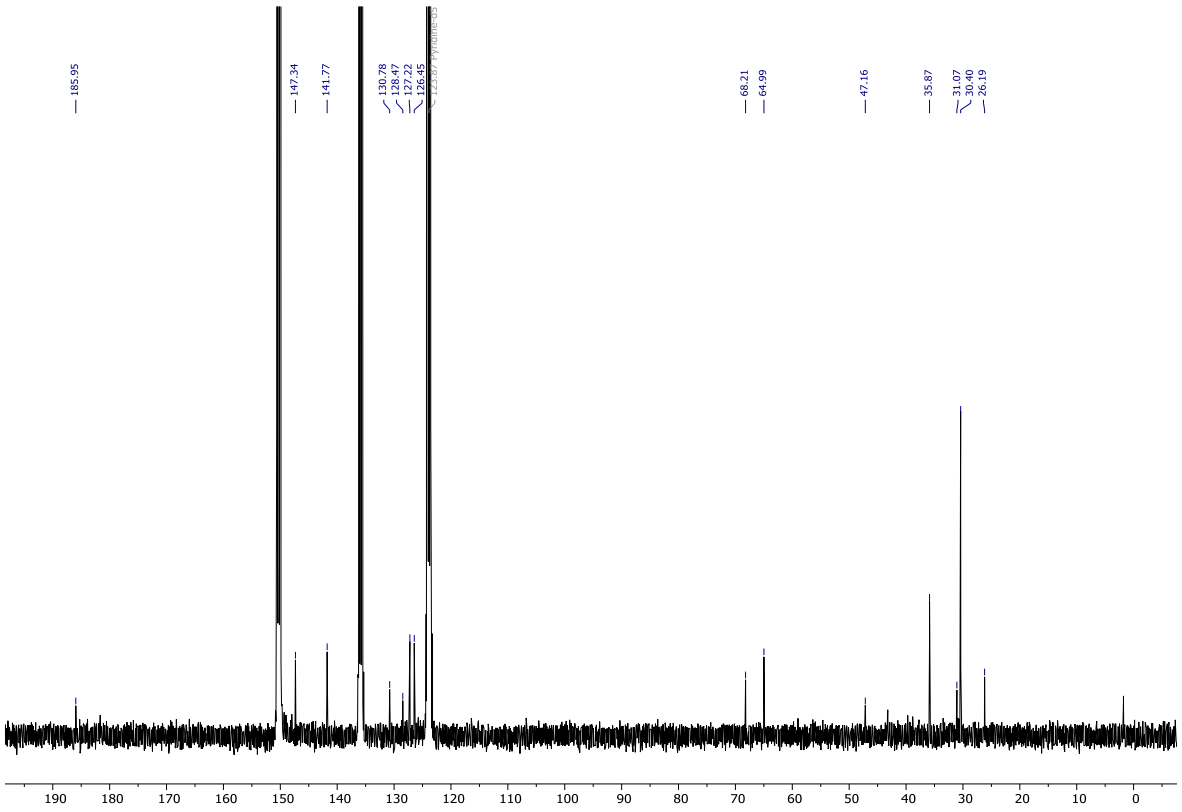

Figure S32. $^{13}C\{^{1}H\}$ NMR spectrum (pyridine-d_5, 125.13 MHz, 300 K) of [{*NCN*^{Me4}}Sb(S_2C-C_6H_2-$^{t}Bu_2$-3,5-O-4)] (**13**).

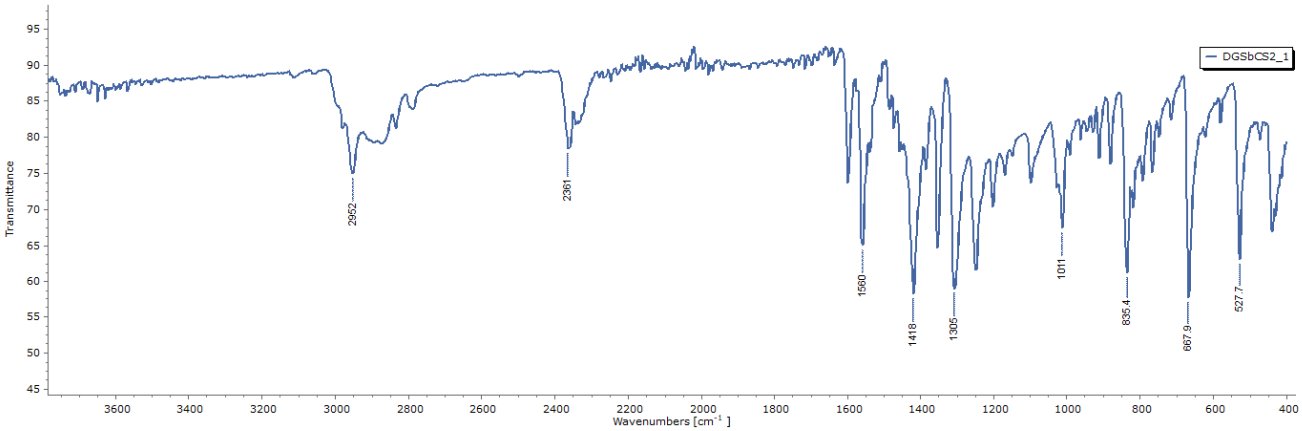

Figure S33. Infrared spectrum (Nujol mull) of [{*NCN*^{Me4}}Sb(S_2C-C_6H_2-$^{t}Bu_2$-3,5-O-4)] (**13**).

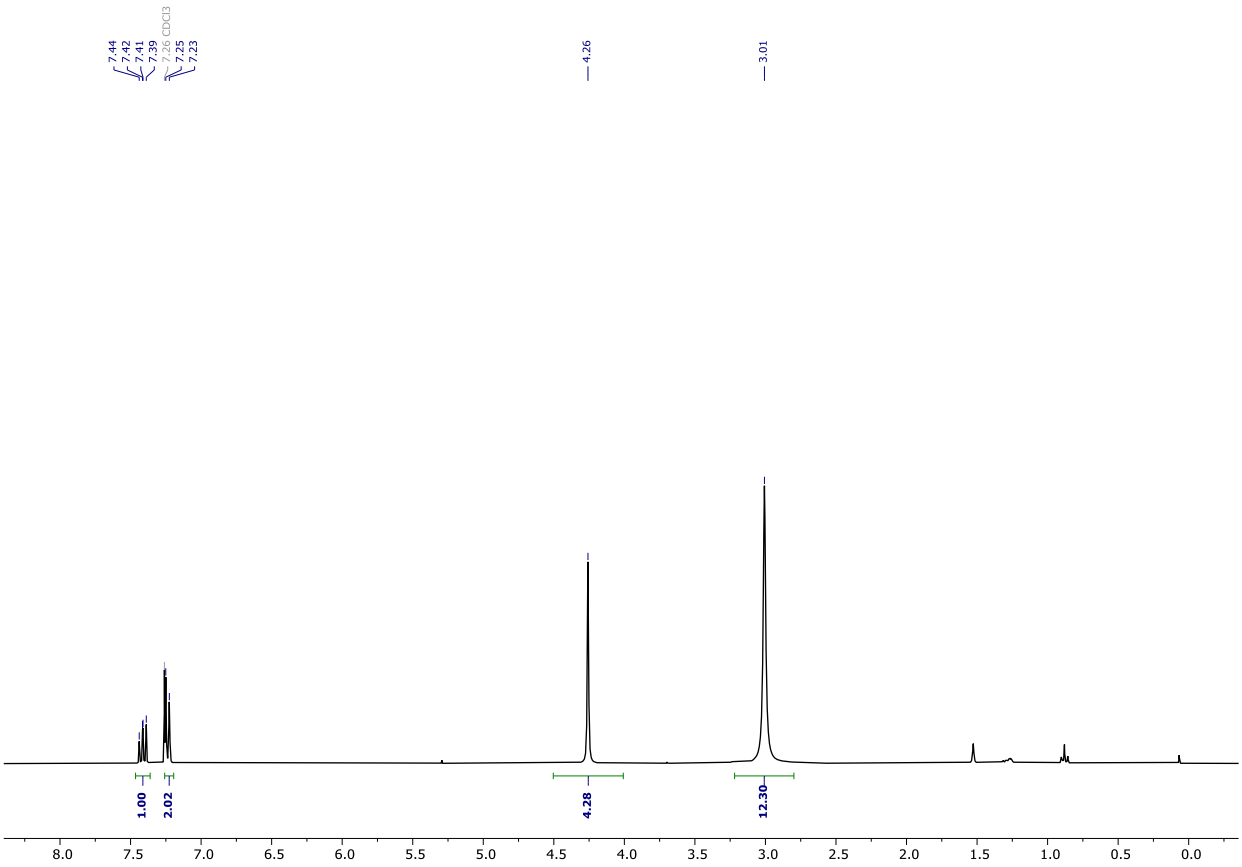

Figure S34. ^{1}H NMR spectrum ($CDCl_3$, 500.13 MHz, 300 K) of [{*NCN*^{Me4}}SbI_2].

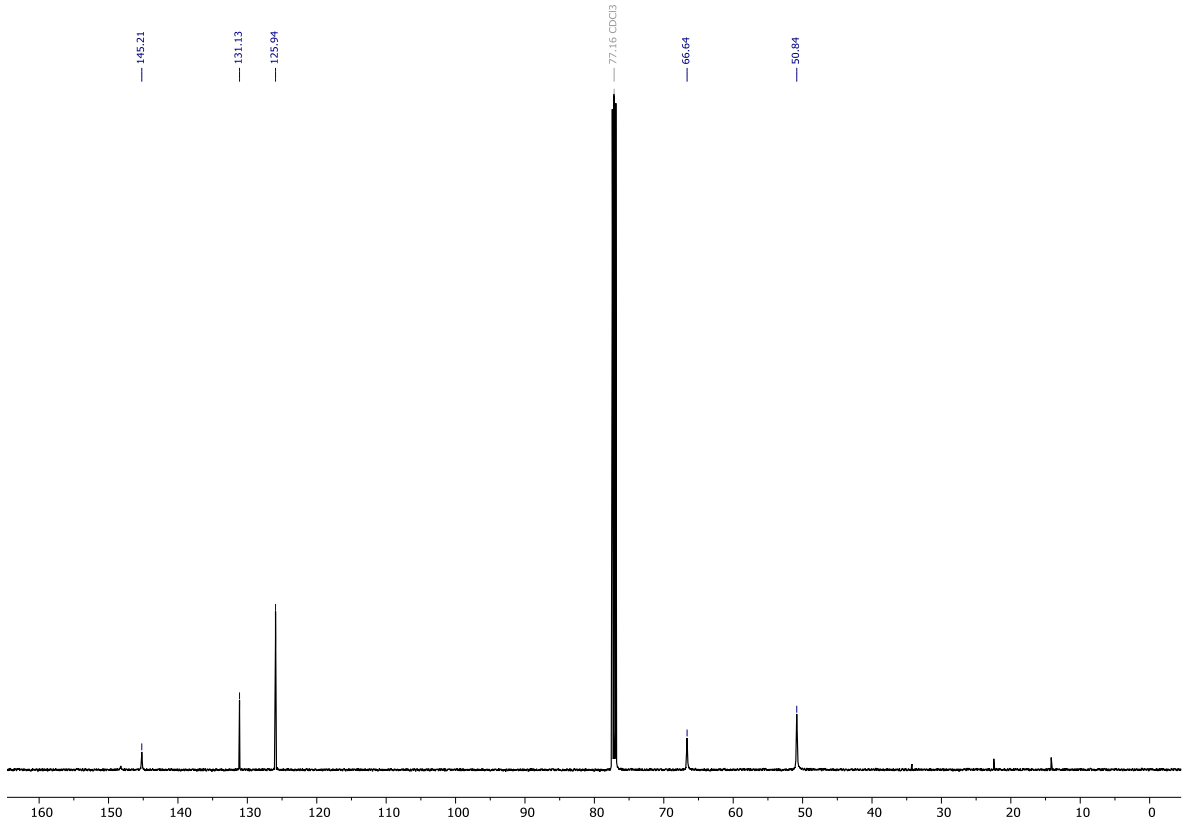

Figure S35. $^{13}C\{^{1}H\}$ NMR spectrum ($CDCl_3$, 125.13 MHz, 300 K) of [{*NCN*^{Me4}}SbI_2].

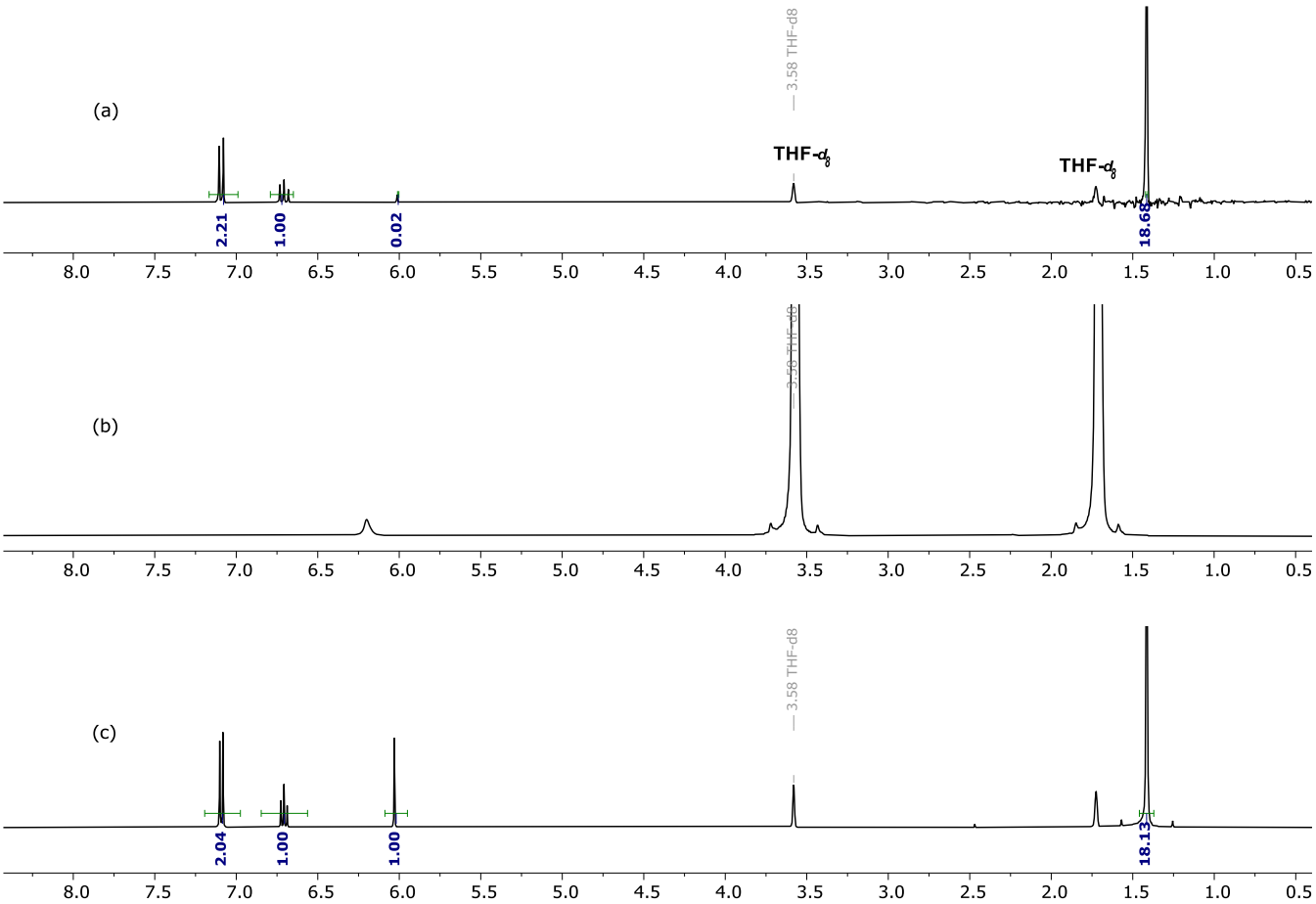

Figure S36. Comparative NMR data for deuteration labelling: (a) ^{1}H NMR spectrum of 2,6-^{t}Bu$_2$-C$_6$H$_3$OD (THF-d_8, 400.13 MHz, 300 K); (b) ^{2}H NMR of 2,6-^{t}Bu$_2$-C$_6$H$_3$OD (THF containing 5% THF-d_8, 61.37 MHz, 300 K); (c) ^{1}H NMR spectrum (THF-d_8, 400.13 MHz, 300 K) of 2,6-^{t}Bu$_2$-C$_6$H$_3$OH.

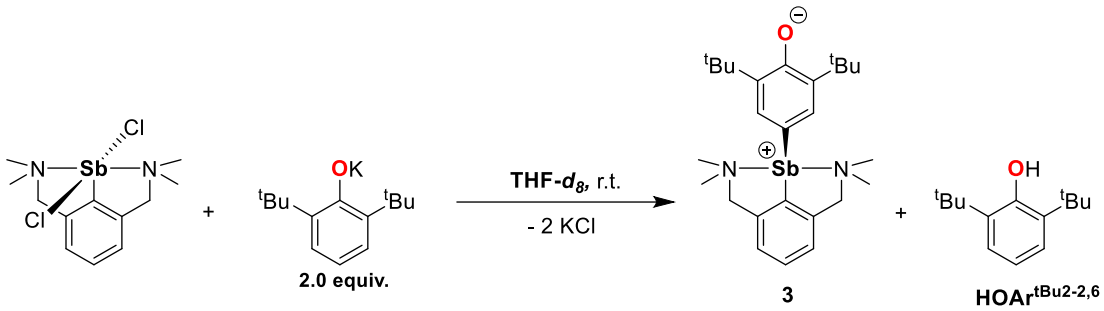

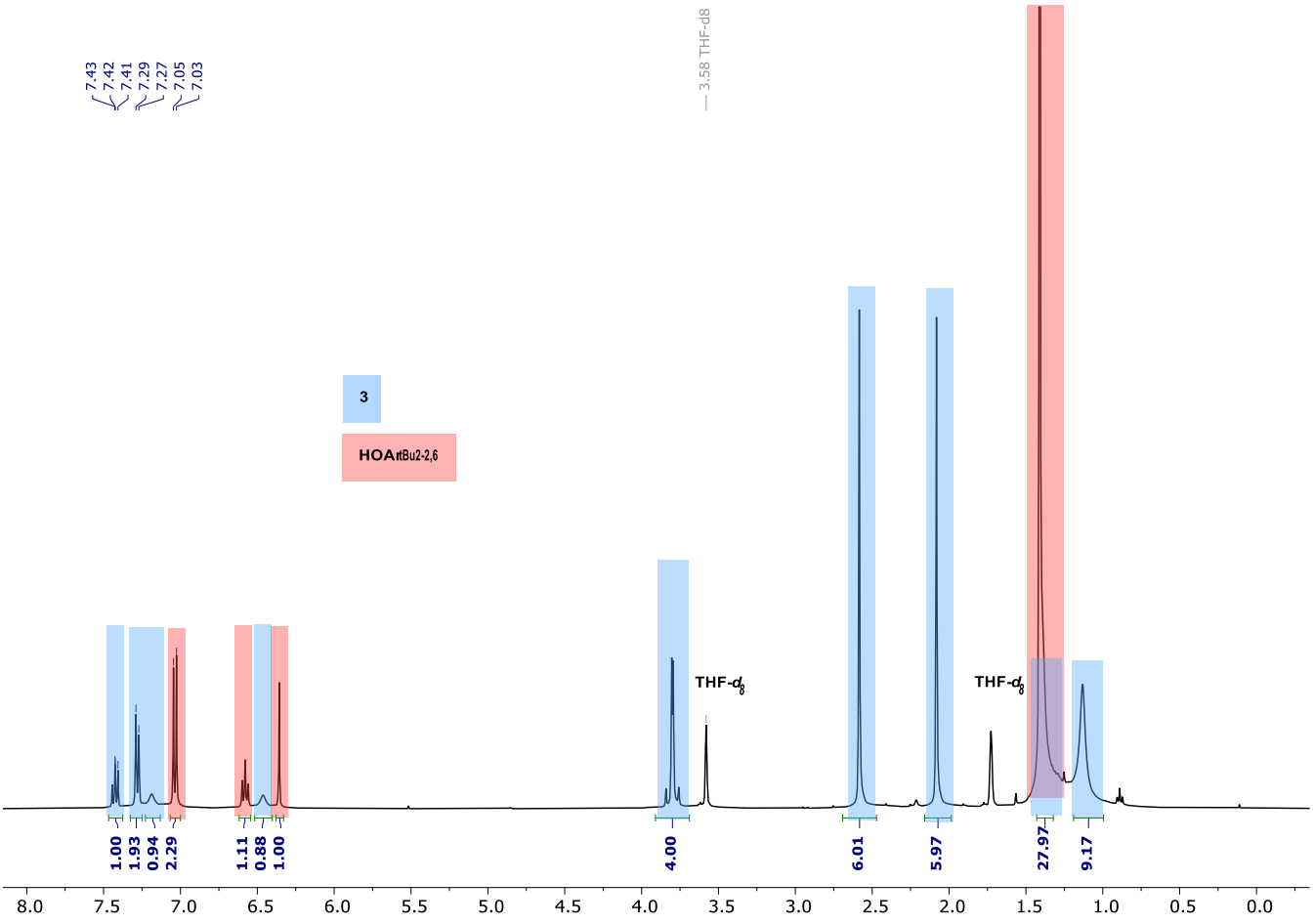

Figure S37. ^{1}H NMR spectrum (THF-d_8, 400.13 MHz, 300 K) of the *in situ* reaction of [{*NCN*^{Me4}}SbCl$_2$] with 2.0 equivalents of [{2,6-^{t}Bu$_2$-C$_6$H$_3$O}K].

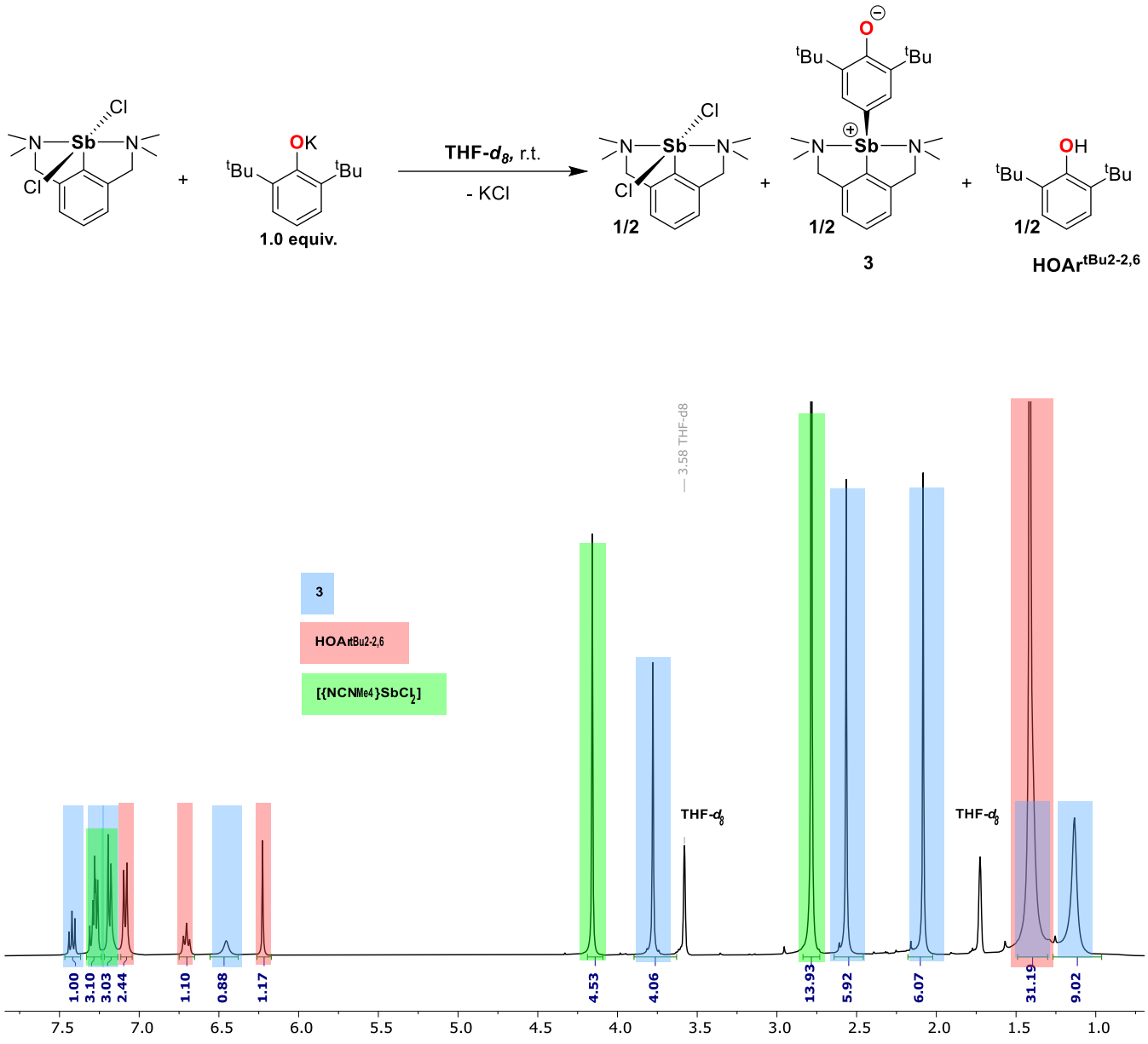

Figure S38. ^{1}H NMR spectrum (THF-d_8, 400.13 MHz, 300 K) of the *in situ* reaction of [{*NCN*^{Me4}}SbCl$_2$] with 1.0 equivalent of [{2,6-^{t}Bu$_2$-C$_6$H$_3$O}K].

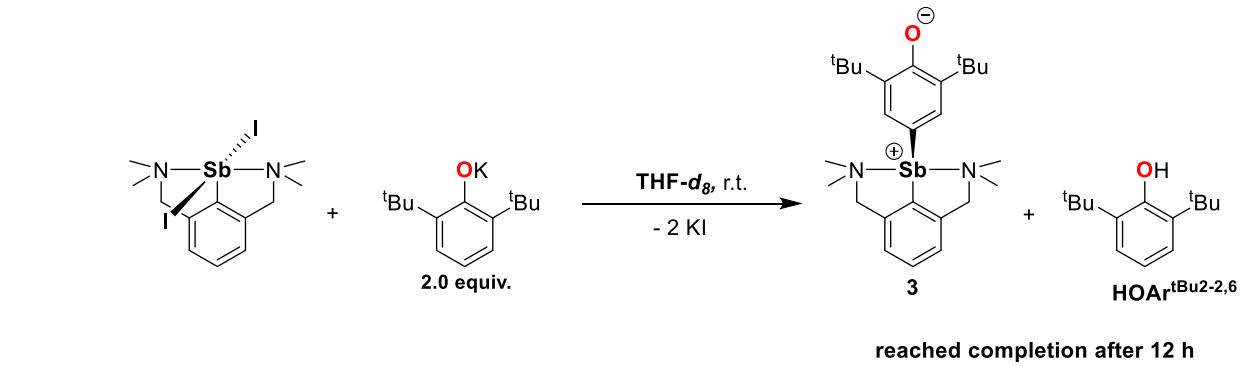

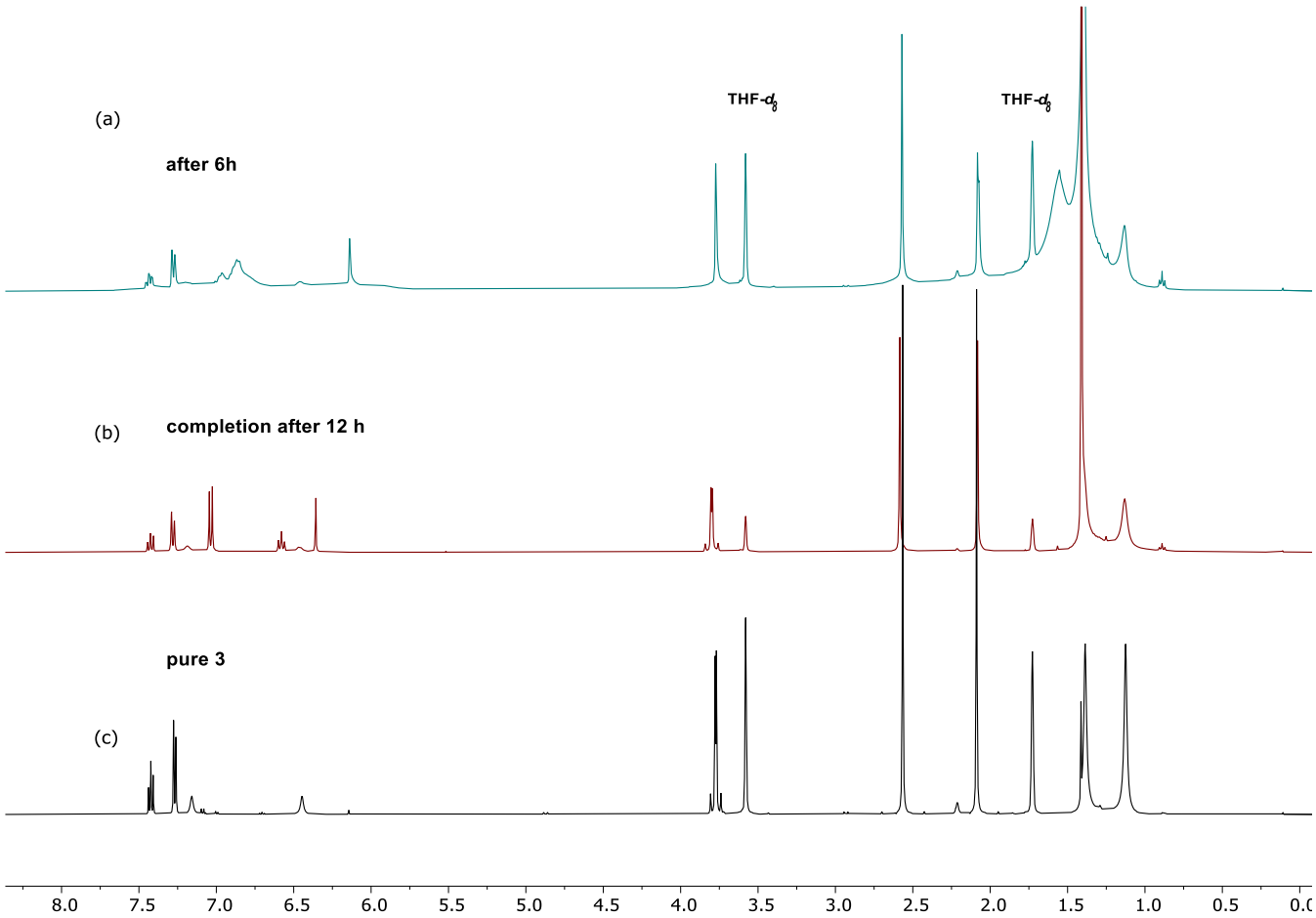

Figure S39. ^{1}H NMR spectra (THF-d_8, 400.13 MHz, 300 K) of the *in situ* reaction of [{*NCN*^{Me4}}SbI$_2$] with 2.0 equivalents of [{2,6-^{t}Bu$_2$-C$_6$H$_3$O}K] after (a) 6 h and (b) 12 h. For comparison, (c) provides the ^{1}H NMR spectrum (THF-d_8, 400.13 MHz, 300 K) of [{*NCN*^{Me4}}Sb(C$_6$H$_2$-^{t}Bu$_2$-3,5-O-4)] (**3**).

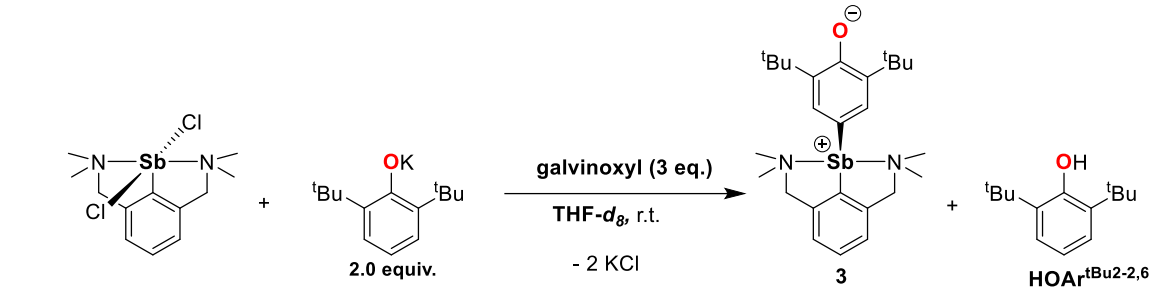

no observable effect on the formation of the expected products

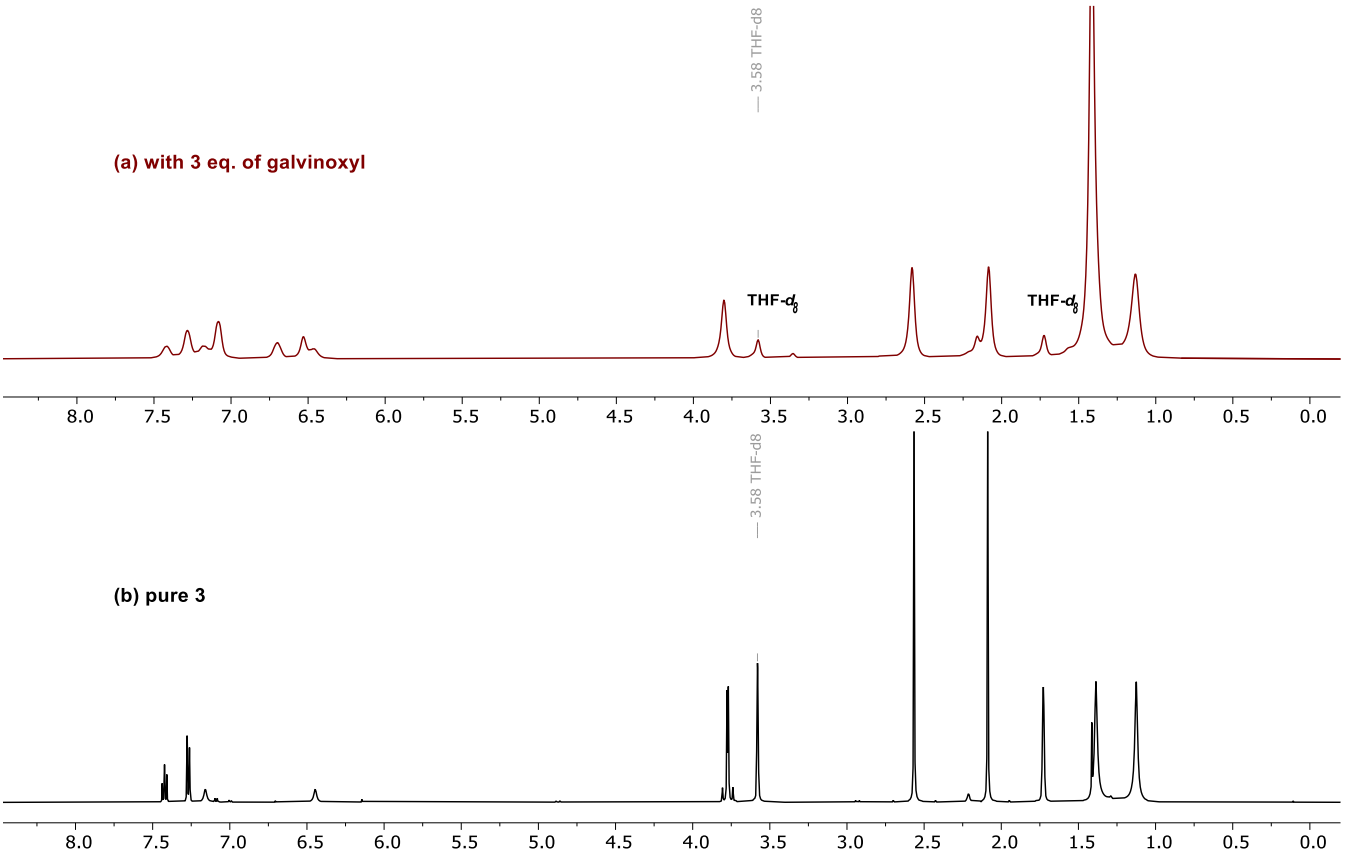

Figure S40. Stacked ^{1}H NMR spectra (THF-d_8, 400.13 MHz, 300 K) of: (a) the *in situ* reaction of [{*NCN*^{Me4}}SbCl$_2$] with [{2,6-^{t}Bu$_2$-C$_6$H$_3$O}K] (2 equiv.) in the presence of galvinoxyl (3 equiv) and (b) ^{1}H NMR spectrum (THF-d_8, 400.13 MHz, 300 K) of [{*NCN*^{Me4}}Sb(C$_6$H$_2$-^{t}Bu$_2$-3,5-O-4)] (**3**).

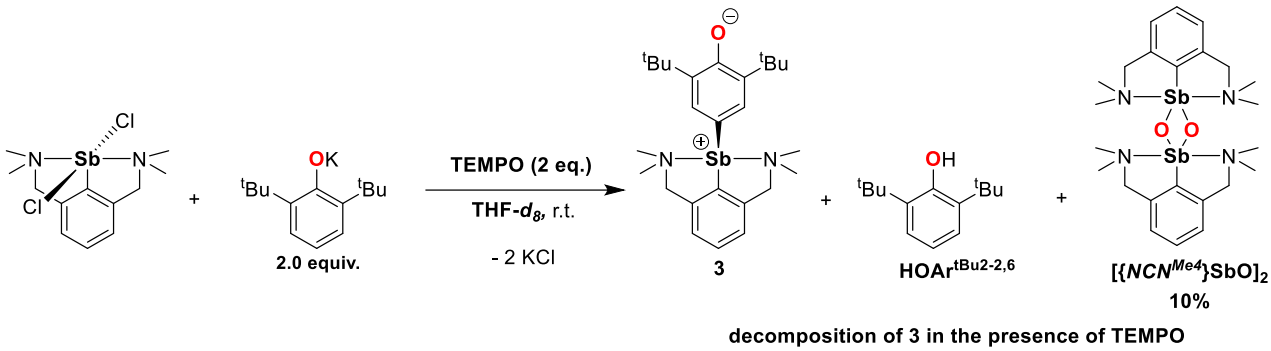

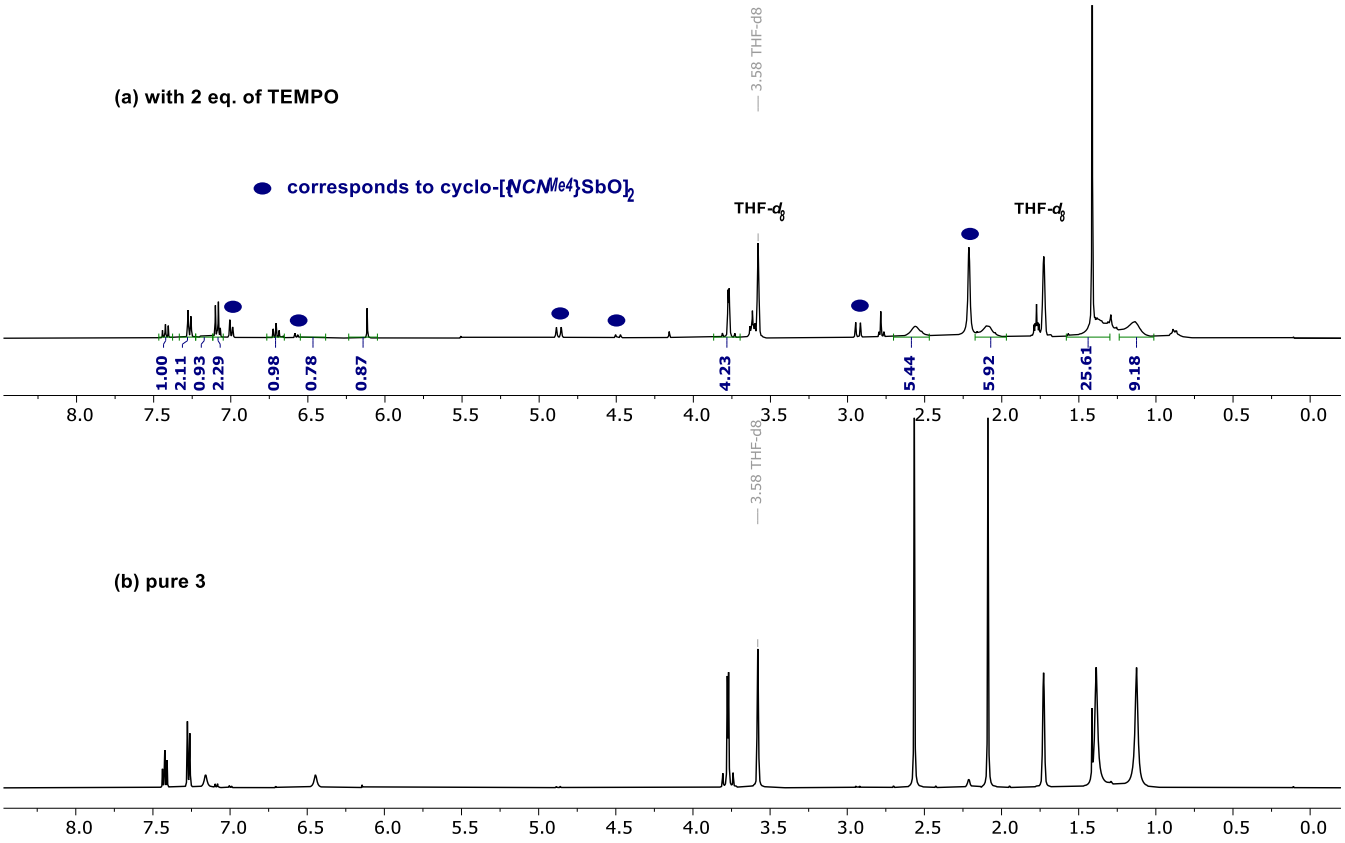

Figure S41. Stacked ^{1}H NMR spectra (THF-d_8, 400.13 MHz, 300 K) of: (a) the *in situ* reaction of [{*NCN*^{Me4}}SbCl$_2$] with [{2,6-^{t}Bu$_2$-C$_6$H$_3$O}K] (2 equiv.) in the presence of TEMPO (2 equiv.) and (b) ^{1}H NMR spectrum (THF-d_8, 400.13 MHz, 300 K) of [{*NCN*^{Me4}}Sb(C$_6$H$_2$-^{t}Bu$_2$-3,5-O-4)] (**3**).

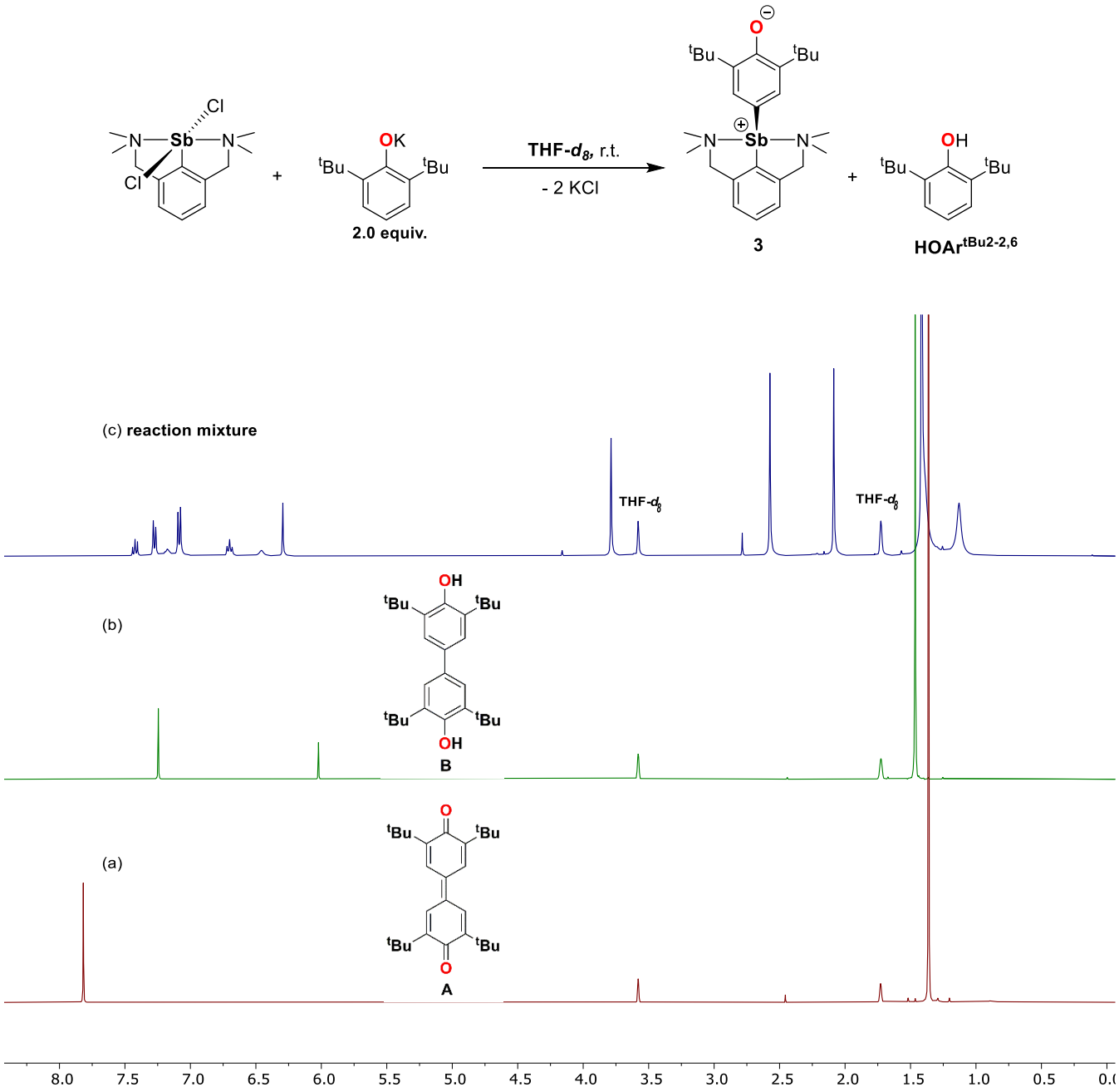

Figure S42. Comparison of the ^{1}H NMR spectra (THF-d_8, 400.13 MHz, 300 K) for (a) 3,3',5,5'-tetra-*tert*-butyldiphenoquinone (**A**), (b) 3,3',5,5'-tetra-*tert*-butyl-[1,1'-biphenyl]-4,4'-diol (**B**), and (c) the *in situ* reaction of [{*NCN*^{Me4}}SbCl$_2$] with 2.0 eq. of [{2,6-^{t}Bu$_2$-C$_6$H$_3$O}K]. It confirms that **A** and **B** are not formed during the synthesis of **3**.

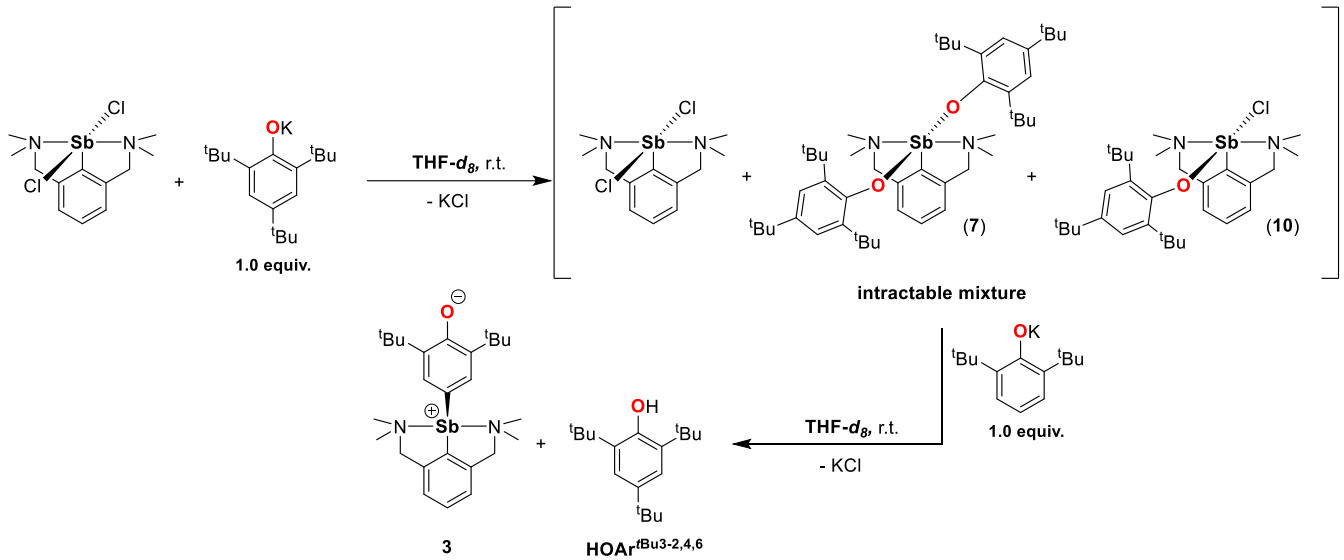

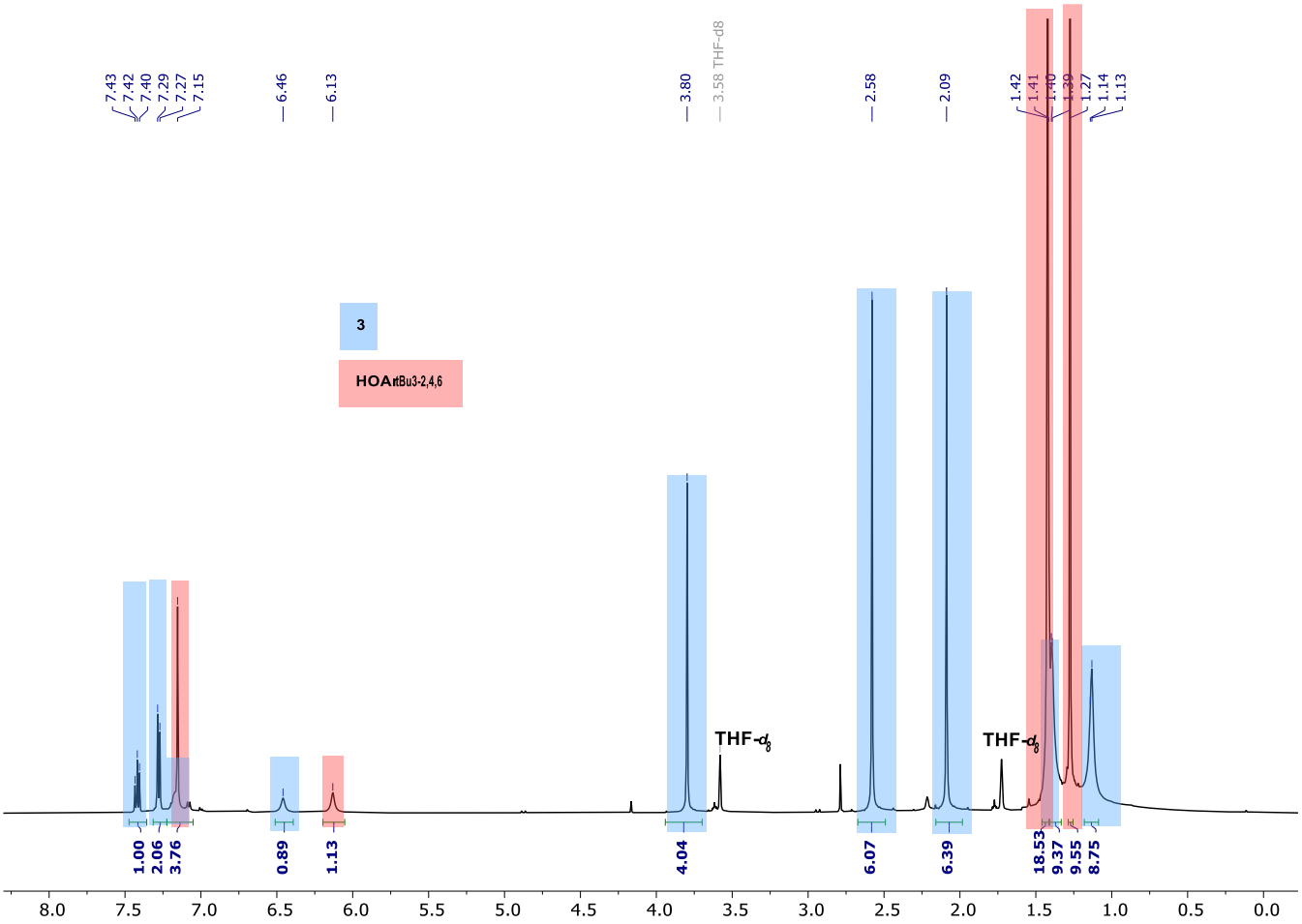

Figure S43. ^{1}H NMR spectrum (THF-d_8, 400.13 MHz, 300 K) of the *in situ*, two-step reaction of [{*NCN*^{Me4}}SbCl$_2$] with, first, [{2,4,6-^{t}Bu$_3$-C$_6$H$_2$O}K] (1.0 eq.) and then [{2,6-^{t}Bu$_2$-C$_6$H$_2$O}K] (1.0 eq.).

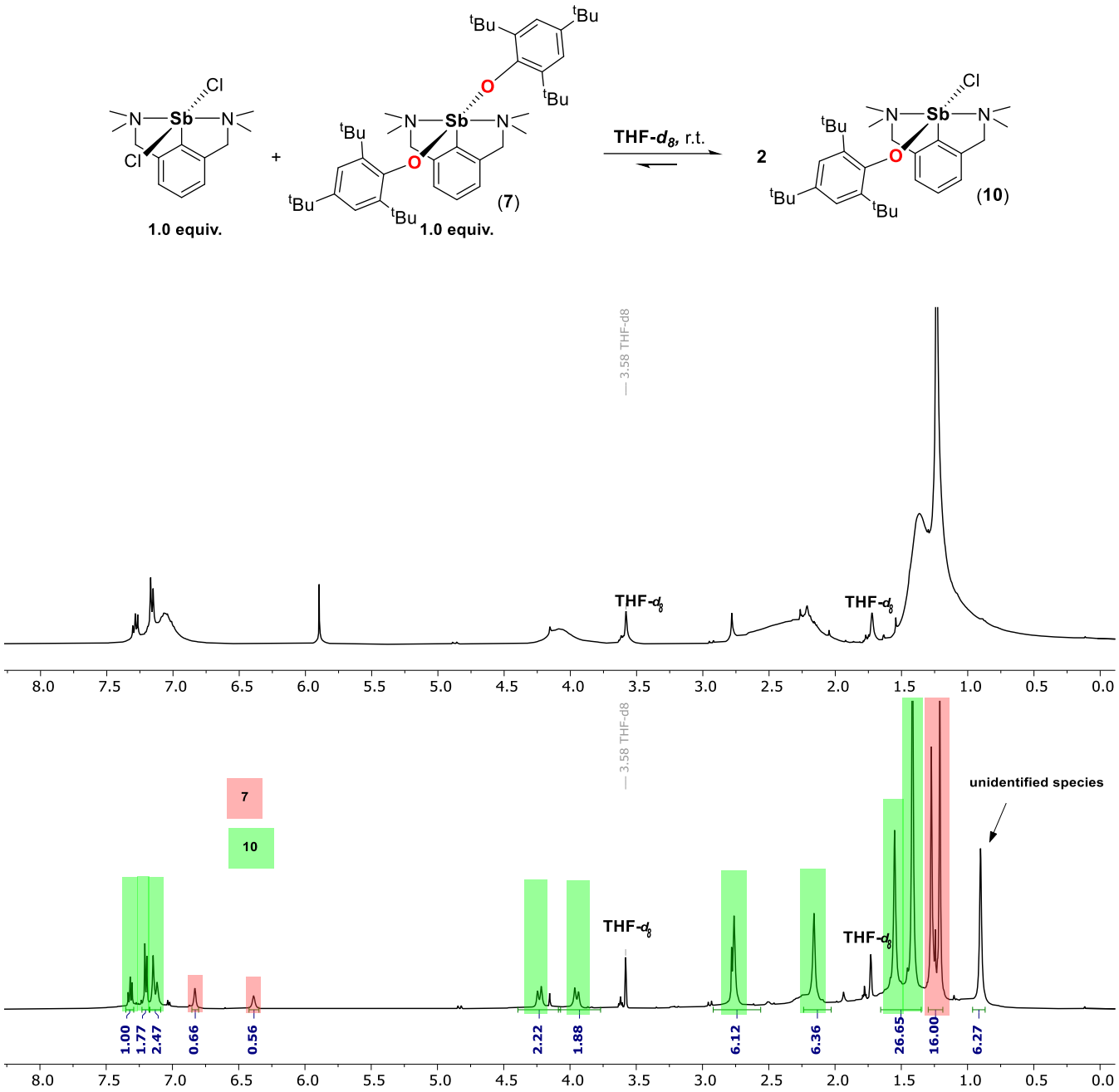

Figure S44. Stacked ^{1}H NMR spectra (THF-d_8, 400.13 MHz) of the 1:1 mixture of [{*NCN*^{Me4}}SbCl$_2$] and [{*NCN*^{Me4}}Sb(OC$_6$H$_2$-^{t}Bu$_3$-2,4,6)$_2$] (**7**) at 25 °C (top) and −35 °C (bottom)

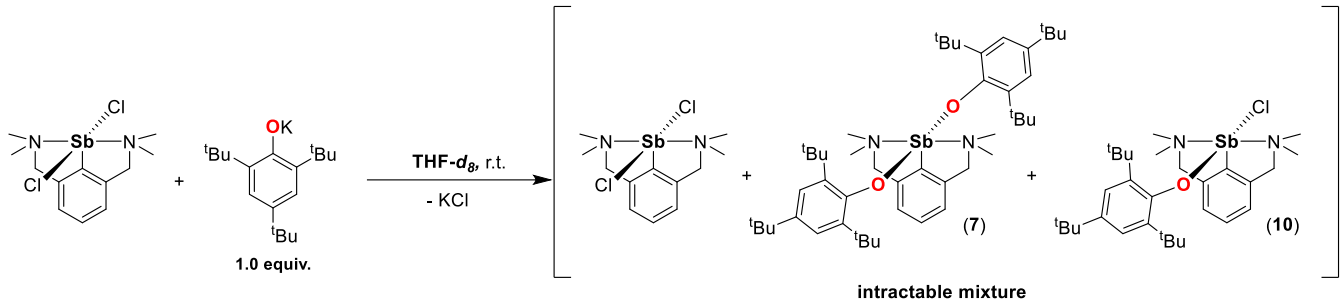

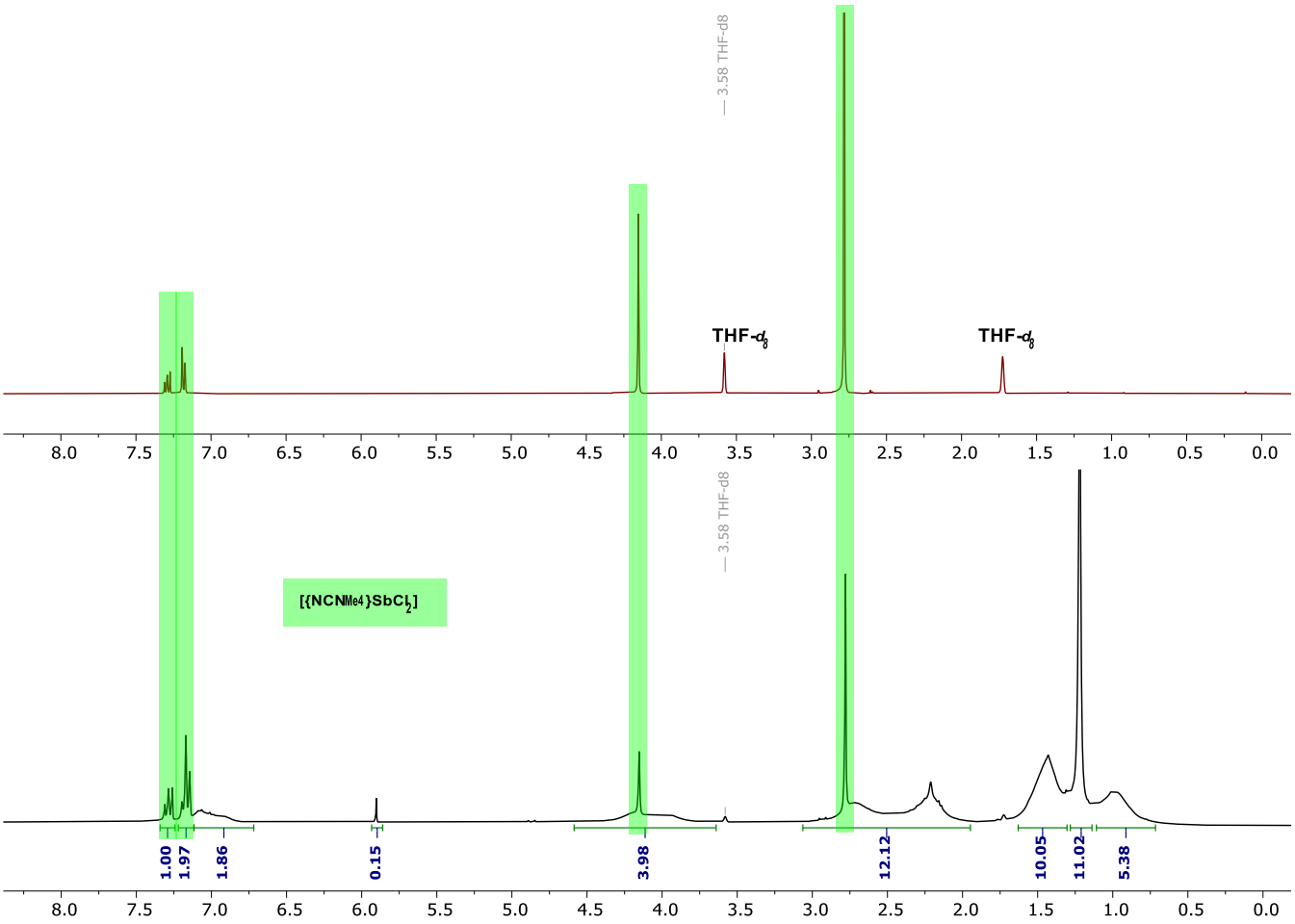

Figure S45. Stacked ^{1}H NMR spectra (THF-d_8, 400.13 MHz, 300 K) of (bottom) the *in situ* reaction of [{*NCN*^{Me4}}SbCl$_2$] with 1.0 equivalent of [{2,4,6-^{t}Bu$_3$-C$_6$H$_2$O}K] and (top) the parent antimony dichloride [{*NCN*^{Me4}}SbCl$_2$].

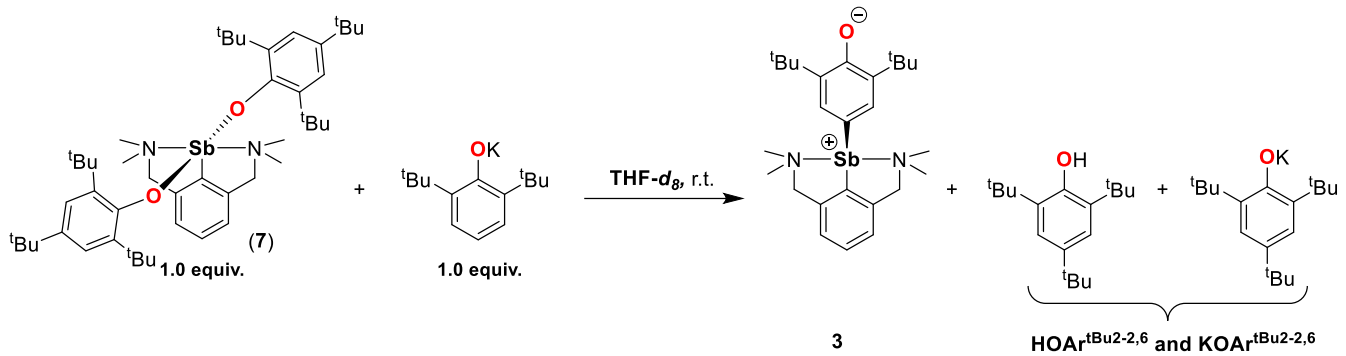

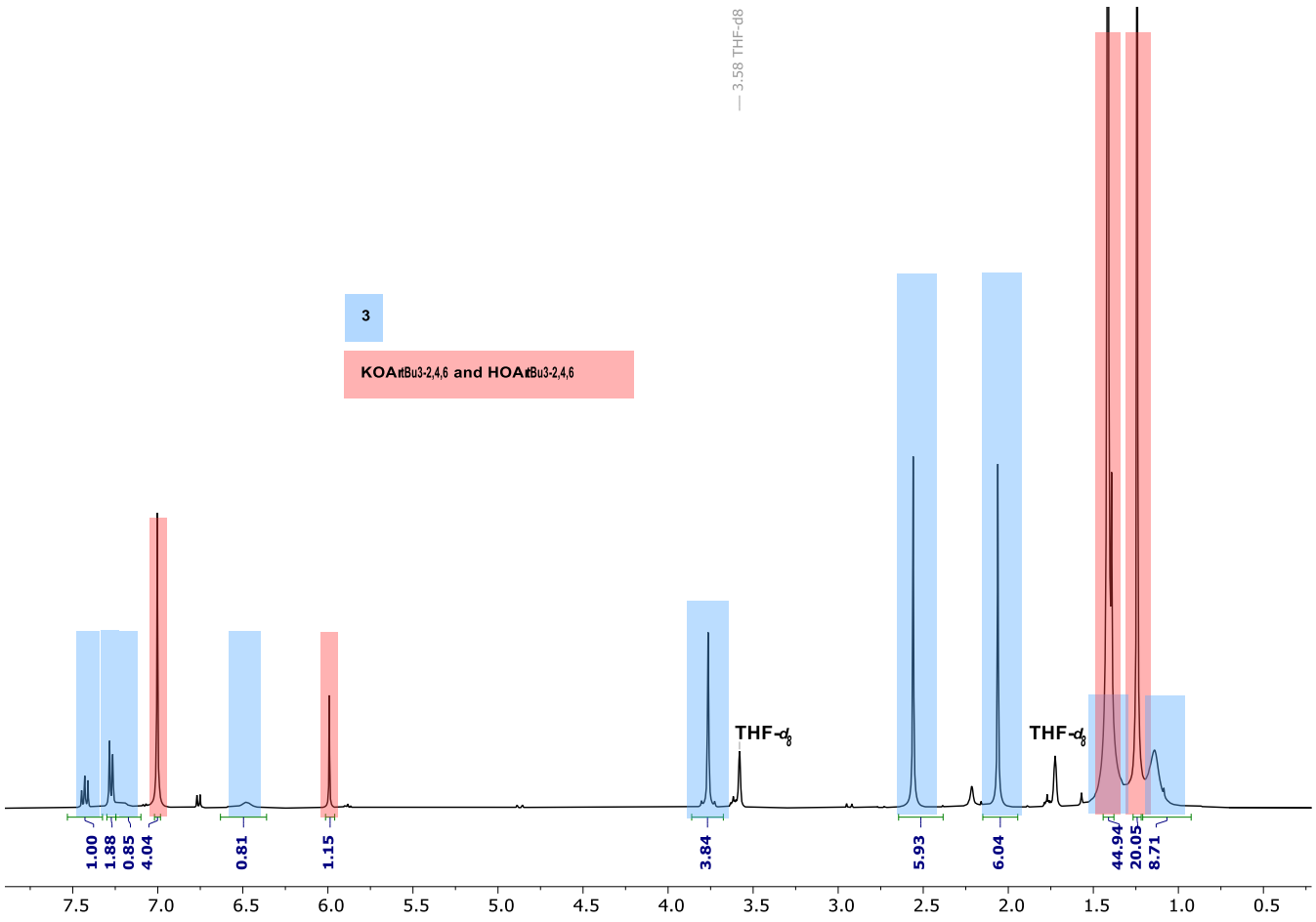

Figure S46. ^{1}H NMR spectrum (THF-d_8, 400.13 MHz, 300 K) of the *in situ* equimolar reaction of [{*NCN*^{Me4}}Sb(OC$_6$H$_2$-^{t}Bu$_3$-2,4,6)$_2$] (**7**) with [{2,6-^{t}Bu$_2$-C$_6$H$_2$O}K].

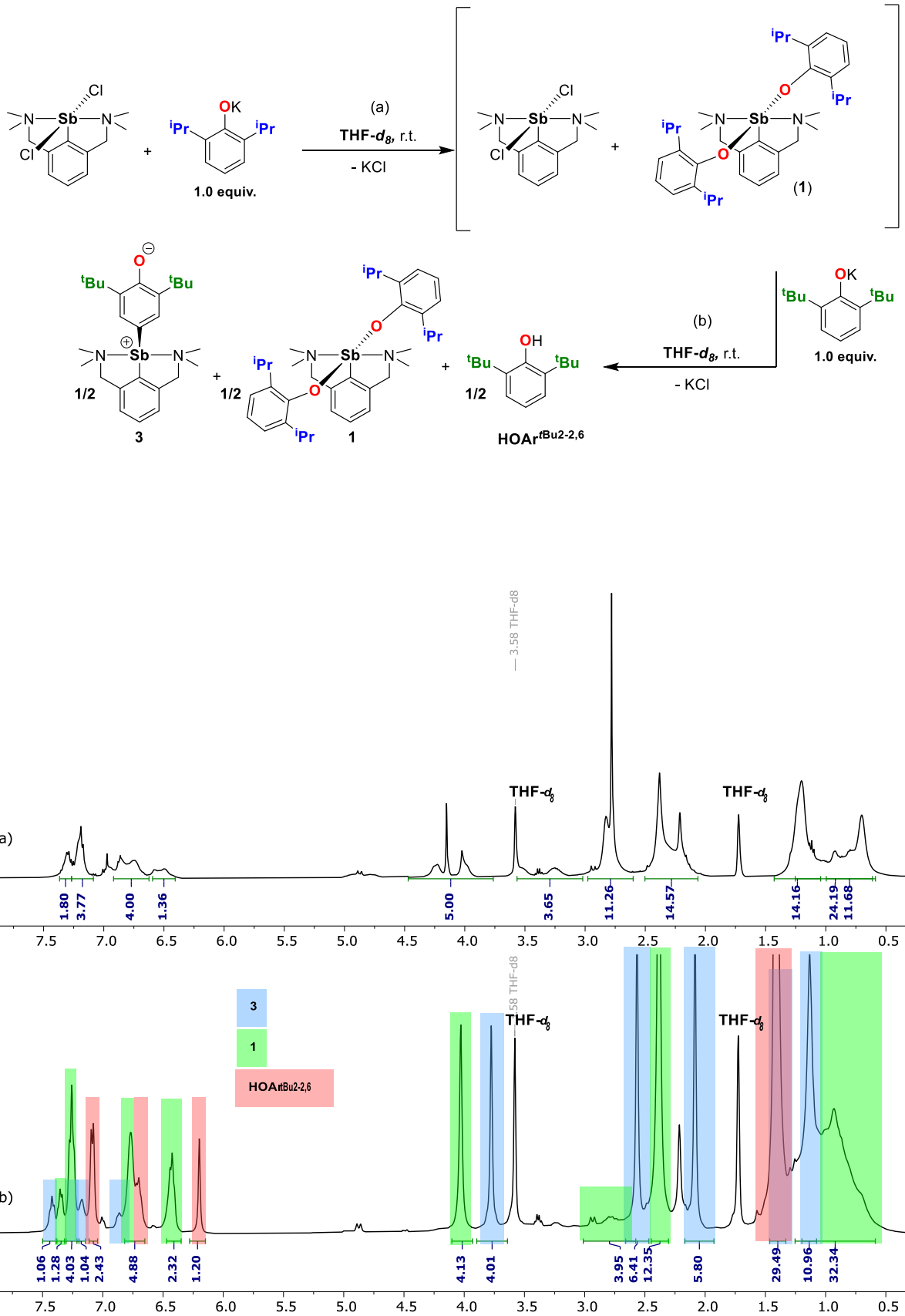

Figure S47. Stacked ^{1}H NMR spectra (THF-d_8, 400.13 MHz, 300 K) of the *in situ*, two-step reaction of [{*NCN*^{Me4}}SbCl$_2$] with (a) 1.0 eq. of [{2,6-^{i}Pr$_2$-C$_6$H$_3$O}K] followed by (b) further addition of 1.0 eq. of [{2,6-^{t}Bu$_2$-C$_6$H$_2$O}K].

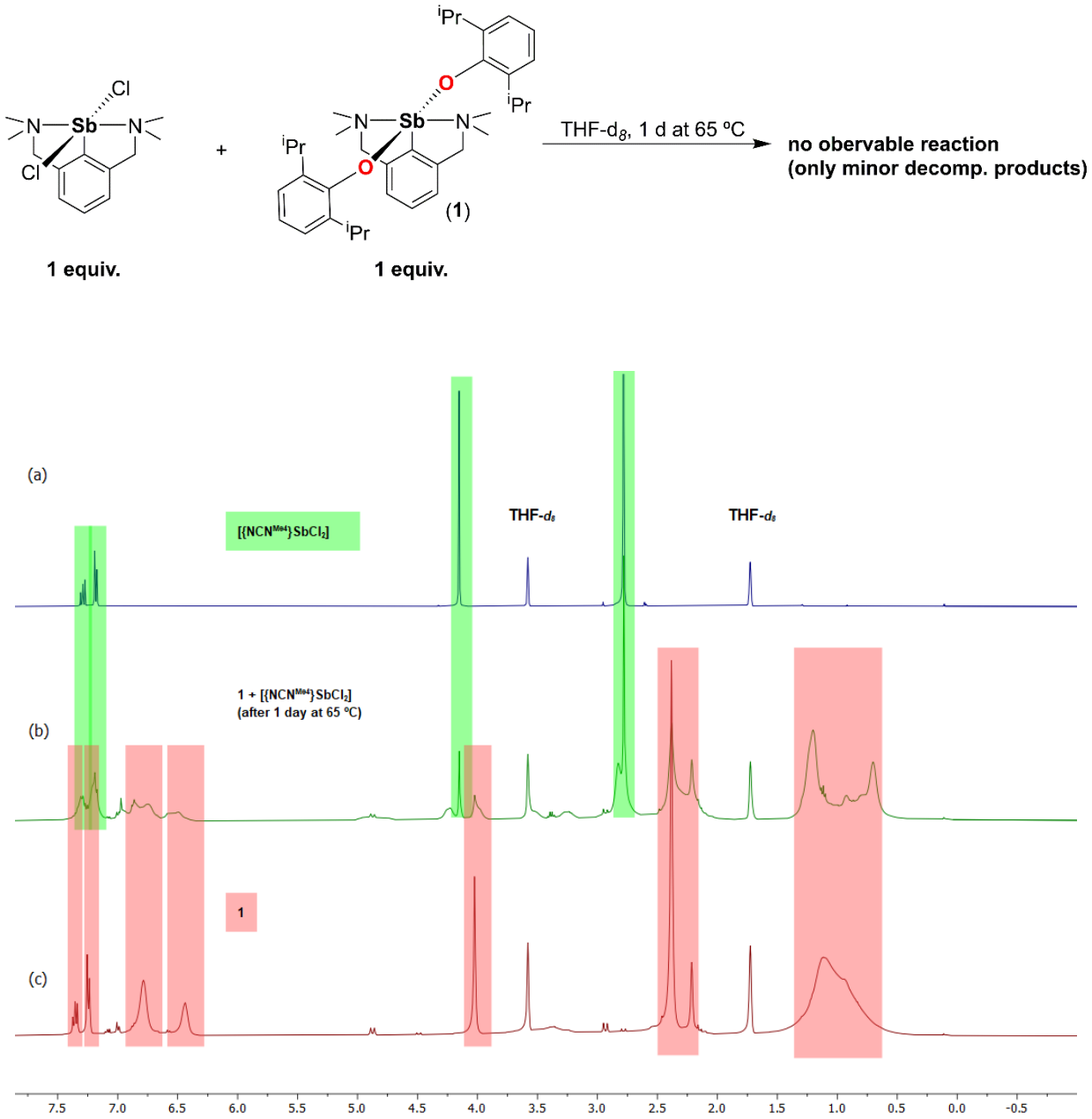

Figure S48. Stacked ^{1}H NMR spectra (THF-d_8, 400.13 MHz, 300 K) of (a) [{*NCN*^{Me4}}SbCl$_2$]; (b) the 1:1 mixture of [{*NCN*^{Me4}}SbCl$_2$] and [{*NCN*^{Me4}}Sb(OC$_6$H$_3$-^{i}Pr$_2$-2,6)$_2$] after heating for 1 d at 65 °C, and (c) [{*NCN*^{Me4}}Sb(OC$_6$H$_3$-^{i}Pr$_2$-2,6)$_2$].

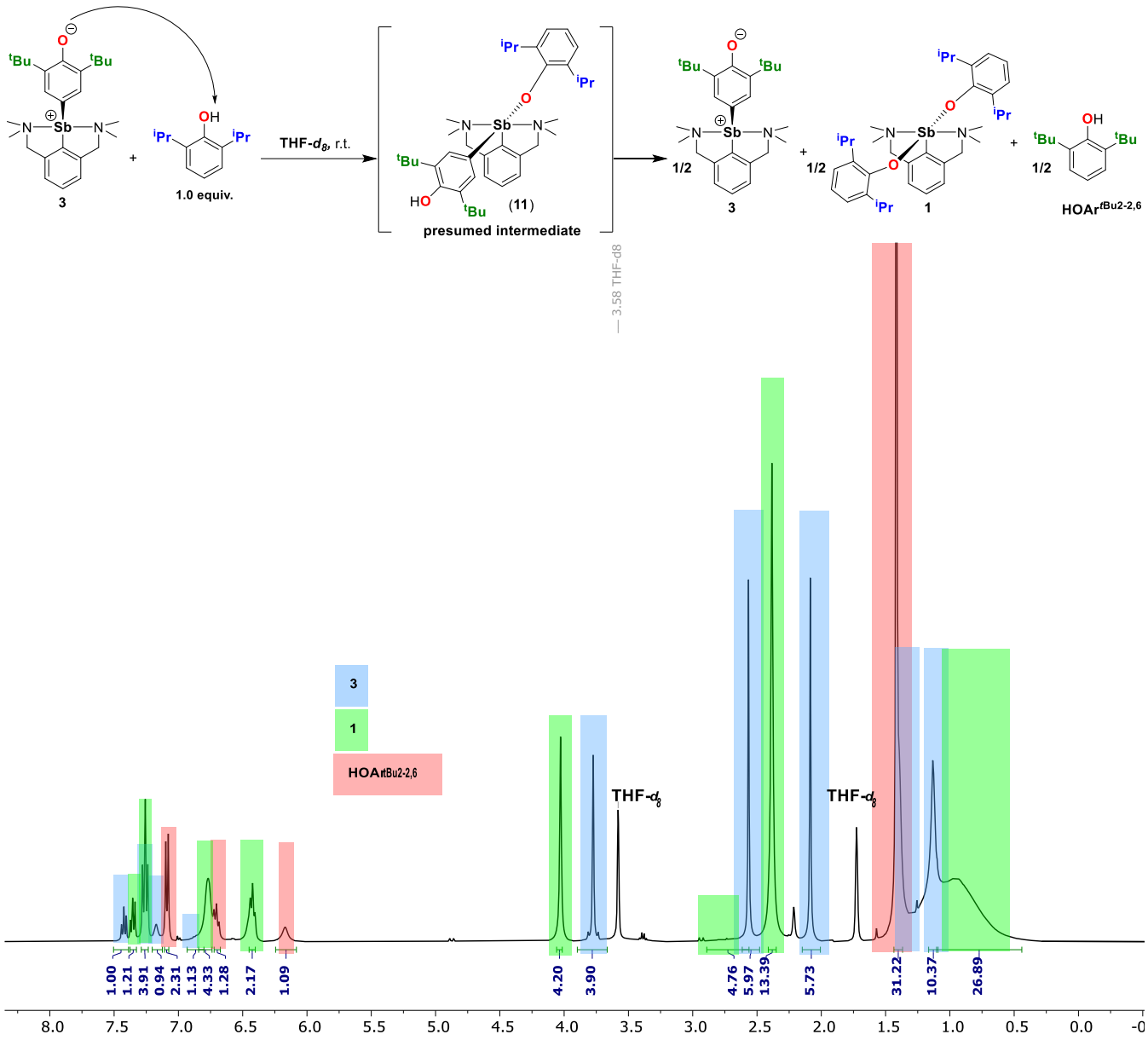

Figure S49. ^{1}H NMR spectrum (THF-d_8, 400.13 MHz, 300 K) of the *in situ* equimolar reaction of [{*NCN*^{Me4}}Sb(C$_6$H$_2$-^{t}Bu$_2$-3,5-O-4)] (**3**) with 2,6-^{i}Pr$_2$-C$_6$H$_3$OH.

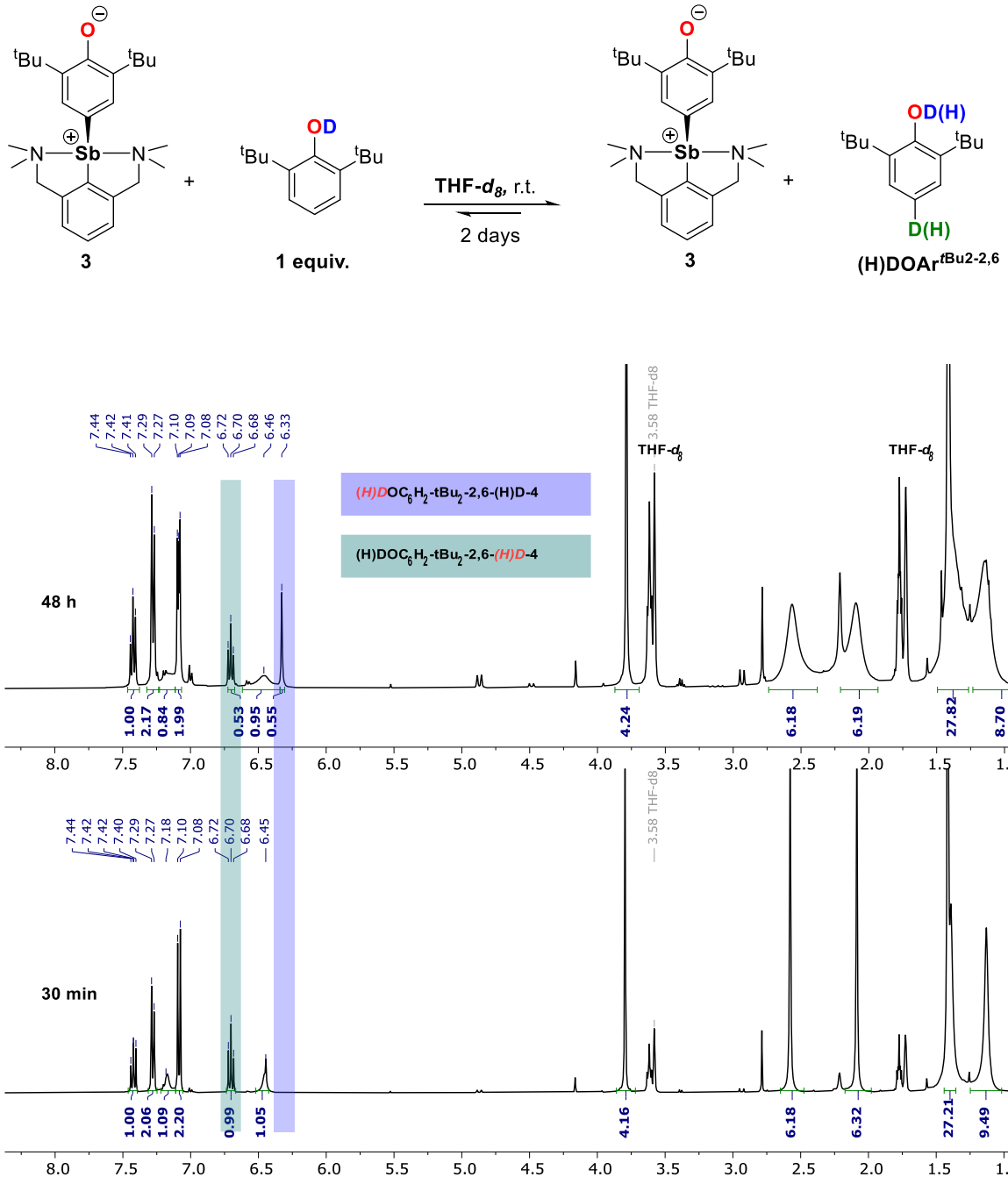

Figure S50. Stacked ^{1}H NMR spectra (THF-d_8, 400.13 MHz, 300 K) of the equimolar mixture of [{*NCN*^{Me4}}Sb(C$_6$H$_2$-^{t}Bu$_2$-3,5-O-4)] (**3**) and 2,6-^{t}Bu$_2$-C$_6$H$_3$OD after 30 min (bottom) and 48 h (top).

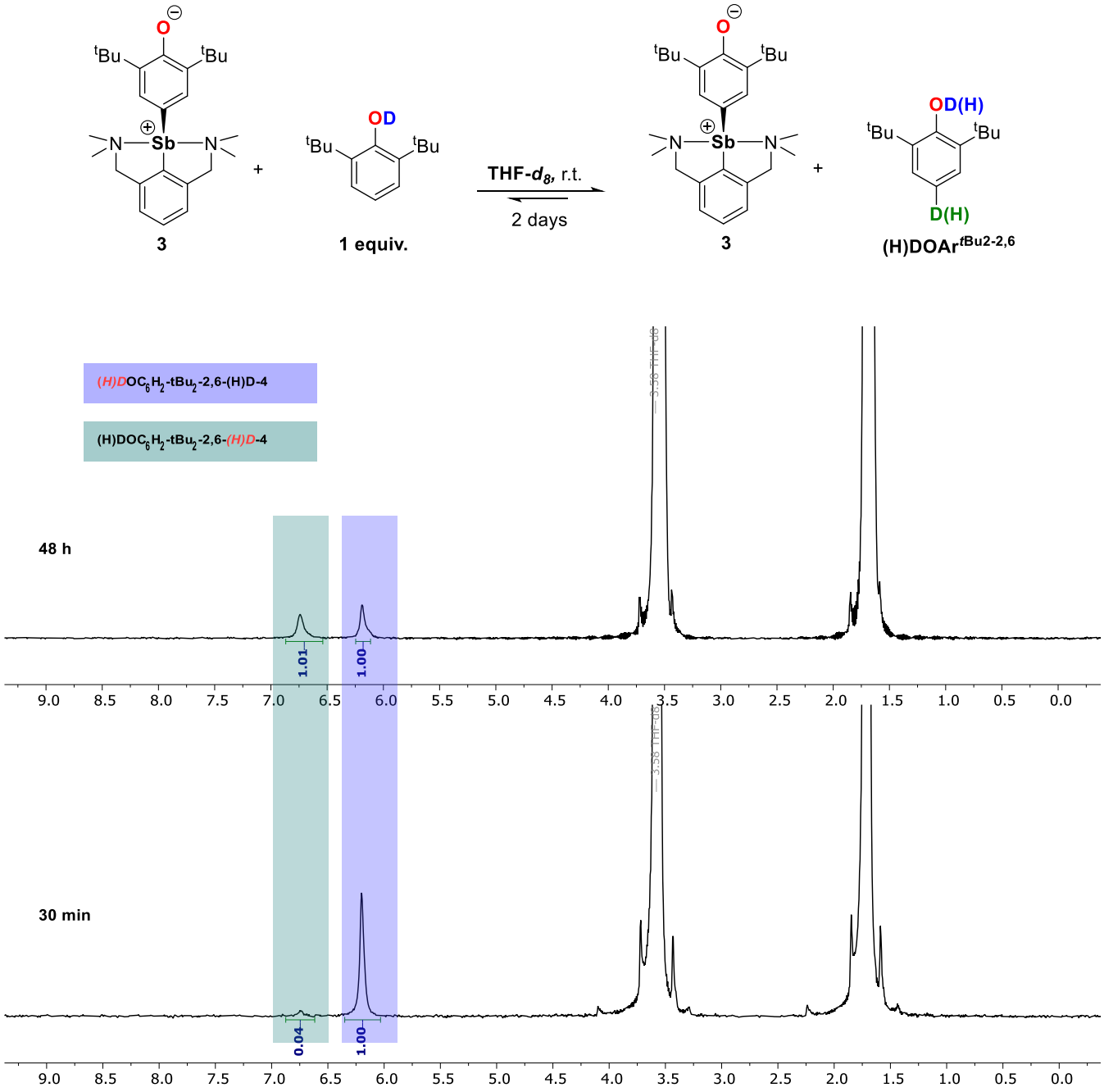

Figure S51. Stacked ^{2}H NMR spectra (THF containing 5% THF-d_8, 61.37 MHz, 300 K) of the equimolar mixture of [{*NCN*^{Me4}}Sb(C$_6$H$_2$-^{t}Bu$_2$-3,5-O-4)] (**3**) and 2,6-^{t}Bu$_2$-C$_6$H$_3$OD after 30 min (bottom) and 48 h (top).

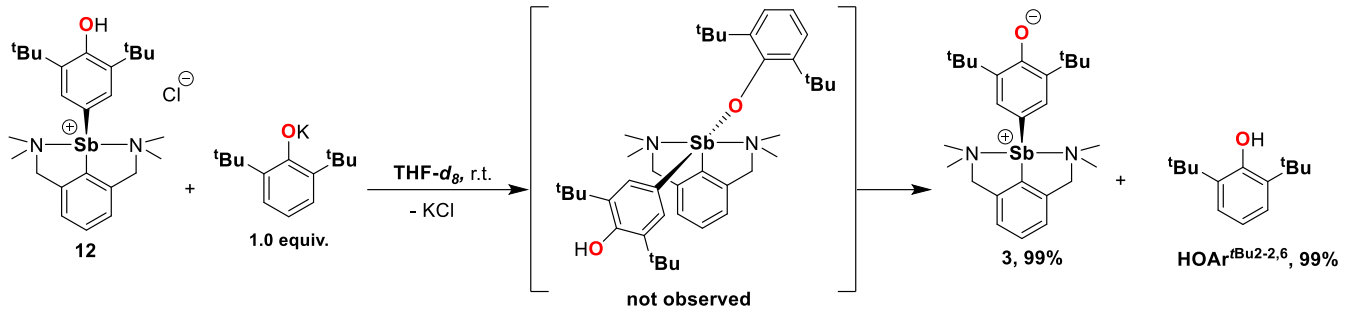

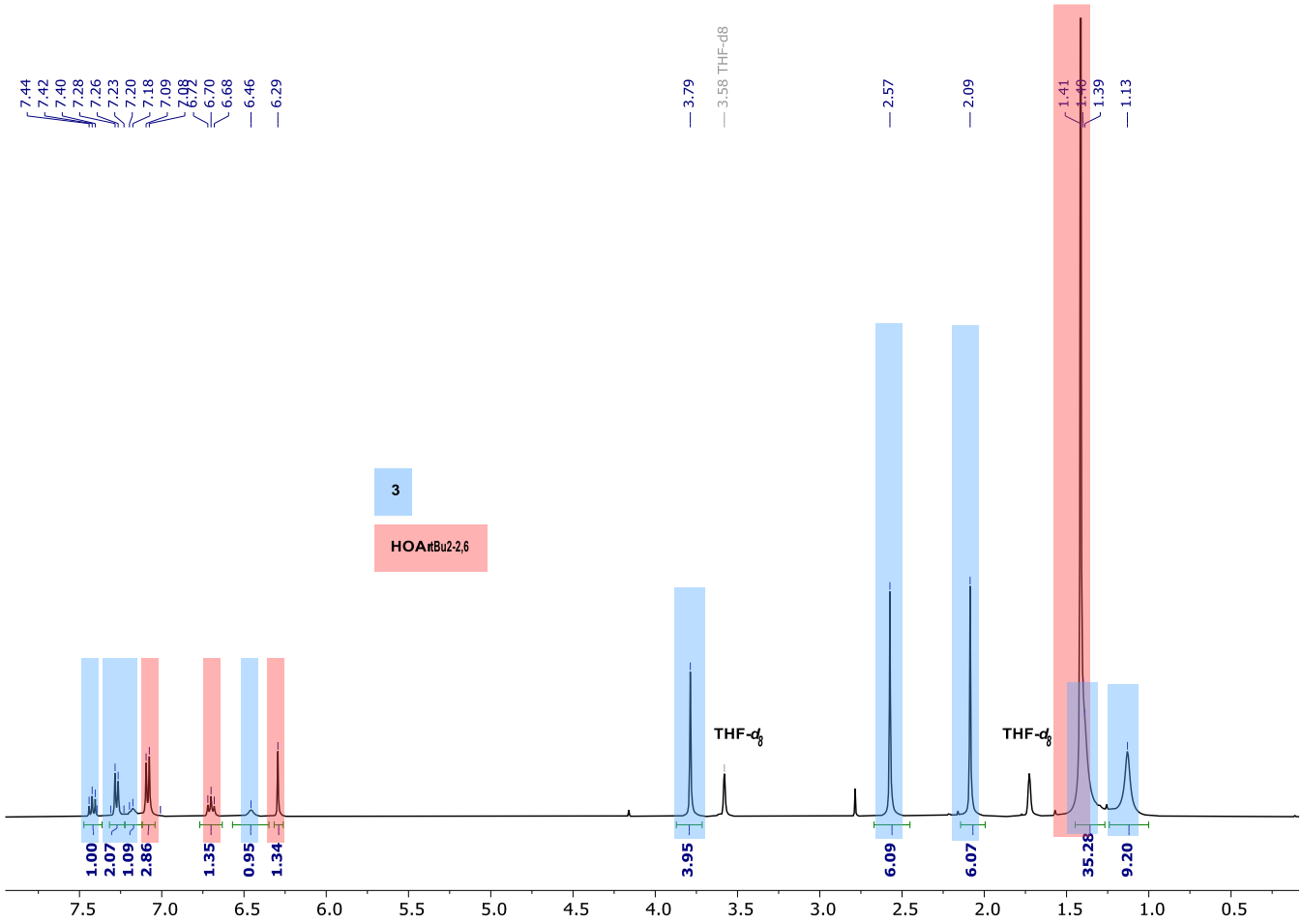

Figure S52. ^{1}H NMR spectrum (THF-d_8, 400.13 MHz, 300 K) of the *in situ* equimolar reaction of [{*NCN*^{Me4}}Sb(C$_6$H$_2$-^{t}Bu$_2$-3,5-OH-4)][Cl] (**12**) with [{2,6-^{t}Bu$_2$-C$_6$H$_3$O}K].

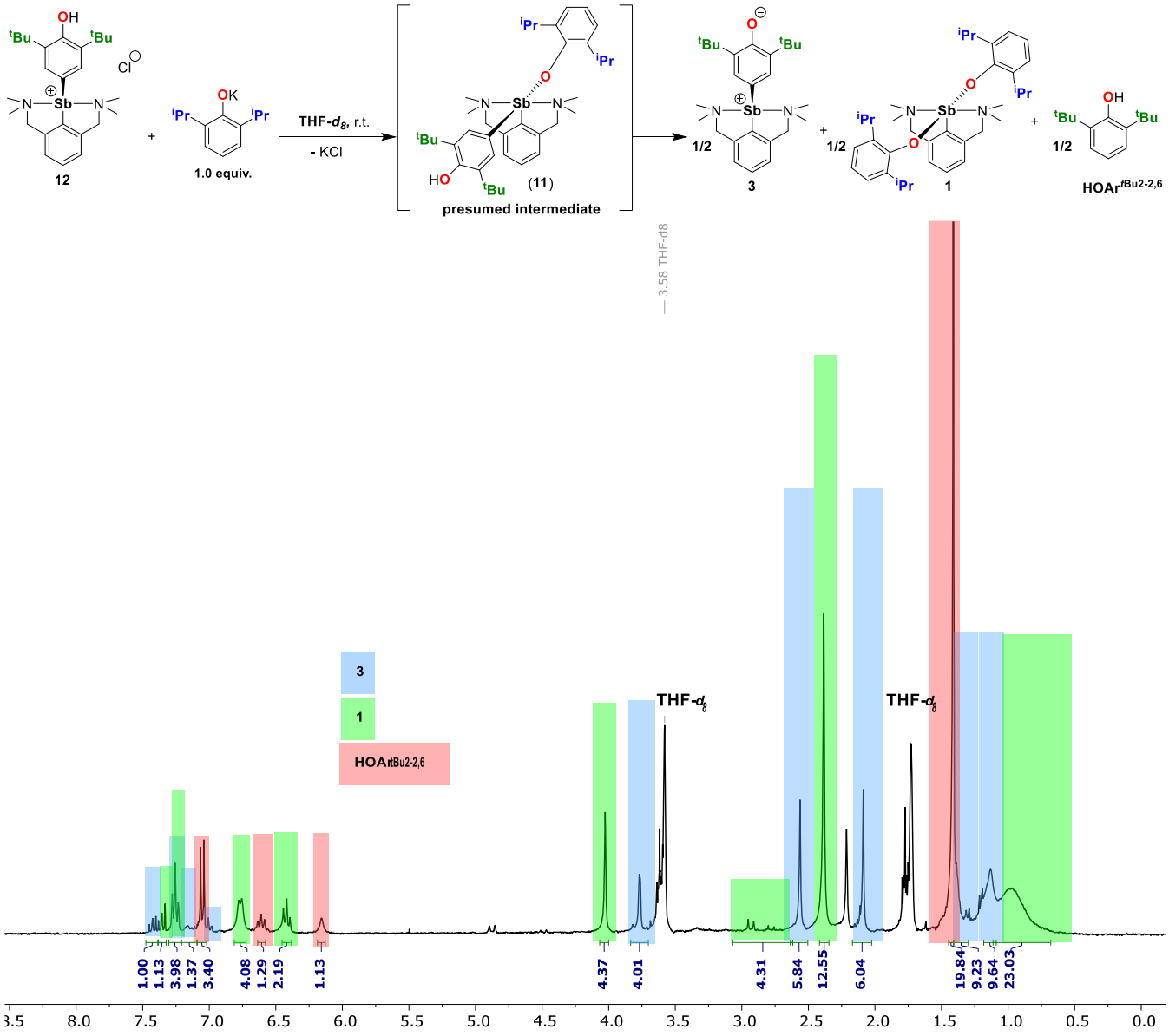

Figure S53. ^{1}H NMR spectrum (THF-d_8, 400.13 MHz, **300 K**) of the *in situ* equimolar reaction of [{*NCN*^{Me4}}Sb(C_6H_2-$^{t}Bu_2$-3,5-OH-4)][Cl] (**12**) with [{2,6-$^{i}Pr_2$-C_6H_3O}K].

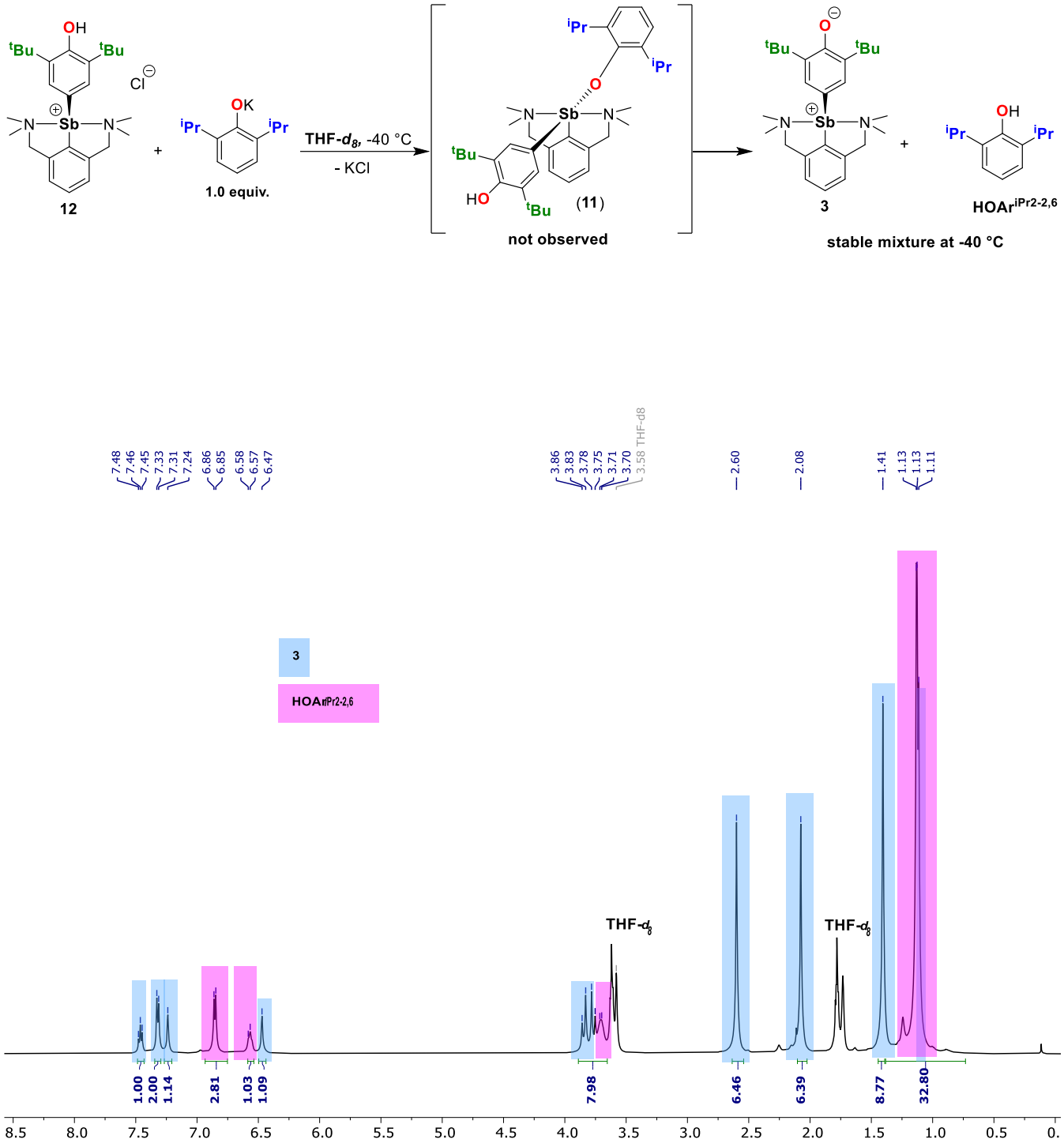

Figure S54. ^{1}H NMR spectrum (THF-d_8, 400.13 MHz, **233 K**) of the *in situ* equimolar reaction of [{*NCN*^{Me4}}Sb(C$_6$H$_2$-^{t}Bu$_2$-3,5-OH-4)][Cl] (**12**) with [{2,6-^{i}Pr$_2$-C$_6$H$_3$O}K].

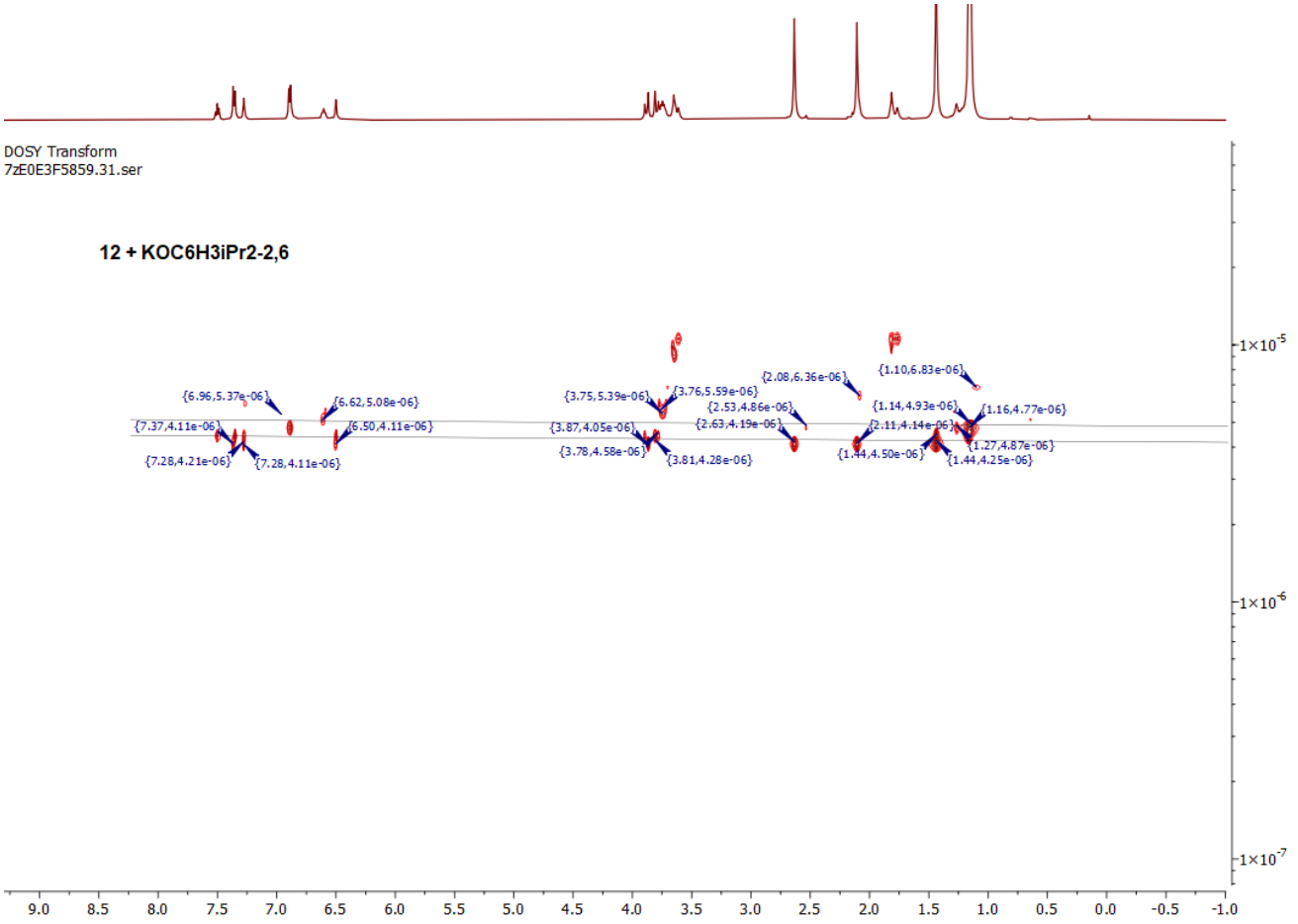

Figure S55. DOSY NMR spectrum (THF-d_8, 400.13 MHz, 233 K) of the *in situ* equimolar reaction of [{*NCN*^{Me4}}Sb(C_6H_2-^{t}Bu$_2$-3,5-OH-4)][Cl] (**12**) with [{2,6-^{i}Pr$_2$-C_6H_3O}K].

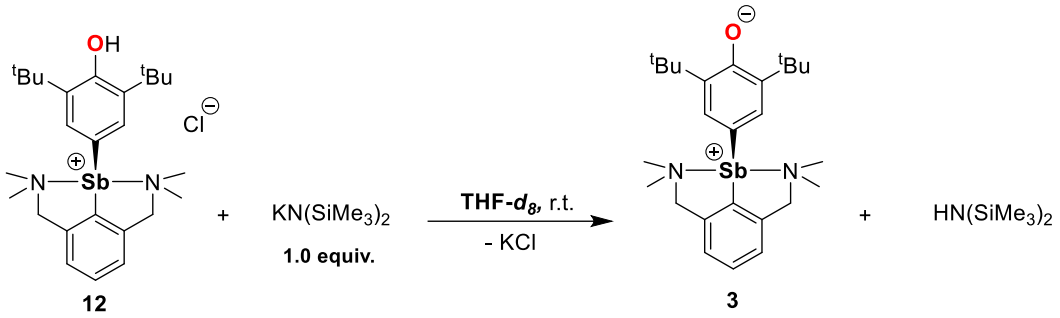

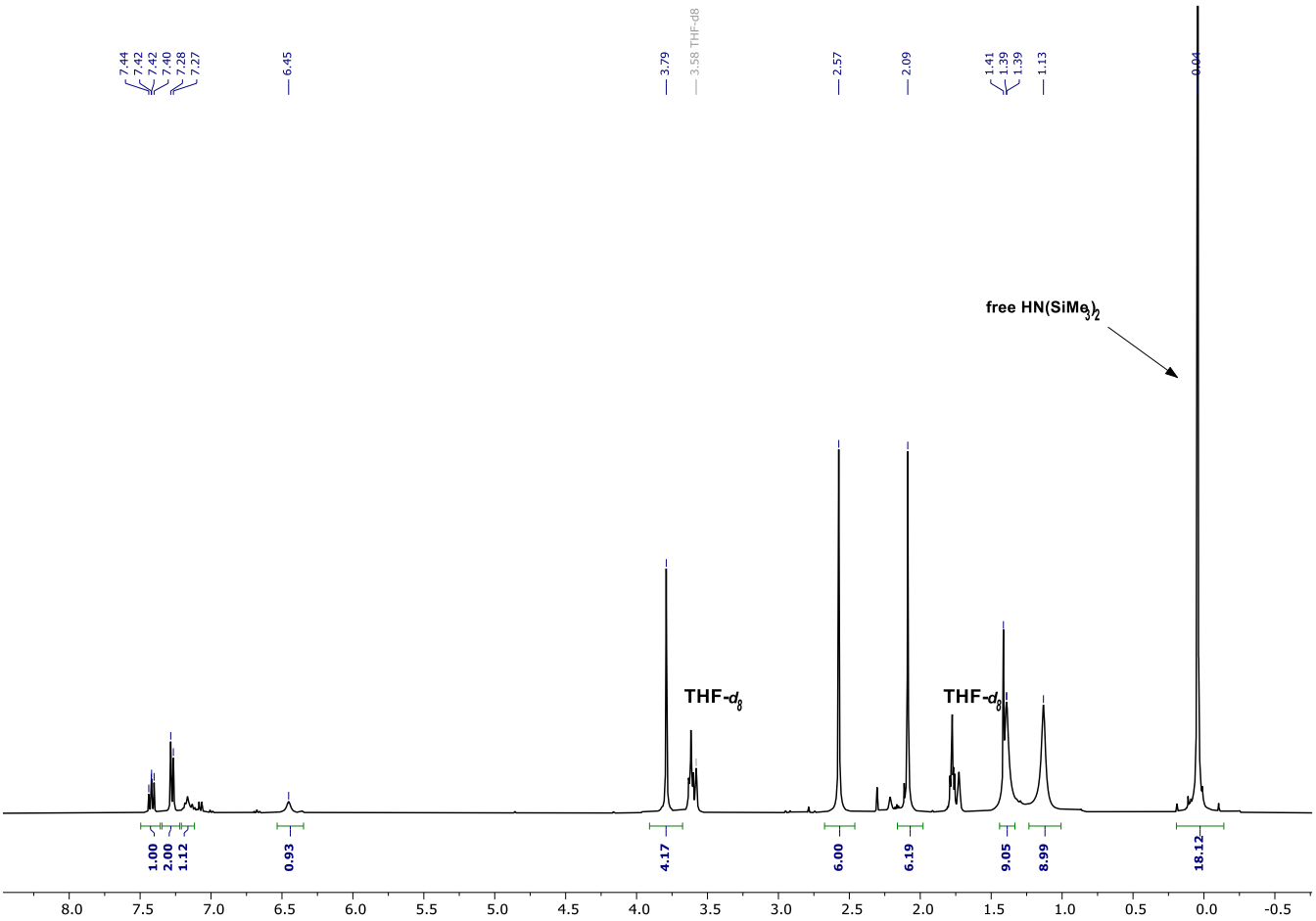

Figure S56. ^{1}H NMR spectrum (THF-d_8, 400.13 MHz, 300 K) of the *in situ* equimolar reaction of [{*NCN*^{Me4}}Sb(C$_6$H$_2$-^{t}Bu$_2$-3,5-OH-4)][Cl] (**12**) with KN(SiMe$_3$)$_2$.

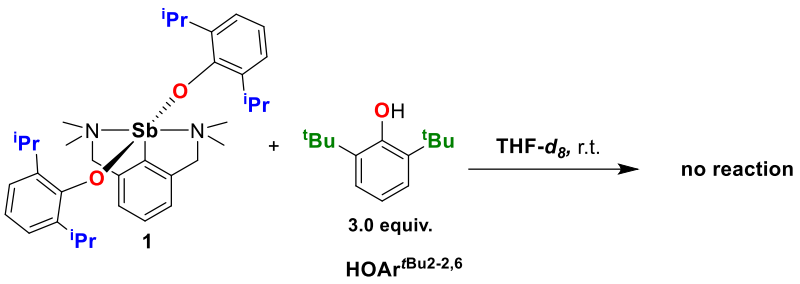

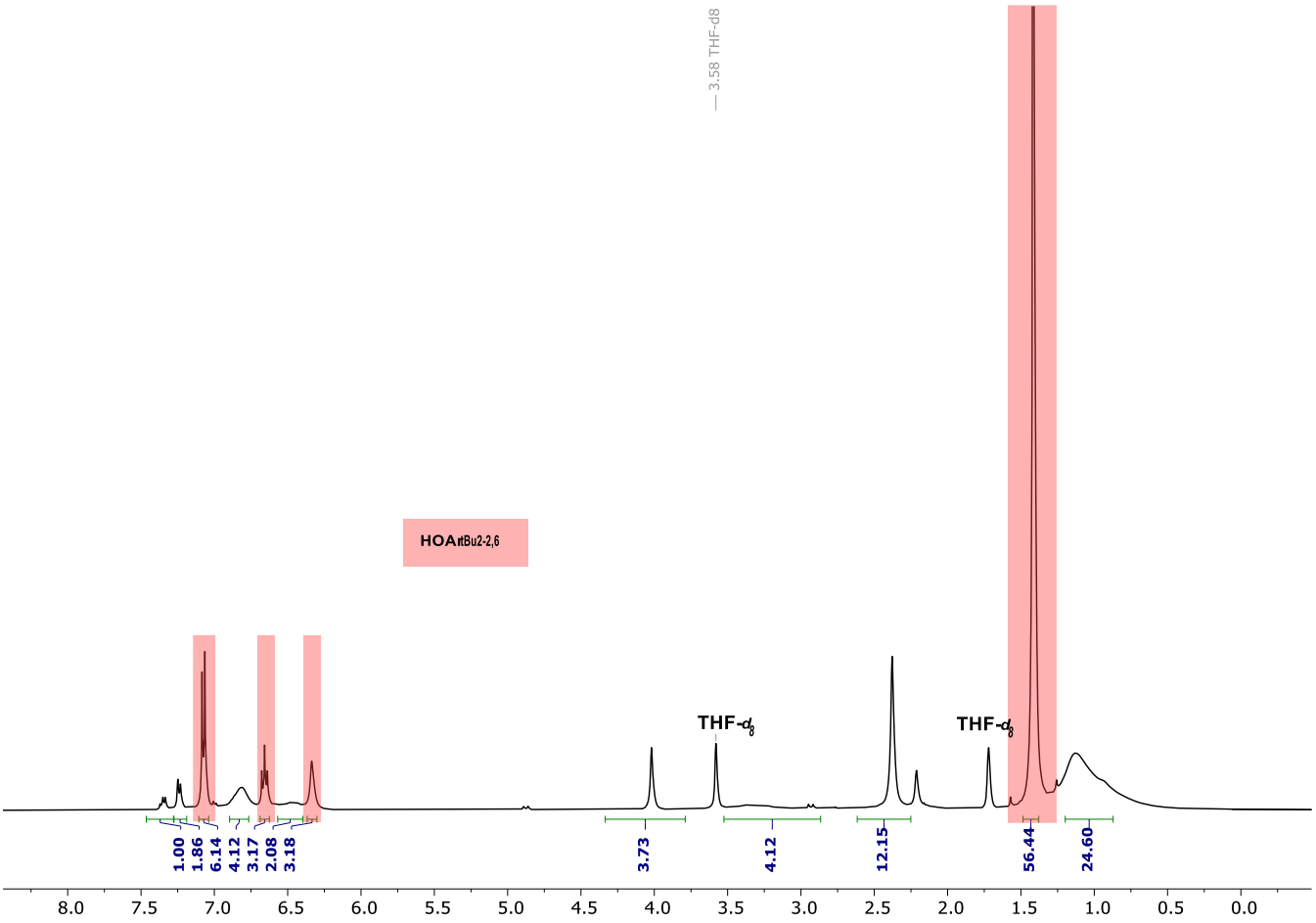

Figure S57. ^{1}H NMR spectrum (THF-d_8, 400.13 MHz, 300 K) of the *in situ* mixture of [{*NCN*^{Me4}}Sb(OC$_6$H$_3$-^{i}Pr$_2$-2,6)$_2$] (**1**) with 2,6-^{t}Bu$_2$-C$_6$H$_3$OH.

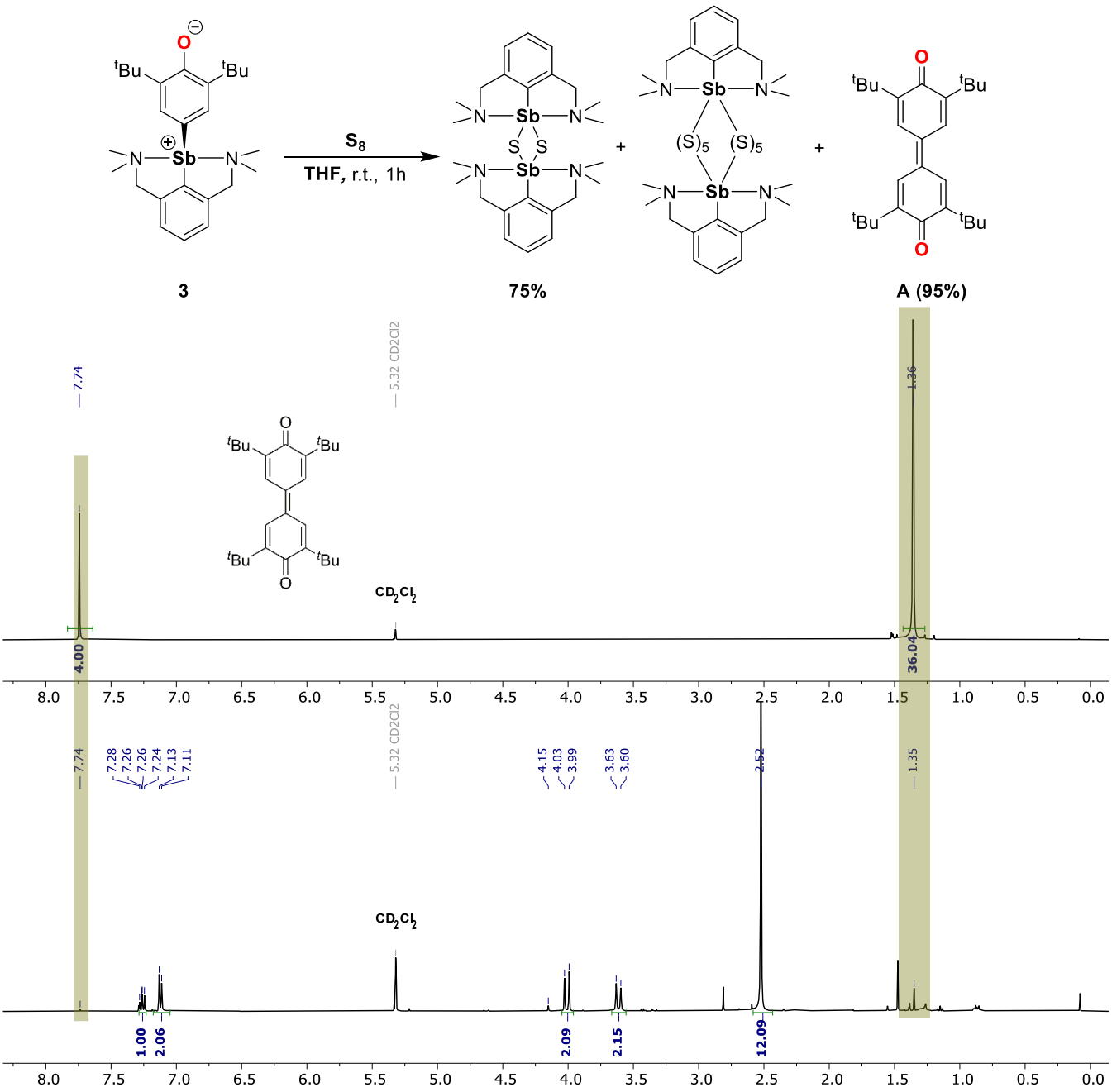

Figure S58. Stacked NMR spectra: ^{1}H NMR (CD_2Cl_2, 400.13 MHz, 300 K) spectrum of [{*NCN*^{Me4}}Sb(μ^{2}-S)]$_2$ (bottom) and ^{1}H NMR (THF-d_8, 400.13 MHz, 300 K) spectrum of 3,3',5,5'-tetra-*tert*-butyldiphenoquinone (**A**) (top).

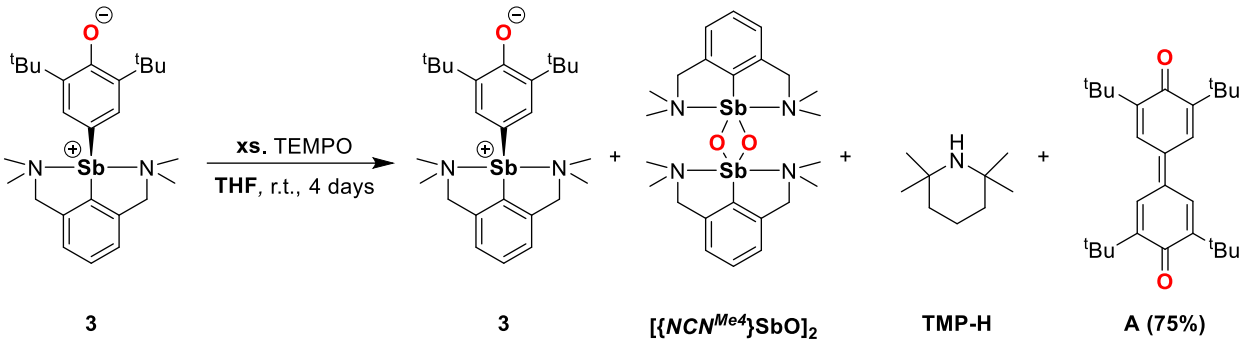

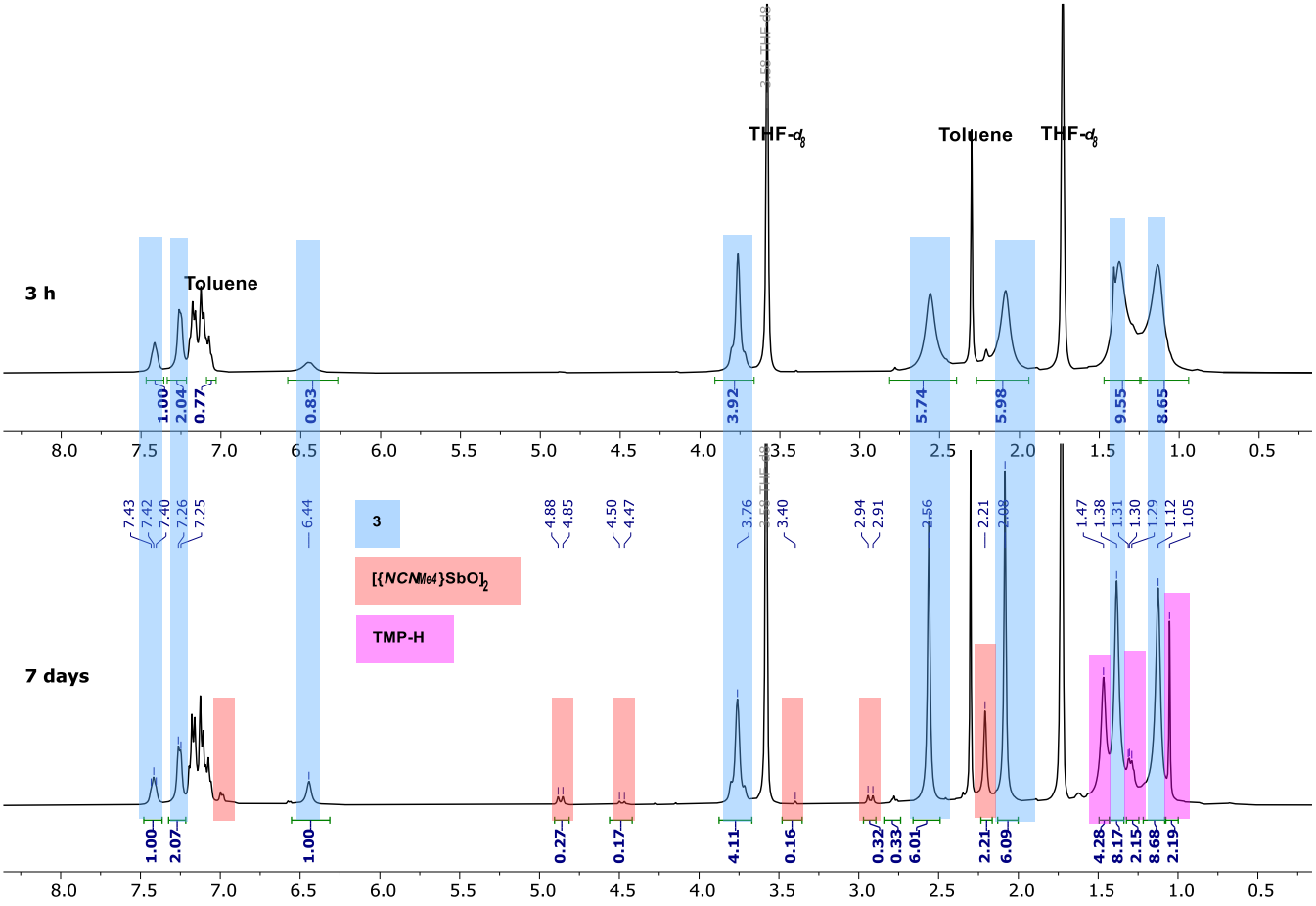

Figure S59. Stacked ^{1}H NMR spectra (THF-d_8, 400.13 MHz, 300 K) of a mixture of [{*NCN*^{Me4}}Sb(C$_6$H$_2$-^{t}Bu$_2$-3,5-O-4)] (**3**) and TEMPO (3 equivalents) after 3 h (top) and 7 d (bottom). Note that the starting compound **3** contained some residual toluene which is visible in the NMR spectra.

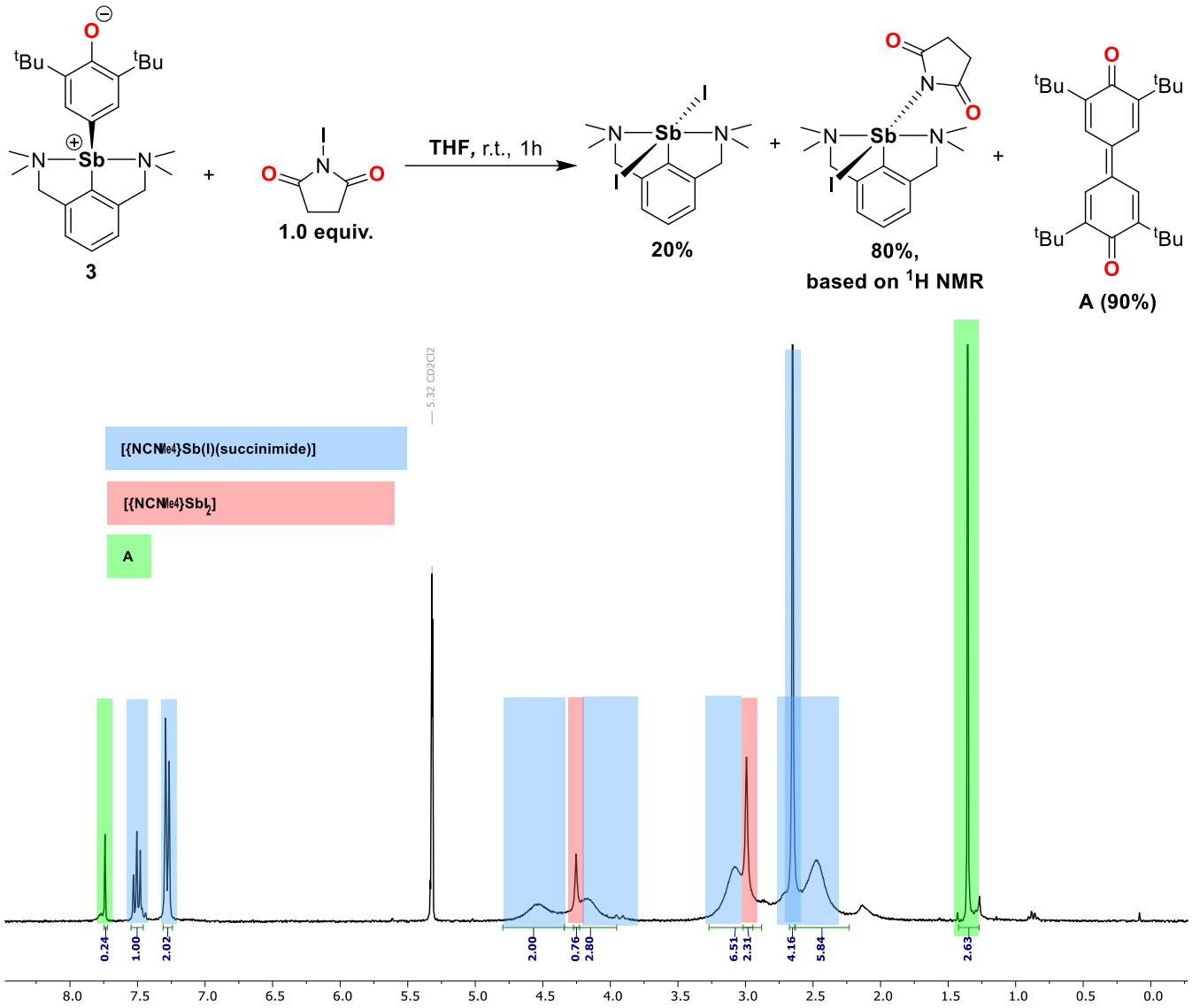

Figure S60. Reaction of [{*NCN*^{Me4}}Sb(C_6H_2-^{t}Bu$_2$-3,5-O-4)] (**3**) with *N*-iodosuccinimide: ^{1}H NMR spectrum (CD_2Cl_2, 400.13 MHz, 300 K) of the yellow material that precipitated from THF. It consists of a mixture of compound assumed to be [{*NCN*^{Me4}}Sb(I)(succinimide)] (ca. 80%) and [{*NCN*^{Me4}}SbI_2] (ca. 20%).

Conductivity measurements

Solutions (5 mM) in THF (5 mL) of the following compounds were prepared under an inert atmosphere (argon). The electrode of the conductivity meter was immersed in each solution under positive flow of argon.

Table S1. Molar conductivity of targeted antimony species.

5 mM solution in THF	**Λ (μS cm^{-1})**	**Λ_m (mS cm^2 mol^{-1})**
Blank – no compound	0.000	N/A
$Sb(C_6H_2Me_3\text{-}2,4,6)_3$	0.000	0.0
[{*NCN*^{Me4}}$SbCl_2$]	0.091	9.1
[{*NCN*^{Me4}}$Sb(OC_6H_3\text{-}^iPr_2\text{-}2,6)_2$] (**1**)	0.212	21.2
[{*NCN*^{Me4}}$Sb(C_6H_2\text{-}^tBu_2\text{-}3,5\text{-}O\text{-}4)$] (**3**)	0.272	27.2
[{*CN*^{Me2}}$Sb(OC_6H_3\text{-}^tBu_2\text{-}2,6)_2$] (**5**)	0.348	34.8
$[Na(OEt_2)_4]^+.[H_2N\{B(C_6F_5)_3\}_2]^-$	220	22,000

Crystallographic data.

Table S2. X-ray diffraction crystallography details.

	Complex number	Experiment number	CCDC number
[{*NCN*^{Me4}}Sb(C_6H_2-^{t}Bu$_2$-3,5-O-4)]	**3**	DG404	2335992
[{*NCN*^{iPr4}}Sb(C_6H_2-^{t}Bu$_2$-3,5-O-4)]	**4**	DG167	2335993
[{*CN*^{Me2}}Sb(C_6H_2-^{t}Bu$_2$-3,5-O-4)]$_4$	**6$_4$**	DG383	2335994
[{*NCN*^{Me4}}Sb(C_6H_2-^{t}Bu$_2$-3,5-OH-4)][Cl]	**12**	DG408	2335995
[{*NCN*^{Me4}}Sb(C_6H_2-^{t}Bu$_2$-3,5-OH-4)]$^+$[H_2N{$B(C_6F_5)_3$}$_2$]$^-$	**12'**	DG398	2335996
[{*NCN*^{Me4}}Sb(S_2C-C_6H_2-^{t}Bu$_2$-3,5-O-4)] (13)	**13**	DG337	2335997
[{*NCN*^{Me4}}SbI_2]	[{*NCN*^{Me4}}SbI_2]	DG419x2	2335998

[{*NCN*^{Me4}}Sb(C_6H_2-^{t}Bu$_2$-3,5-O-4)] (3) ($C_{26}H_{39}N_2OSb$); M = 517.34. A suitable crystal for X-ray diffraction single crystal experiment (yellow prism, dimensions = 0.400 x 0.280 x 0.100 mm) was selected and mounted on the goniometer head of a D8 Venture (Bruker-AXS) diffractometer equipped with a CMOS-PHOTON70 detector, using Mo-$K\alpha$ radiation (λ = 0.71073 Å, multilayer monochromator) at T = 150(2) K. Crystal structure has been described in triclinic symmetry and P -1 (I.T.#2) centric space group (R_{int} = 0.0263). Cell parameters have been refined as follows: a = 9.8727(10), b = 10.5653(9), c = 14.2599(14) Å, α = 107.461(3), β = 93.163(3), γ = 113.351(3)°, V = 1276.7(2) Å^3. Number of formula unit Z is equal to 2 and calculated density d and absorption coefficient µ values are 1.346 g.cm^{-3} and 1.099 mm^{-1} respectively. Crystal structure was solved by dual-space algorithm using *SHELXT* program,[13] and then refined with full-matrix least-squares methods based on F^2 (*SHELXL*[14]). All non-Hydrogen atoms were refined with anisotropic atomic displacement parameters. H atoms were finally included in their calculated positions and treated as riding on their parent atom with constrained thermal parameters. A final refinement on F^2 with 5840 unique intensities and 281 parameters converged at ωR_F^2 = 0.0388 (R_F = 0.0158) for 5583 observed reflections with $I > 2\sigma(I)$.

[{*NCN*^{iPr4}}Sb(C_6H_2-^{t}Bu$_2$-3,5-O-4)] (4) ($C_{34}H_{55}N_2OSb$); M = 629.55. A suitable crystal for X-ray diffraction single crystal experiment (clear light orange block, dimensions = 0.122 x 0.081 x 0.028 mm) was selected and mounted on a MiTeGen microMounts cryoloop using Paratone oil and data were collected on a Bruker D8 VENTURE diffractometer using Mo-Kα radiation (0.71073 Å) from a IµS 3.0 micro focus source, at low temperature (110 K). Crystal structure has been described in monoclinic symmetry and P 1 21/n 1 acentric space group (R_{int} = 0.0361). Cell parameters have been refined as follows: a = 9.7653(3), b = 21.1742(7), c = 15.8732(5) Å, α = 90.00, β = 100.8090(10), γ = 90.00 °, V = 3223.91(18) Å^3. Number of formula unit Z is equal to 4 and calculated density d and absorption coefficient µ values are 1.297 g.cm^{-3} and 0.883 mm^{-1} respectively. For structure solving and refinement the Bruker APEX4 software package was used.[15] The structures were solved by dual methods (SHELXT-2014/5)[13] and refined by full matrix least-squares procedures based on F^2 with all measured reflections (SHELXL-2019/1).[14,16] The structures were refined with anisotropic thermal parameters for non-H atoms. Hydrogen atoms were placed in fixed, idealized positions and refined with a riding model and a mutual isotropic thermal parameter. A final refinement on F^2 with 7997 unique intensities and 388 parameters converged at ωR_F^2 = 0.0440 (R_F = 0.0192) for 7161 observed reflections with $I > 2\sigma(I)$.

[{*CN*^{Me2}}Sb(C_6H_2-^{t}Bu$_2$-3,5-O-4)]$_4$ (6$_4$) ($C_{92}H_{128}N_4O_4Sb_4$); M = 1840.98. A suitable crystal for X-ray diffraction single crystal experiment (colourless stick, dimensions = 0.180 x 0.120 x 0.080 mm) was selected and mounted on the goniometer head of a D8 Venture (Bruker-AXS) diffractometer equipped with a CMOS-PHOTON70 detector, using Mo-$K\alpha$ radiation (λ = 0.71073 Å, graphite monochromator) at T = 150(2) K. Crystal structure has been described in tetragonal symmetry and I -4 (I.T.#82) acentric space group (R_{int} = 0.0452). Cell parameters have been refined as follows: a = 21.5783(13), b = 21.5783, c = 9.3024(6) Å, V = 4331.4(6) Å^3. Number of formula unit Z is equal to 2 and calculated density d and absorption coefficient µ values are 1.412 g.cm^{-3} and 1.285 mm^{-1} respectively. Crystal structure was solved by dual-space algorithm using *SHELXT* program,[13] and then refined with full-matrix least-squares methods based on F^2 (*SHELXL*[14]). All non-Hydrogen atoms were refined with anisotropic atomic displacement parameters. H atoms were finally included in their calculated positions and treated as riding on their parent atom with constrained thermal parameters. A final refinement on F^2 with 4929 unique intensities and 244 parameters converged at ωR_F^2 = 0.0647 (R_F = 0.0259) for 4782 observed reflections with $I > 2\sigma(I)$.

[{*NCN*^{Me4}}Sb(C_6H_2-^{t}Bu_2-3,5-OH-4)][Cl] (12) ($C_{26}H_{40}N_2OSb•CD_2Cl_2•Cl$); *M* = 640.74. A suitable crystal for X-ray diffraction single crystal experiment (colourless prism, dimensions = 0.250 x 0.070 x 0.050 mm) was selected and mounted on the goniometer head of a D8 Venture (Bruker-AXS) diffractometer equipped with a CMOS-PHOTON70 detector, using Mo-*Kα* radiation (*λ* = 0.71073 Å, multilayer monochromator) at *T* = 150(2) K. Crystal structure has been described in monoclinic symmetry and *C c*(I.T.#9) acentric space group (R_{int} = 0.0402). Cell parameters have been refined as follows: *a* = 9.7009(8), *b* = 17.2182(17), *c* = 18.3636(18) Å, *β* = 102.303(3)°, *V* = 2996.9(5) Å^3. Number of formula unit *Z* is equal to 4 and calculated density *d* and absorption coefficient μ values are 1.420 g.cm^{-3} and 1.210 mm^{-1} respectively. Crystal structure was solved by dual-space algorithm using *SHELXT* program,[13] and then refined with full-matrix least-squares methods based on F^2 (*SHELXL*[14]). All non-Hydrogen atoms were refined with anisotropic atomic displacement parameters. Except H1O introduced in the structural model through Fourier difference maps analysis, H atoms were finally included in their calculated positions and treated as riding on their parent atom with constrained thermal parameters. A final refinement on F^2 with 6833 unique intensities and 321 parameters converged at ωR_F^2 = 0.0579 (R_F = 0.0252) for 6762 observed reflections with $I > 2\sigma(I)$.

[{*NCN*^{Me4}}Sb(C_6H_2-^{t}Bu_2-3,5-OH-4)]$^+$[H_2N{$B(C_6F_5)_3$}$_2$]$^-$ (12') ($C_{36}B_2F_{30}N•C_{26}H_{40}N_2OSb$); *M* = 1556.34. A suitable crystal for X-ray diffraction single crystal experiment (colourless prism, dimensions = 0.200 x 0.140 x 0.100 mm) was selected and mounted on the goniometer head of a D8 Venture (Bruker-AXS) diffractometer equipped with a CMOS-PHOTON70 detector, using Mo-*Kα* radiation (*λ* = 0.71073 Å, multilayer monochromator) at *T* = 150(2) K. Crystal structure has been described in triclinic symmetry and *P* -1 (I.T.#2) centric space group (R_{int} = 0.0378). Cell parameters have been refined as follows: *a* = 11.7279(12), *b* = 14.3207(15), *c* = 19.0667(19) Å, *α* = 88.065(4), *β* = 81.938(4), *γ* = 78.543(4)°, *V* = 3107.4(6) Å^3. Number of formula unit *Z*is equal to 2 and calculated density *d* and absorption coefficient μ values are 1.663 g.cm^{-3} and 0.580 mm^{-1} respectively. Crystal structure was solved by dual-space algorithm using *SHELXT* program,[13] and then refined with full-matrix least-squares methods based on F^2 (*SHELXL*[14]). All non-Hydrogen atoms were refined with anisotropic atomic displacement parameters. Except H1O, H24A/B/C, H25A/B/C and H26A/B/C introduced in the structural model through Fourier difference maps analysis, H atoms were finally included in their calculated positions and treated as riding on their parent atom with constrained thermal parameters. A final refinement on $F^2$with 14171 unique intensities and 929 parameters converged at ωR_F^2 = 0.0765 (R_F = 0.0357) for 12665 observed reflections with $I > 2\sigma(I)$.

[{*NCN*^{Me4}}Sb(S_2C-C_6H_2-^{t}Bu_2-3,5-O-4)] (13) ($C_{27}H_{39}N_2OS_2Sb•C_5H_5N$); *M* = 672.57. A suitable crystal for X-ray diffraction single crystal experiment (gold prism, dimensions = 0.120 x 0.120 x 0.110 mm) was selected and mounted on the goniometer head of a D8 Venture (Bruker-AXS) diffractometer equipped with a CMOS-PHOTON70 detector, using Mo-*Kα* radiation (*λ* = 0.71073 Å, multilayer monochromator) at *T* = 150(2) K. Crystal structure has been described in monoclinic symmetry and *P* $2_1/n$ (I.T.#14) centric space group (R_{int} = 0.0369). Cell parameters have been refined as follows: *a* = 10.2127(10), *b* = 25.780(2), *c* = 12.4202(13) Å, *β* = 93.905(4)°, *V* = 3262.4(5) Å^3. Number of formula unit *Z* is equal to 4 and calculated density and absorption coefficient μ values are 1.369 g.cm^{-3} and 1.002 mm^{-1} respectively. Crystal structure was solved by dual-space algorithm using *SHELXT* program,[13] and then refined with full-matrix least-squares methods based on F^2 (*SHELXL*[14]). All non-Hydrogen atoms were refined with anisotropic atomic displacement parameters. H atoms were finally included in their calculated positions and treated as riding on their parent atom with constrained thermal parameters. A final refinement on F^2 with 7447 unique intensities and 362 parameters converged at ωR_F^2 = 0.0494 (R_F = 0.0238) for 6847 observed reflections with $I > 2\sigma(I)$.

[{*NCN*^{Me4}}SbI_2] ($C_{12}H_{19}I_2N_2Sb$); *M* = 566.84. A suitable crystal for X-ray diffraction single crystal experiment (yellow prism, dimensions = 0.090 x 0.080 x 0.040 mm) was selected and mounted on the goniometer head of a D8 Venture (Bruker-AXS) diffractometer equipped with a CMOS-PHOTON70 detector, using Mo-*Kα* radiation (*λ* = 0.71073 Å, multilayer monochromator) at *T* = 150(2) K. Crystal structure has been described in monoclinic symmetry and *P* 2_1 (I.T.#4) acentric space group (R_{int} = 0.0416). Cell parameters have been refined as follows: *a* = 8.7432(9), *b*= 17.2545(17), *c*= 16.9471(18) Å, *β* = 101.901(4), *V* = 2501.7(4) Å^3. Number of formula unit *Z* is equal to 6 and calculated density and absorption coefficient μ values are 2.258 g.cm^{-3} and 5.341 mm^{-1} respectively. Crystal structure was solved by dual-space algorithm using *SHELXT* program,[13] and then refined with full-matrix least-squares methods based on F^2 (*SHELXL*[14]). All non-Hydrogen atoms were refined with anisotropic atomic displacement parameters. H atoms were finally included in their calculated positions and treated as riding on their parent atom with constrained thermal parameters. A final refinement on F^2 with 11348 unique intensities and 473 parameters converged at ωR_F^2 = 0.0726 (R_F = 0.0342) for 11038 observed reflections with $I > 2\sigma(I)$.

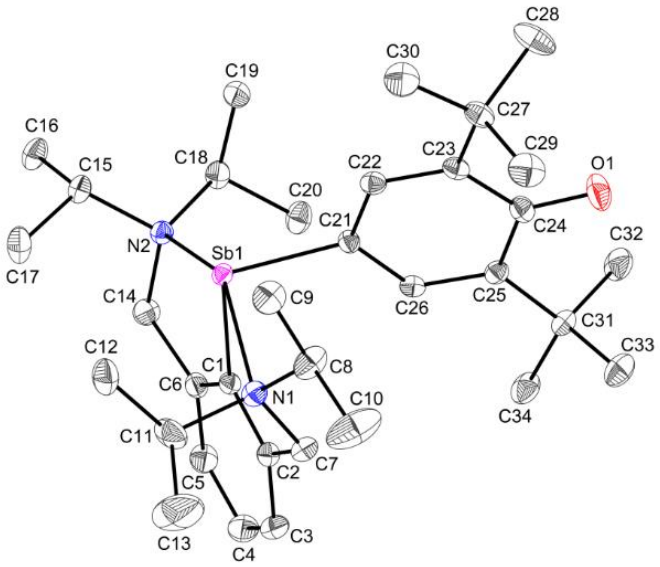

Figure S61. View of the molecular structure of [{*NCN*^{iPr4}}Sb(C_6H_2-^{t}Bu_2-3,5-O-4)] (**4**). H atoms omitted for clarity. Ellipsoids at the 50% probability level. Only one of the two enantiomers (pS_{N1}, pS_{N2}) in the asymmetric unit is shown. Selected distances (Å) and angles (°): Sb1−C1 = 2.1219(12), Sb1−C21 = 2.0882(14), Sb1−N1 = 2.5473(13), Sb1−N2 = 2.5666(12), C21−C22 = 1.4095(18), C21−C26 = 1.4042(17), C22−C23 = 1.3813(21), C23−C24 = 1.4559(19), C24−C25 = 1.4599(18), C25−C26 = 1.3785(18), C24−O1 = 1.2689(18); C1−Sb1–C13 = 98.81(5), C1−Sb1−N1 = 74.63(4), C1−Sb1−N2 = 74.22(5), C21−Sb1−N1 = 89.50(5), C21−Sb1−N2 = 107.69(5), N1−Sb1−N2 = 146.300(4).

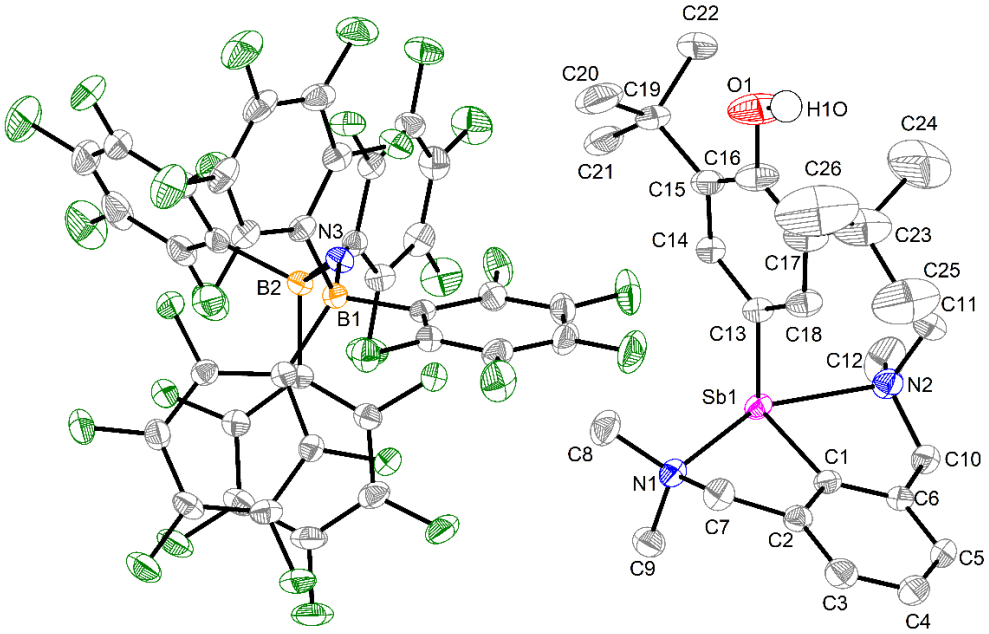

Figure S62. View of the molecular structure of [{*NCN*^{Me4}}Sb(C_6H_2-^{t}Bu_2-3,5-OH-4)][H_2N{$B(C_6F_5)_3$}$_2$] (**12'**). H atoms (except OH) omitted for clarity. Only the main components of the disordered ^{t}Bu groups are depicted. Ellipsoids at the 50% probability level. Selected distances (Å) and angles (°): Sb1−C1 = 2.0964(19), Sb1−C13 = 2.118(2), Sb1−N1 = 2.3956(19), Sb1−N2 = 2.4374(19), C13−C14 = 1.391(3), C13−C18 = 1.385(3), C14−C15 = 1.391(3), C15−C16 = 1.397(4), C16−C17 = 1.403(4), C17−C18 = 1.390(3), O1−C16 = 1.380(3), O1−H1(O) = 0.76(3); C1−Sb1−C13 = 101.02(8), C1−Sb1−N1 = 74.97(7), C1−Sb1−N2 = 74.68(7), C13−Sb1−N1 = 91.18(7), C13−Sb1−N2 = 94.01(8), N1−Sb1−N2 = 149.64(6).

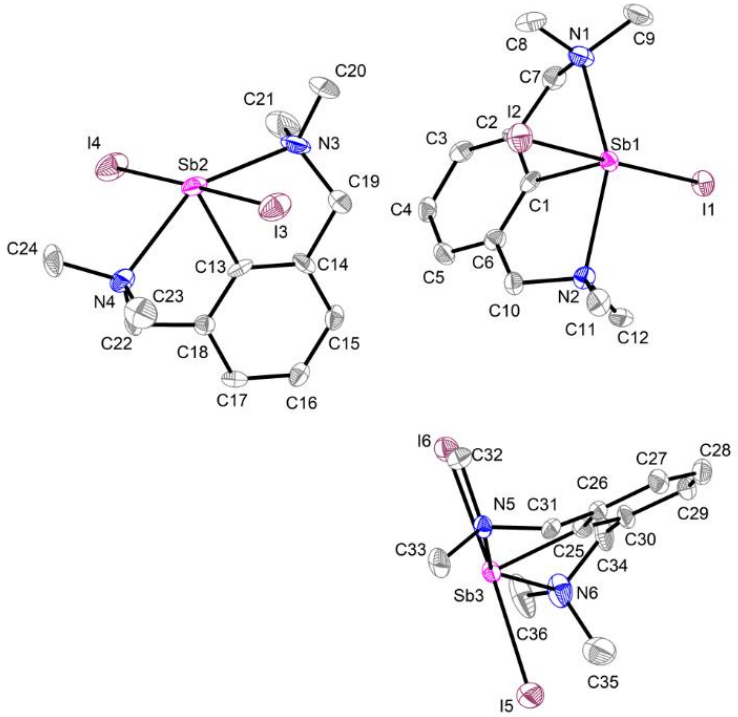

Figure S63. View of the molecular structure of [{*NCN*^{Me4}}SbI_2]. H atoms omitted for clarity. Ellipsoids at the 50% probability level. Selected distances (Å) and angles (°): Sb1−C1 = 2.102(10), Sb1−I1 = 3.0496(9), Sb1−I2 = 2.9749(10), Sb1−N1 = 2.493(8), Sb1−N2 = 2.466(8), I1−Sb1–I2 = 178.55(3), C1−Sb1−I1 = 89.7(2), C1−Sb1−I2 = 91.7(2), N1−Sb1−N2 = 147.9(3); Sb2−C13 = 2.130(9), Sb2−I3 = 2.9693(11), Sb2−I4 = 3.0067(11), Sb2−N3 = 2.471(10), Sb2−N4 = 2.480(9), I3−Sb2–I4 = 179.26(4), C13−Sb2−I3 = 89.1(3), C13−Sb2−I4 = 90.6(3), N3−Sb2−N4 = 148.2(3); Sb3−C25 = 2.125(10), Sb3−I5 = 2.9812(11), Sb3−I6 = 3.0199(10), Sb3−N5 = 2.470(8), Sb3−N6 = 2.456(9), I5−Sb3–I6 = 177.57(3), C25−Sb3−I5 = 92.3(3), C25−Sb3−I6 = 90.1(3), N5−Sb3−N6 = 147.6(3).

Discussion of metric parameters in the XRD structures of complexes 3 and 12.

For [{*NCN*^{Me4}}Sb(C_6H_2-^{t}Bu$_2$-3,5-O-4)] (**3**):

The molecular solid-state structure of **3** features a four-coordinate metalloid in a pseudotrigonal bipyramidal arrangement (see Fig. 3 in the manuscript). The *NCN*^{Me4} ligand adopts a distorted T-shape geometry about Sb (N1−Sb1−N2 = 148.10(4)°). The short Sb1−N1 and Sb1−N2 interatomic distances (2.4458(11) and 2.4436(11) Å) match those in [{*NCN*^{Me4}}$SbCl_2$] (2.422(8) and 2.491(9) Å)[3] and testify to two strong N→Sb dative bonds. The oxyaryl ligand is almost orthogonal to the plane delineated by Sb1-C1-N1-N2 (C1−Sb1−C13 = 101.02(5)°), and the coordination geometry about Sb is best described as see-saw (τ_4 = 0.66).[17] The Sb−$C_{oxyaryl}$ bond length (Sb1−C13 = 2.0862(12) Å) is below the low end of Sb−C_{aryl} distances in four-coordinate arylantimony(III) complexes. For instance, the Sb−C_{aryl} bonds in **3** itself (Sb1−C1 = 2.1134(13) Å) and in [{*NCN*^{Me4}}Sb−O−B(C_6F_5)$_3$] (2.102(2) Å)[18] are short compared to neutral compounds, e.g. in [{*NCN*^{Me4}}Sb($SC_6H_3Me_2$-2,6)$_2$] (2.1799(12) Å) having only one coordinated pendant arm,[19] or in [{2-(Me_2NCH_2)C_6H_4}SbX_2] (X = Cl, 2.147(5) Å; Br, 2.147(3) Å; I, 2.150(4) Å).[20] The Sb−$C_{oxyaryl}$ interatomic distance in **3** is comparable with the value found for the few reported Sb=C double bonds, e.g. in the stibaenol [Mes*C(O)Sb=C(OH)Mes*] (Mes* = C_6H_2^{t}Bu$_3$-2,4,6; Sb–C = 2.078(3) Å),[21] and in the pnictinidenes [{BDI^{DiPP}}(Cl)MSb^{Me}cAAC] (M = Al, Sb−C = 2.078(4) Å; M = In, Sb−C = 2.083(4) Å)[22] and [{BDI^{DiPP}}Ga(X)Sb^{Me}cAAC] (X = Cl, Sb−C = 2.083(4) Å; X = Br, Sb−C = 2.089(1) Å),[23] where ^{Me}cAAC = [$H_2C(CMe_2)_2NAr$]C and {BDI^{DiPP}} = HC[C(Me)N-2,6-^{i}Pr$_2$$C_6H_3$]$_2$. The Sb−C13 bond in **3** is hence intermediary between single and double Sb(III)−carbon bonds. The C16−O1 distance in **3** (1.2708(16) Å) also ranges between the values of single and double carbon-oxygen bonds, e.g. as in 3,3',5,5'-tetra-*tert*-butyl-(1,1'-biphenyl)-4,4'-diol (compound **B** in the manuscript; 1.385(4) and 1.391(3) Å)[24] and in 2,6-di-*tert*-butyl-1,4-benzoquinone (1.2456(6) and 1.2570(6) Å).[25] The C−O length in the 2,4,6-tri-*tert*-butylphenoxyl radical (**C**) is 1.246(2) Å.[26] The carbon-carbon interatomic distances in the oxyaryl ring in **3** vary in the range 1.3777(17)-1.4572(18) Å, as reported for **C**.[26] It hence feels legitimate to consider that this fragment exhibits partial quinoidal behaviour. Last, the non-planarity of the Sb1−C1−C2−C7−N1 and Sb1−C1−C6−C10−N2 rings induces chirality, and **3** crystallises as 1:1 mixture of (*p*R_{N1}, *p*R_{N2}) and (*p*S_{N1}, *p*S_{N2}) isomers.[27]

For [{*NCN*^{Me4}}Sb(C_6H_2-^{t}Bu$_2$-3,5-OH-4)][Cl] (**12**):

The geometry about the four-coordinate Sb atom in **12** (see Fig. 5 in the manuscript) is *pseudo*-trigonal bipyramidal. Complex **12** forms a loose ion pair. At a distance of 3.6761(14) Å, the closest Cl^- in the asymmetric unit is too remote from the metalloid to consider covalent bonding. By comparison, the Sb−Cl interatomic distances in [{*NCN*^{Me4}}$SbCl_2$] are 2.591(3) and 2.600(3) Å.[3] The Cl^- anion is engaged in H-bonding with the OH group (OH···Cl = 2.1538(341) Å), resulting in the assembly of monodimensional chains. Accordingly, the O1−H1(O) bond is stretched (0.909(6) Å).[28] The OH···Cl bond impacts the orientation of the OH group; the C16−O1−H1(O) plane is uncharacteristically *orthogonal* to the best plane delineated by the six carbon atoms. Complexes **12** and **3** present noticeable structural differences, compare for instance the distances to C13 belonging to the organoligand, 2.141(4) in **12** vs 2.0862(12) Å in **3**. The C−$O_{hydroxyl}$ distance in **12** (C16−O1 = 1.373(4) Å) is longer than the corresponding C−O_{oxy} one in **3** (1.2708(16) Å). The C_i−C_{i+1} distances (i = 13−17) in **12** exhibit only slight variations. Overall, the discrepancies in the metric parameters from **3** to **12** indicate protonation of the O atom, re-aromatisation of the C13−C14−C15−C16−C17−C18 ring, and loss of quinoidal character. The molecular solid-state structure of **12'** was also elucidated (Fig. S62). Typically with this anion,[29] there is no interaction between [H_2N{$B(C_6F_5)_3$}$_2$]$^-$ and the cation. Only minor differences between the metric parameters of the cations in **12** and **12'** can be noted, confirming that the chloride is loosely linked to the cationic Sb(III) centre in the former.[30]

Theoretical calculations

Computational Details

Geometry optimizations were carried out within the formalism of the density functional theory (DFT) with the Gaussian 16 package,[31] using the PBE0 functional[32] and the Def2-TZVP basis set from EMSL Basis Set Exchange Library,[33,34] together with Grimme's empirical DFT-D3(BJ) corrections[35] All the optimized geometries were characterized as true minima by vibrational analysis. The natural atomic orbital (NAO) charges and Wiberg bond indices were computed with the NBO 6.0 program.[36] Computed Gibbs free energies correspond to T = 298 K.

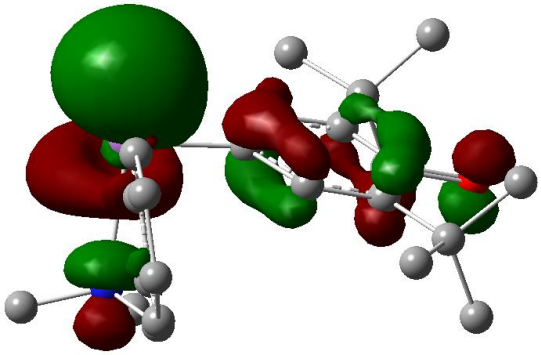

Figure S64. The LUMO of the elusive monomer [{*CN*^{Me2}}Sb(C_6H_2-^{t}Bu_2-3,5-O-4)] (**6**).

Table S3. Relevant DFT-computed data for bisphenolate complexes. Bond distances are given in Å, with their associated Wiberg bond index in brackets. Bond angles are given in °.

		[{*NCN*^{Me4}}Sb(OR)$_2$]					[{*CN*^{Me2}}Sb(OR)$_2$]
		R = C_6H_3-Me-2,6 **(not synthesized)**	R = C_6H_3-^{i}Pr$_2$-2,6 (**1**)	R = C_6H_3-^{t}Bu$_2$-2,6	R = C_6H_3-^{t}Bu$_3$-2,4,6 (**7**)	R = C_6H_2-^{t}Bu$_2$-2,4 (**8**)	R = C_6H_3-^{t}Bu$_2$-2,6] (**5**)
HOMO-LUMO gap (eV)		4.40	4.32	4.14	4.03	4.41	3.75
Sb-O		2.183 [0.289]	2.187 [0.244]	2.243 [0.192]	2.241 [0.191]	2.173 [0.308]/2.178 [0.304]	2.181 [0.276]/2.164 [0.315]
Sb-N		2.457 [0.219]	2.458 [0.183]	2.476 [0.149]	2.479 [0.148]	2.466 [0.234]	2.312 [0.301]
Sb-C		2.117 [0.654]	2.115 [0.574]	2.116 [0.482]	2.116 [0.479]	2.116 [0.678]	2.126 [0.667]
O-C		1.327 [1.111]	1.330 [1.100]	1.331 [1.118]	1.3321 [1.114]	1.329 [1.099]/1.331 [1.110]	1.345 [1.084]/1.334 [1.086]
O-Sb-O		167	168	174	174	170	167
N-Sb-N		148	148	148	148	148	
N-Sb-C		74	74	74	74	74	78
Sb-O-Ar		133	128	128	126	141/124	113/157
NAO atomic charges	**Sb**	1,19	1,19	1,20	2.13	1.76	1,88
	O	-0,65	-0,67	-0,69	-0.95	-0.90/-0.88	-0,92
	N	-0,41	-0,41	-0,41	-0.49	-0.43/-0.44	-0,47
	C	-0,35	-0,35	-0,35	-0.65	-0.43	-0,51

Table S4. Relevant DFT-computed data for the oxyaryl complex [{*NCN*^{Me4}}Sb(C_6H_2-^{t}Bu$_2$-3,5-O-4)] (**3**) and related species. Bond distances are given in Å, with their associated Wiberg bond index in brackets. Bond angles are given in °.

		[{*NCN*^{Me4}}Sb(C_6H_2-R$_2$-3,5-O-4)]			**[{*CN*^{Me2}}Sb(C_6H_2-^{t}Bu$_2$-3,5-O-4)]**	**[{*NCN*^{Me4}}Sb(C_6H_2-^{t}Bu$_2$-3,5-OH-4)]$^+$ (cation of salts 12 and 12')**
		R = Me	R = ^{i}Pr	R = ^{t}Bu (**3**)	R = ^{t}Bu (**6**)	
HOMO-LUMO gap (eV)		3.27	3.32	3.36	2.85	5.24
Sb-C(aryl)		2.041 [1.033]	2.044 [1.021]	2.047 [1.011]	2.029 [1.152]	2.110 [0.869]
Sb-C(*NCN*^{Me4})		2.127 [0.799]	2.126 [0.800]	2.125 [0.800]	2.140 [0.825]	2.105 [0.815]
Sb-N		2.543 [0.206] 2.522 [0.210]	2.538 [0.211] 2.513 [0.216]	2.529 [0.215] 2.507 [0.220]	2.445 [0.259]	2.458 [0.273] 2.425 [0.280]
O-C		1.242 [1.555]	1.244 [1.531]	1.247 [1.505]	1.24 [1.554]	1.347 [1.060]
N-Sb-C		73	73	73	75	74
N-Sb-N		146	146	146	-	149
N-Sb-C(aryl)		95 91	95 91	95 90	94	93 90
C-Sb-C		101	100	100	98	98
NAO atomic charges	**Sb**	1.19	1.19	1.20	1.11	1.28
	C(aryl)	-0.55	-0.55	-0.54	-0.51	-0.43
	O	-0.65	-0.67	-0.69	-0.65	-0.65
	N	-0.41	-0.41	-0.41	-0.40	-0.41
	C(*NCN*^{Me4})	-0.35	-0.41	-0.35	-0.36	-0.38

References

1 Thermo Xcalibur Qual Browser, Thermo Fisher Scientific Inc., Waltham, MA, 02454, 2016.
2 C. Bibal, S. Mazières, H. Gornitzka and C. Couret, *Polyhedron*, 2002, **21**, 2827-2834.
3 D. A. Atwood, A. H. Cowley and J. Ruiz, *Inorg. Chim. Acta*, 1992, **198-200**, 271-274.
4 C. J. Carmalt, A. H. Cowley, R. D. Culp, R. A. Jones, S. Kamepalli and N. C. Norman, *Inorg. Chem.*, 1997, **36**, 2770-2776.
5 G. Duneș and C. Silvestru, *New J. Chem.*, 2024, **48**, 5523-5529.
6 S. J. Lancaster, A. Rodriguez, A. Lara-Sanchez, M. D. Hannant, D. A. Walker, D. L. Hughes and M. Bochmann, *Organometallics*, 2002, 21, 451-453.
7 MestReNova, Mestrelab Research S.L., Feliciano Barrera 9B, Bajo, 15706 Santiago de Compostela, Spain, 2020.
8 G. R. Fulmer, A. J. M. Miller, N. H. Sherden, H. E. Gottlieb, A. Nudelman, B. M. Stoltz, J. E. Bercaw and K. I. Goldberg, *Organometallics*, 2010, **29**, 2176-2179.
9 L. Dostál, R. Jambor, A. Růžička, R. Jirásko, V. Lochař, L. Beneš and F. de Proft, *Inorg. Chem.*, 2009, **48**, 10495-10497.
10 L. Dostál, R. Jambor, A. Růžička, M. Erben, R. Jirásko, E. Černošková and J. Holeček, *Organometallics*, 2009, **28**, 2633-2636.
11 A. Ahmed, R. A. Bragg, J. Clayden, L. W. Lai, C. McCarthy, J. H. Pink, N. Westlund and S. A. Yasin, *Tetrahedron*, 1998, **54**, 13277-13294.
12 Y. Yamamoto, X. Chen, S. Kojima, K. Ohdoi, M. Kitano, Y. Doi and K.-Y. Akiba, *J. Am. Chem. Soc.*, 1995,**117**, 3922-3932.
13 G. M. Sheldrick, *Acta Cryst.*, 2015, **A71**, 3-8.
14 G.M. Sheldrick, *Acta Cryst.*, 2015, **C71**, 3-8.
15 Bruker, APEX4, Bruker AXS Inc., Madison, Wisconsin, USA, 2012.
16 J. Lübben, C. M. Wandtke, C. B. Hübschle, M. Ruf, G. M. Sheldrick and B. Dittrich, *Acta Cryst.*, 2019, **A75**, 50–62.
17 L. Yang, D. R. Powell and R. P. Houser, *Dalton Trans.*, **2007**, 955-964.
18 R. Kather, T. Svoboda, M. Wehrhahn, E. Rychagova, E. Lork, L. Dostál, S. Ketkov and J. Beckmann, *Chem. Commun.*, 2015, **51**, 5932-5935.
19 G. Duneş, A. Soran and C. Silvestru, *Dalton Trans.*, 2022, **51**, 10406-10419.
20 L. M. Opris, A. Silvestru, C. Silvestru, H. J. Breunig and E. Lork, *Dalton Trans.*, 2003, 4367-4374.
21 C. Jones, J. W. Steed and R. C. Thomas, *J. Chem. Soc., Dalton Trans.*, 1999, 1541-1542.
22 J. Krüger, C. Wölper and S. Schulz, *Organometallics*, 2022, **41**, 3788-3793.
23 J. Krüger, C. Wölper, L. John, L. Song, P. R. Schreiner and S. Schulz, *Eur. J. Inorg. Chem.*, 2019, 1669-1678.
24 M. A. Jackisch, F. R. Fronczek, C. C. Geiger, P. S. Hale, W. H. Daly and L. G. Butler, *Acta Crystallogr., Sect. C. Struct. Chem.*, 1990, **C46**, 919-922.
25 G. G. Aleksandrov, Y. T. Struchkov, D. I. Kalinin and M. G. Neigauz, *Zh. Strukt. Khim.*, 1973, **14**, 797-803.
26 V. W. Manner, T. F. Markle, J. H. Freudenthal, J. P. Roth and J. M. Mayer, *Chem. Commun.*, 2008, 256-258.
27 IUPAC Nomenclature of Organic chemistry, Pergamon Press, Oxford, **1979**.
28 Note that the position of H1(O) atoms in **12** was not idealised but localised by Fourier difference map analysis.
29 Y. Sarazin, D. L. Hughes, N. Kaltsoyannis, J. A. Wright and M. Bochmann, *J. Am. Chem. Soc.*, 2007, **129**, 881-894.
30 The only significant difference between the metric parameters of the cations in **12** and **12'** is the length of the O−H bond, which is much larger in **12** (0.909(6) Å) because of OH···Cl hydrogen bonding than in **12'** (0.76(3) Å); the O1−H1(O) bond in **12'** is coplanar with the aromatic ring, whereas it was orthogonal in **12**.
31 Gaussian 16, Revision C.01, M. J. Frisch, G. W. Trucks, H. B. Schlegel, G. E. Scuseria, M. A. Robb, J. R. Cheeseman, G. Scalmani, V. Barone, G. A. Petersson, H. Nakatsuji, X. Li, M. Caricato, A. V. Marenich, J. Bloino, B. G. Janesko, R. Gomperts, B. Mennucci, H. P. Hratchian, J. V. Ortiz, A. F. Izmaylov, J. L. Sonnenberg, D. Williams-Young, F. Ding, F. Lipparini, F. Egidi, J. Goings, B. Peng, A. Petrone, T. Henderson, D. Ranasinghe, V. G. Zakrzewski, J. Gao, N. Rega, G. Zheng, W. Liang, M. Hada, M. Ehara, K. Toyota, R. Fukuda, J. Hasegawa, M. Ishida, T. Nakajima, Y. Honda, O. Kitao, H. Nakai, T. Vreven, K. Throssell, J. A. Montgomery, Jr., J. E. Peralta, F. Ogliaro, M. J. Bearpark, J. J. Heyd, E. N. Brothers, K. N. Kudin, V. N. Staroverov, T. A. Keith, R. Kobayashi, J. Normand, K. Raghavachari, A. P. Rendell, J. C. Burant, S. S. Iyengar, J. Tomasi, M. Cossi, J. M. Millam, M. Klene, C. Adamo, R. Cammi, J. W. Ochterski, R. L. Martin, K. Morokuma, O. Farkas, J. B. Foresman, and D. J. Fox, Gaussian, Inc., Wallingford CT, 2016.
32 (*a*) J. P. Perdew, K. Burke and M. Ernzerhof, *Phys. Rev. Lett.*, 1996, **77**, 3865-3868; (*b*) C. Adamo and V. Barone, *J. Chem. Phys.*, 1999, **110**, 6158-6170.
33 A. Schaefer, H. Horn and R. J. Ahlrichs, *Chem. Phys*., 1992, **97**, 2571-2577.
34 A. Schaefer, C. Huber and R. J. Ahlrichs, *Chem. Phys*., 1994, **100**, 5829-5835.
35 S. Grimme, *J. Comput. Chem.*, 2006, **27**, 1787-1799.
36 E. D. Glendening, J. K. Badenhoop, A. E. Reed, J. E. Carpenter, J. A. Bohmann, C. M. Morales, C. R. Landis and F. Weinhold, F. NBO 6.0; Theoretical Chemistry Institute, University of Wisconsin, Madison, WI, 2013, http://nbo6.chem.wisc.edu.

Author Contributions

Gabriel Duneş carried out the synthetic and spectroscopic experimental work and participated to the data analysis and their processing, and to the preparation of the manuscript. Marie Cordier solved the crystallographic structures. Alpar Pöllnitz participated to the synthetic experimental work. Samia Kahlal and Jean-Yves Saillard performed the theoretical calculations and their analysis, and participated to the preparation of the manuscript. Cristian Silvestru participated to data analysis, planning of experimental work and manuscript preparation. Yann Sarazin was the lead scientist; he secured the funding, participated to experiment planning, to data analysis, and to the writing of the manuscript.